Anul XLI **1996**

S T U D I A

UNIVERSITATIS BABEŞ-BOLYAI

PHYSICA

1

R e d a c ţ i a : 3400 CLUJ-NAPOCA str. Gheorghe Bilaşcu nr.24 Telefon : 194315,int.167

S U M A R - C O N T E N T S - S O M M A I R E

SOLID STATE PHYSICS

SPECTROSCOPY

PLASMA PHYSICS

METAMAGNETIC TRANSITIONS IN $Y(Co_XNi_{1-X})_3$ COMPOUNDS

E. BURZO[1], R. TETEAN[1]

ABSTRACT. The magnetic measurements on $Y(Co_XNi_{1-X})_3$ compounds were performed in the temperature range 5-300 K and fields up to 9 T. Metamagnetic transitions involving nickel atoms, are observed in the low temperature range, for compounds with $0.9 \leq x \leq 0.6$. Finally the magnetic behavior of the above system is analyzed.

INTRODUCTION

The YCo_3 and YNi_3 compounds crystallize in a $PuNi_3$-type structure having R3m space group[1]. In the above lattice the 3d transition metal atoms occupy three types of sites. The cobalt and nickel magnetic moments are dependent on the characteristic environment of a given site. The neutron diffraction studies show values of cobalt moments of 0.55(3), 0.79(4) and 0.04(1) μ_B [2]. Very weak nickel moments were reported in YNi_3,namely 0.057(3), 0.073(3) and 0.065(3) μ_B respectively [3].

The high field measurements performed on YCo_3 show the presence of two field induced successive transitions at B_1=60 T and B_2=82 T [4]. These metamagnetic transitions are believed to occur at different crystallographic Co sites and are considered to come from a special shape of density of state near the Fermi level.

[1] "Babeş-Bolyai" University, Faculty of Physics, 3400 Cluj-Napoca, Romania.

By gradual substitution of cobalt by nickel in YCo_3 we expect that the magnetic behaviour of the pseudobinary compounds will be modified. The presence, in the same compound, of very weak nickel moments in addition to Co ones can results in interesting magnetic properties.

EXPERIMENTAL

The $Y(Co_XNi_{1-X})_3$ compounds were prepared by arc melting the constituent elements in a purified argon atmosphere. A small excess of yttrium was used to compensate the loss of weight during melting. The samples were remelted several times in order to ensure a good homogeneity. The alloys were then heat treated at 950°C for 10 days.

The X-ray analyses show that the compounds crystallize in a $PuNi_3$ - type structure in all the composition range. The lattice parameters are only little dependent on composition, Fig. 1. This behaviour may be correlated with nearly the same radius of cobalt and nickel ions.

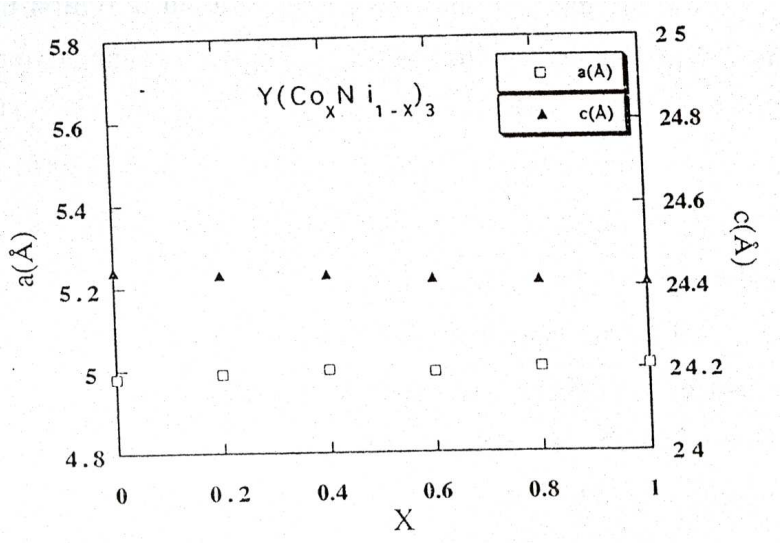

Fig. 1. Composition dependencies of the lattice parameters.

The magnetic measurements were performed in the temperature range 5-300 K and fields up to 9 T. The spontaneous magnetization's, M_s, were

determined from the magnetization isotherms, according to the approach to saturation law $M=M_S(1-a/H)+\chi_0'H$. We denoted by a the coefficient of magnetic hardness and χ_0' is a field independent contribution to susceptibility. The Curie temperatures were determined from the thermal variations of magnetization's in low fields (B ≅ 0.01 T).

EXPERIMENTAL RESULTS AND DISCUSSIONS

Some magnetization isotherms, obtained for the compound having x=0.8 are plotted in Fig. 2. A transition towards a state having somewhat higher magnetization is induced by an applied field of 5-6 T, at low temperatures (5K). The variation of magnetization (of metamagnetic type) at above transition is dependent on composition-Fig. 3.

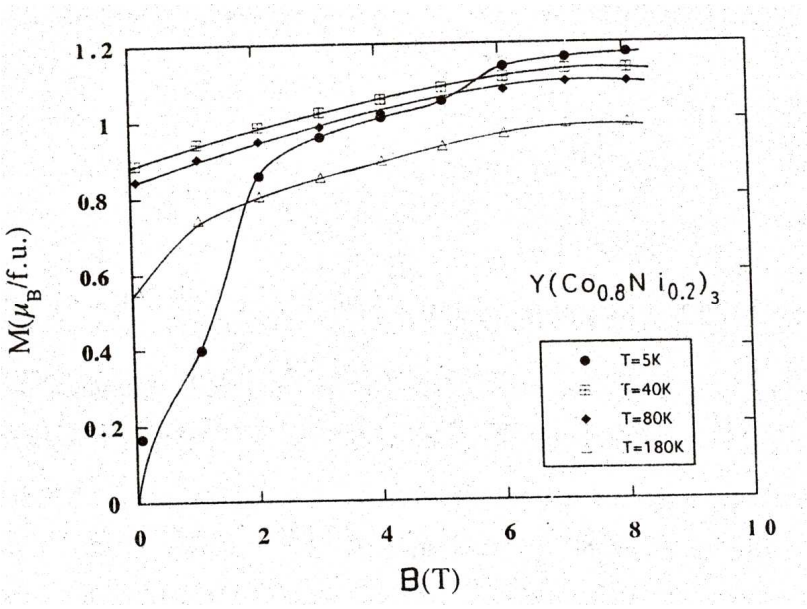

Fig. 2. Magnetization isotherms determined in $Y(Co_{0.8}Ni_{0.2})_3$ compound, at 5K**.**

The increase in the magnetization at the critical field is of 0.012 μ_B (x=0.9), 0.07 μ_B (x=0.8) and 0.03 μ_B (x=0.6). We attribute these transitions to the nickel atoms whose magnetization's increase under the action of external field.

Similar transitions have been observed for cobalt in $ThCo_5$ where two states of different magnetization's are induced by an applied magnetic field [5]. In our case, the transition is not so sharp as in $ThCo_5$. We attributed the observed behavior to a distribution of exchange fields and consequently of the critical fields during this ferromagnetic-ferromagnetic type transition determined by the presence of both Co and Ni atoms in lattice.

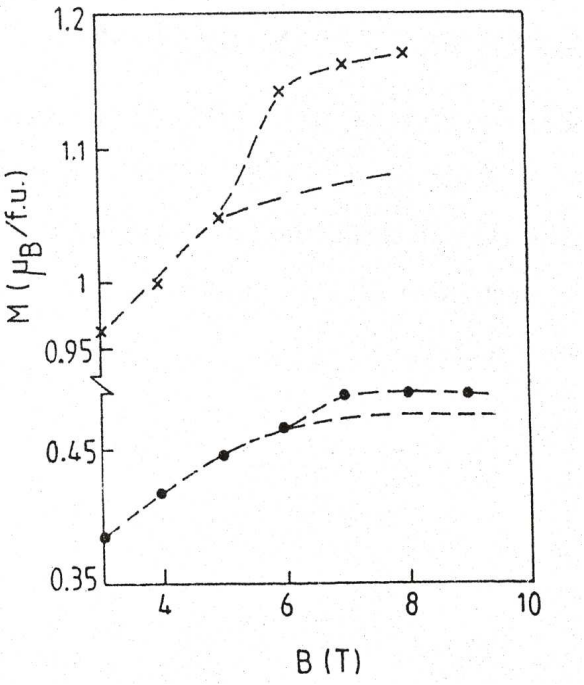

Fig. 3. Metamagnetic transitions in $Y(Co_xNi_{1-x})_3$ compounds with x=0.8 and 0.6, at 5k.

There are experimental evidence that in observed metamagnetic transition nickel is involved. The high magnetization state in YCo_3 is observed in fields more than one order of magnitude greater than experimentally observed in the present study. In $Y(Co_XNi_{1-X})_3$ the critical field is little dependent on composition even the exchange interactions decrease strongly when cobalt is replaced by nickel. Also, the observed changes in the magnetization is of the order of magnitude of nickel moment induced when replacing yttrium by gadolinium in YNi_3 [6]. In this case the meanvalue of nickel moment increase from 0.07 μ_B (Y) up to 0.15 μ_B (Gd).

The neutron diffraction studies performed on $Er(Fe_XNi_{1-X})_3$ [7] show that Ni atoms prefer the 18 h sites. We suppose that a similar substitutional preference takes place in $Y(Co_XNi_{1-X})_3$. We note that in $R\bar{3}m$ **Error! Switch argument not specified.** - type structure the ratio of the atoms in h: c: b sites is 2: 1/2: 2/3.

In a first approximation we suppose that the nickel magnetic moment of h site in $Y(Co_XNi_{1-X})_3$ is the same as that determined in YNi_3 ($0.065\mu_B$). In this case the nickel contribution to the magnetization in $Y(Co_XNi_{1-X})_3$ will be $0.019\mu_B$ (x=0.1); $0.040\mu_B$ (x=0.2) and $0.078\mu_B$ (x=0.4). By comparing the induced nickel moment in $GdNi_3$, we expect an increase of Ni moment at the metamagnetic transition of the same magnitude as nickel moments in YNi_3.

These agree with experimental data, except for the compound with x=0.6. Probably that in this case the high decrease of the exchange interactions, as evidenced by changes in Curie temperatures, will influence significantly the nickel moments.

If we suppose that the decrease of the nickel moment is proportional to the exchange field, from the value evidenced in compound with x=0.1, the induced moment will be about half than that expected, in agreement with the experimental data.

The temperature dependencies of the magnetization's are plotted in Fig. 4. Except for the compound with x=0.2 the samples are ferromagnetically ordered. Both the saturation magnetization's and Curie temperatures decrease as cobalt is replaced by nickel up to x=0.2.

As seen in Fig. 5 the compound with x=0.2 seems to be non magnetic. The disappearance of the ferromagnetism can be explained qualitatively by assuming that a local minimum in the density of states exist between the Fermi levels corresponding to YCo_3 and Yni_3.

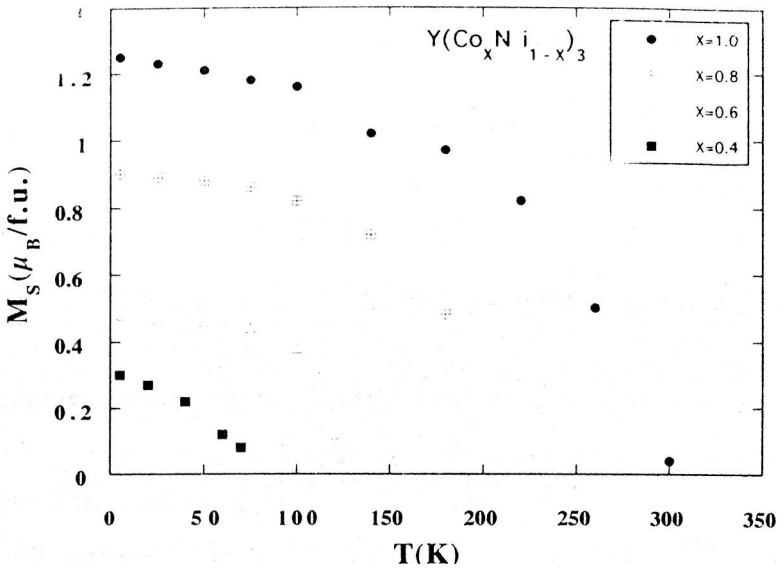

Fig. 4. The thermal variations of spontaneous magnetizations.

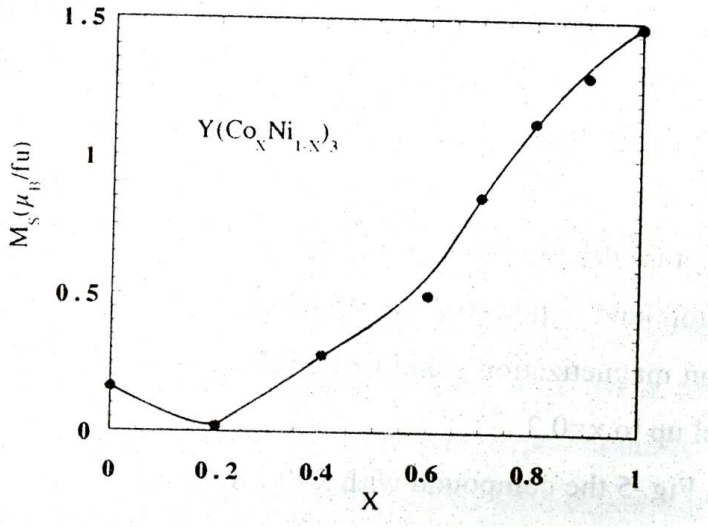

Fig. 5. The composition dependence of the magnetizations, at 5 K.

We analyzed the influence of external magnetic field on the magnetization's of $Y(Co_{0.2}Ni_{0.8})_3$ compound. The magnetization isotherm obtained at 5K is shown in Fig. 6. The magnetic moment increases linearly with a slope of ~ $(300)^{-1}$ μ_B/T, up to 5 T and then saturates to a value of 0.018 μ_B.

We note that the induced moments per unit field in linear region is close to that determined in cobalt compounds [8,9]. It will be interesting to study this compound in higher external fields, some magnetic transition being expected.

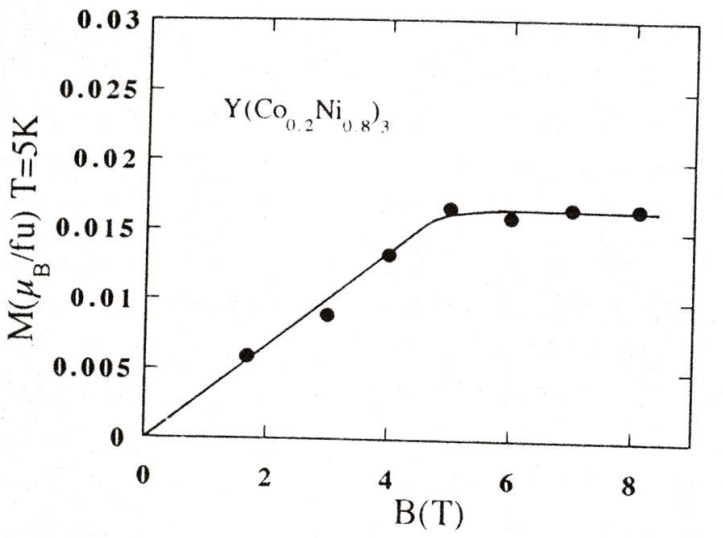

Fig. 6. Field dependence of magnetization in $Y(Co_{0.8}Ni_{0.2})_3$, at 5K.

We conclude that in $Y(Co_XNi_{1-X})_3$ system the metamagnetic transitions are present, these being attributed to the contributions of nickel atoms.

REFERENCES

1. E. F. Bertaut, R. Lemaire, J. Schweizer, *Bull.Soc. Miner. Cryst. 88*, 580 (1965).
2. E. Krén, J. Schweizer, F. Tasset, *Phys. Rev. 186*, 479 (1969).
3. D. Gignoux, R. Lemaire, P. Molho and F. Tasset. J. Magn. *Magn. Mat. 21*, 307 (1980).
4. T. Goto, H. Aruga Katori, T. Sakakibabara, M. Yamaguchi, *Physica* B *177*, 255 (1992).
5. D.Givord, J. Laforest, R. Lemaire, *J.Appl.Phys*., *50*, 7489 (1979).
6. E. Burzo, J. Laforest, *Compte Rend.Acad.Sci.Paris* B *274*, 114 (1972).
7. D. Tharp, Y. Yang, W. James, W. Yelon, D. Xie, J. Yang, *J. Appl.Phys. 61* 4249 (1987).
8. E. Burzo, *Solid State Commun. 20*, 569 (1976).
9. E. Burzo, J. Less Common. *Metals 77*, 251 (1981).

MAGNETIC PROPERTIES OF $LaMn_6Al_6$ AND $CeMn_6Al_6$

M. COLDEA[1], I. BURDA[1], R. COLDEA[1], D. ANDREICA[1]

ABSTRACT. The occurrence of a Mn moment in $LaMn_6Al_6$ and $CeMn_6Al_6$ is strongly correlated with the critical value d=2.61 Å of Mn-Mn distance below which the Mn moments collapses. A progressive change from a Ce^{4+} state at very low temperature to an intermediate valence state at room temperature, arising through thermal excitation to the 3+ magnetic state, in $CeMn_6Al_6$ was evidenciated.

INTRODUCTION

The magnetic moment on the Mn sites in RMn_2 (R=Y and rare earth) has been shown to depend strongly on the Mn-Mn distance [1]. A critical value of d=2.67Å was postulated, below which the Mn moments should not be stable. We have also found that a similar phenomena takes place in RMn_4Al_8 (R=Y, Gd) and RMn_6Al_6 (R=Y, Gd, Er) of $ThMn_{12}$ structure type where the critical Mn-Mn distance was estimated to be 2.6 Å [2-4]. In RMn_6Al_6 both the magnetic and the nonmagnetic Mn atoms were observed to coexist. The thermodynamic properties at finite temperatures of these compounds have been described in terms of the self-consistent renormalization (SCR) theory of spin fluctuations, as a transition from the itinerant electron character to the local moment type of the Mn moment. These studies revealed also the importance of performing magnetic measurements in a large temperature range in order to understand the magnetic behavior of the investigated compounds.

[1] "Babeş-Bolyai" University, Faculty of Physics, 3400 Cluj-Napoca, Romania.

The RMn_6Al_6 compounds where R is a light rare earth (R=La-Sm) crystallize in the hexagonal (rhomboedral) Th_2Zn_{17} structure type in spite of the big difference in the compositions of $ThMn_{12}$ and Th_2Zn_{17} [5]. The magnetic susceptibility of $LaMn_6Al_6$ was measured by Felner and Nowik only in the temperature range 1.4K - 170 K [6]. This compound orders antiferromagnetically with T_N=4 K. It was shown that the magnetic susceptibility obeys a Curie-Weiss law in the temperature range 50 - 170 K with the paramagnetic Curie-Weiss temperature θ=-186 K and an effective magnetic moment per Mn atom μ_{ef}=2.6 μ_B, considering that all six Mn atoms in the unit formula contribute with the same value to the total magnetic moment.

RESULTS AND DISCUSSION

The aim of this paper is to study the magnetic state of Mn atoms in $LaMn_6Al_6$ from different crystallographic sites in a large temperature range and through a comparative study to determine the valence state of Ce ions in $CeMn_6Al_6$. The samples $LaMn_6Al_6$ and $CeMn_6Al_6$ were prepared by argon arc melting. The purity of the starting materials was 99.99% for Al and 99,9% for La, Ce and Mn. X-Ray powder diffraction measurements showed that both compounds formed the hexagonal Th_2Zn_{17} structure. No extra lines in the X-Ray diagrams were observed. The lattice parameters agree with those reported in [5]. The unit cell of Th_2Zn_{17} structure contains three formula units. The Th atoms occupy the position 6c and the Zn atoms are distribute over four crystallographic sites, namely 6c, 9d, 18f and 18h (in the Wyckoff notation with the corresponding multiplicity). This structure type can accommodate four formula units of $LaMn_6Al_6$ and $CeMn_6Al_6$, five atomic positions remaining unoccupied. In order to identify the positions of atoms in the unit cell we took into account the data for $CeMn_7Al_{10}$ [7] which crystallizes also in the Th_2Zn_{17} structure type and that the metallic radius of Mn is smaller than that of Al. The best fitting of

the observed and calculated relative intensities of the lines in the X-Ray diagrams was obtained for the following distribution of the atoms in unit cell: the 6c sites are occupied by La(Ce) and Al atoms, the Mn and the remaining Al atoms are distributed at random over the 9d, 18f and 18h sites, the number of Mn atoms in these sites being 6,6 and 12 respectively.

The magnetic susceptibility of these compounds was measured between 100 K and 800K by a Weiss-Forrer magnetic balance with the sensitivity of 10^{-8} emu/g. The temperature dependence of the reciprocal susceptibilities of $LaMn_6Al_6$ and $CeMn_6Al_6$ is shown in figure 1.

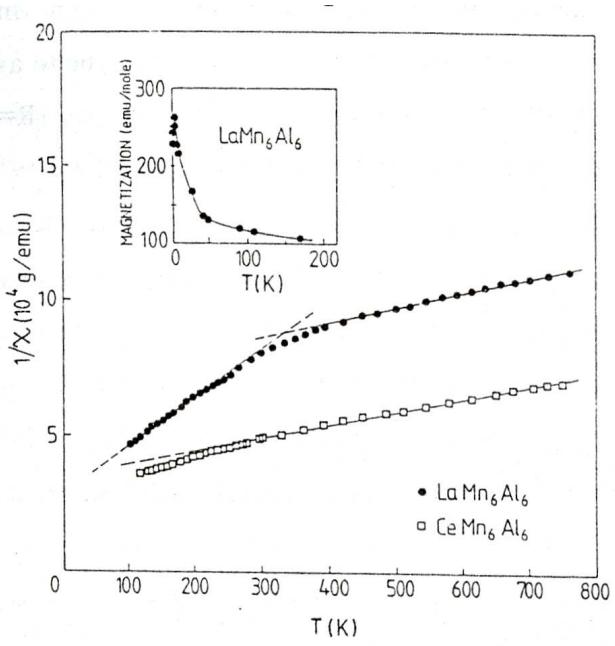

Fig. 1. Thermal variation of the reciprocal susceptibility for $LaMn_6Al_6$ and $CeMn_6Al_6$.

The inset of figure 1 shows the magnetization versus temperature for $LaMn_6Al_6$ measured by Felner and Nowik in a magnetic field of 5 KOe [6]. The $1/\chi(T)$ curve for $LaMn_6Al_6$ presents two linear portions in the temperature ranges of 100K - 280K and 440K - 800K and between these two intervals the slope of the curve changes monotonously. The magnetic susceptibility in these two ranges of temperature fit a Curie-Weiss law modified by a temperature indepedent part χ_0, according to $\chi=C/(T-\theta) + \chi_0$. The values of the Curie constants and the

paramagnetic Curie-Weiss temperatures are C_l=3.82 emu/mol.K and θ_1=-160 K in the low temperature region and C_h=10.98 emu/mol.K and θ_h=-1208 K in the high temperature region. For the effective magnetic moment per Mn atom in the high temperature range results the value $\mu_{Mn}=3.83\mu_B$ which is very close to the Mn^{4+} ion value ($3.87\mu_B$). Approximately the same value of the magnetic moment ($3.92\mu_B$) one obtains in the low temperature region if we consider that only two Mn atoms per unit formula carry a magnetic moment. The results show that the magnetic character of four Mn atoms per unit formula (sixteen Mn atoms in the unit cell) in $LaMn_6Al_6$ changes from an itinerant electron type to a local moment type with increasing temperature. In $LaMn_6Al_6$, as in RMn_6Al_6 (R=Y, Gd, Er) of $ThMn_{12}$ structure type, there are crystallographic sites occupied by Mn atoms for which the Mn-Mn distance $d \leq 2.61$ Å The Mn atoms from these sites have no magnetic moment at low temperatures. The remaining Mn atoms retain their magnetic moments because the Mn-Mn distances are greather than this critical value. These atoms are the six atoms from 18f sites and two Mn atoms from 9d and 18f sites for which the condition for the nearest neighbors $d \leq 2.61$ Å is not fulfilled. The Al atoms from 9d and 18h sites cut the 3d-3d bonds between Mn atoms causing the local 3d band width to become narrower. The antiferromagnetic order at very low temperatures is due only to these Mn atoms (two per unit formula) which retain their magnetic moment at low temperature. The contribution χ_{dh} in the measured susceptibility of the other four Mn atoms per unit formula from 9d and 18h sites may be understood in terms of the SCR theory of spin fluctuations [8]. The temperature dependence of χ_{dh} is the result of the increase of local moments with increasing temperature. The average amplitude $\langle S^2_L \rangle$ of thermally excited longitudinal spin fluctuations saturates at a certain temperature T*, above which the susceptibility is governed by local moment type fluctuations. In $LaMn_6Al_6$ this saturation temperature has the value T*=440 K, where the $1/\chi(T)$ curve deviates from linearity.

The magnetic susceptibility of $CeMn_6Al_6$ exhibits a Curie-Weiss behavior only for T>300 K (Fig.1). The Curie constant and the Curie-Weiss temperature are determined to be C=11.82 emu/mol.K and θ=-716 K, respectively. These values are greater than those obtained for $LaMn_6Al_6$ in the high temperature range. These differences are due to the magnetic moment of Ce ions μ_{Ce}=2.57 μ_B obtained from the relation $C=C_{Mn}+C_h$, considering that μ_{Mn} has the same value as in $LaMn_6Al_6$. Because the μ_{Ce} is close to the free μ^{3+}_{Ce} ion value (2.54 μ_B), the Ce ion of this compound above 300 K is in a trivalent state. Below 300 K, the $1/\chi(T)$ curve has an irregular form what suggests a change in the magnetic state of Ce ions. The contribution of Ce ions in the measured susceptibility for T<300 K has been determined from the difference $\chi_{Ce} = \chi(CeMn_6Al_6) - \chi(LaMn_6Al_6)$. The $\chi_{Ce}(T)$ curve shows a maximum around $T_{max} \approx 200$ K characteristic for the intermediate valence state of Ce ions, and at lower temperature decreases monotonously with lowering temperature. The thermal variation of the Ce susceptibility in $CeMn_6Al_6$ results from a progressive change from a Ce^{4+} state at very low temperature to an intermediate valence state at room temperature, arising through thermal excitation to the 3+ magnetic state.

REFERENCES

1. H.Wada, H. Nakamura, K. Yoshimura, M. Shiga, Y. Nakamura, *J. Magn. Magn. Mater*.70,134 (1987).
2. M. Coldea, R. Coldea, Gh. Borodi, *IEEE Trans.Magnet*.,30,855 (1994).
3. R. Coldea, M. Coldea, I. Pop, *IEEE Trans.Magnet*., 30,852 (1994).
4. R. Coldea, A. Mihuß, M. Coldea, I. Burda, *Phys.Stat.Sol*.(a)(to be published).
5. I. Felner, J. Less.-*Common Metals* 72,241 (1980).
6. I. Felner, Nowik, J.Phys.*Chem.Solids* 43,463 (1982).
7. P. Villars, L. D. Calvert, in: *Pearson's Handbook of Crystallographic Data for Intermetallic Phases, 2nd ed.*, vol.1 (ASM International, Materials Park, Ohio, 1991) p. 711.
8. T. Moriya, J. Magn. *Magn. Mater.* 14,1 (1979).

EPR OF Fe^{3+} IONS IN $70TeO_2$ $25B_2O_3$ 5PbO GLASSES

M. PETEANU[1], I. ARDELEAN[1], V. SIMON[1], S. FILIP[2], G. GYÖRFFY[1]

ABSTRACT. The structural investigation of $70TeO_2 \cdot 25B_2O_3 \cdot 5PbO$ vitreous matrix was performed by means of iron ions paramagnetic resonance. The ions distribution in several structural aggregates was tested over a wide range of concentration. Their valence state was also determined.

INTRODUCTION. Paramagnetic ions are often used as probes in exploring the structure of new vitreous systems, by means of their EPR absorption spectra [1-3]. For the $3d^5$ paramagnetic ions these spectra generally consist in absorption centred at $g_{eff} \cong 4.3$ and $g_{eff} \cong 2.0$ values [1-3].

The $g_{eff} \cong 4.3$ resonance is attributed to isolate ions subjected to strong crystal field effects, acting as principal interaction in the spin Hamiltonian. The theory of the $g \cong 4.3$ absorption was detailed for a variety of distorted vicinities [4-7] options for the most convenient case being available according to the structural peculiarities of the investigated system. Because the intensity of the $g \cong 4.3$ absorption increases when temperature lowers, this cannot be assigned to transitions inside the median Kramers doublet as in the case of the rhombic field model [4], and it seems appropriate to consider the tetragonal distorted field case, resulting in transitions having an isotropic $g = 4.28$ value inside the lowest Kramers doublet [8, 9].

[1] "Babeş-Bolyai" University, Faculty of Physics, 3400 Cluj-Napoca, Romania.
[2] University of Oradea, Department of Physics, 3700, Oradea, Romania.

The $g_{eff} \cong 2.0$ resonance is commonly attributed either to isolated paramagnetic centres of octahedral (tetrahedral) symmetry or to exchange-coupled pairs [10]. Tellurite systems become even more studied because of their interesting properties having numerous applications as semiconductors in microelectronics, etc. The vitreous state formation in binary tellurite systems containing transition metal oxides properties having numerous applications as semiconductors in microelectronics, etc. was investigated in detail [11]. Tellurite systems containing Fe_2O_3 were studied for revealing their electrical properties as well as the structural ones [12, 13]. For obtaining more information concerning tellurite systems we studied the $70TeO_2 \cdot 25B_2O_3 \cdot 5PbO$ vitreous matrix containing Fe_2O_3 by means of electron paramagnetic resonance.

EXPERIMENTAL

The $xFe_2O_3 \cdot (1-x)[70TeO_2 \cdot 25B_2O_3 \cdot 5PbO]$ glass system was studied by means of the EPR spectrometry.

Samples were prepared by mixing the chemical pure reagents TeO_2, H_3BO_3, PbO, and Fe_2O_3 in suitable proportions and melting these oxide mixtures for 6 minutes, in sintered corundum crucibles, at 1250^oC. The melts were poured on a stainless steel plate, at room temperature. Typical glasses were obtained. Their structure was checked by means of X-rays diffraction analysis. Up to x = 20 mol % Fe_2O_3 no crystalline phase was evidenced. The EPR investigations were performed at room temperature by using a JEOL-type spectrometer, operating in the X frequency band (9.46 GHz).

RESULTS AND DISCUSSIONS

Glasses of the system $xFe_2O_3(1-x)[70TeO_2 \cdot 25B_2O_3 \cdot 5PbO]$ were investigated by means of EPR for x varying in the range $0.3 \leq x \leq 20$ mol%. The features of the recorded spectra are detailed in Fig. 1.

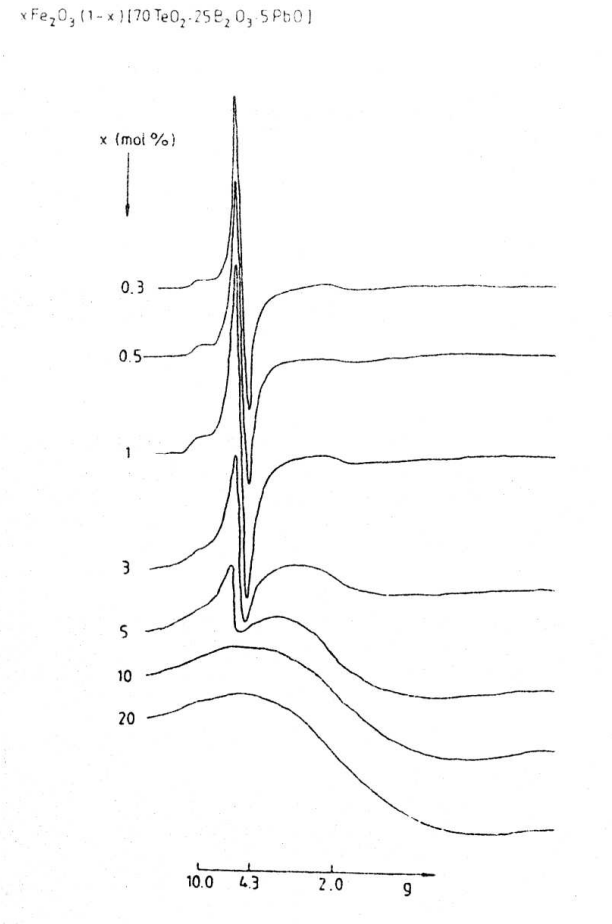

Fig.1. EPR absorption spectra due to Fe^{3+} ions in glasses of the system $70TeO_2{\cdot}25B_2O_3{\cdot}5PbO$.

EPR absorption are due to Fe^{3+} ($3d^5$; $^6S_{5/2}$) ions entering the matrix as paramagnetic species. According to Fig.1 there is a strong dependence of the absorption spectra structure, and the values of the EPR parameters, on the Fe_2O_3 content of the sample. Mainly, the structure of the spectra consists in absorption centred at $g \cong 4.3$ and $g \cong 2.0$ their prevalence depending on concentration. At low Fe^{3+} content resonance's centred at $g \cong 4.3$ prevail in the spectrum. As shown in Fig. 1 their intensity rises on a short concentration range, then suddenly decreases, becoming favoured the absorption at $g \cong 2.0$. This evolution may be easier followed by considering the concentration dependence on the EPR parameters, i.e. the line-height I, the line-width ΔH, and the intensity of the

absorption line approximated as $J = I \cdot (\Delta H)^2$. The concentration dependence of these parameters is plotted in Fig. 2 and 3 for the absorption centred at $g \cong 4.3$ and $g \cong 2.0$ respectively.

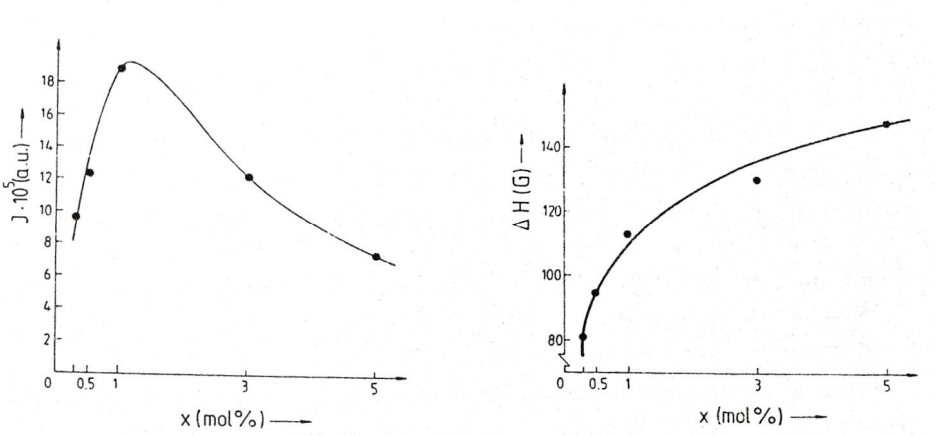

Fig. 2. Line-intensity (a) and line-width (b) dependence on the Fe_2O_3 content of the sample, corresponding to absorption at $g \cong 4.3$.

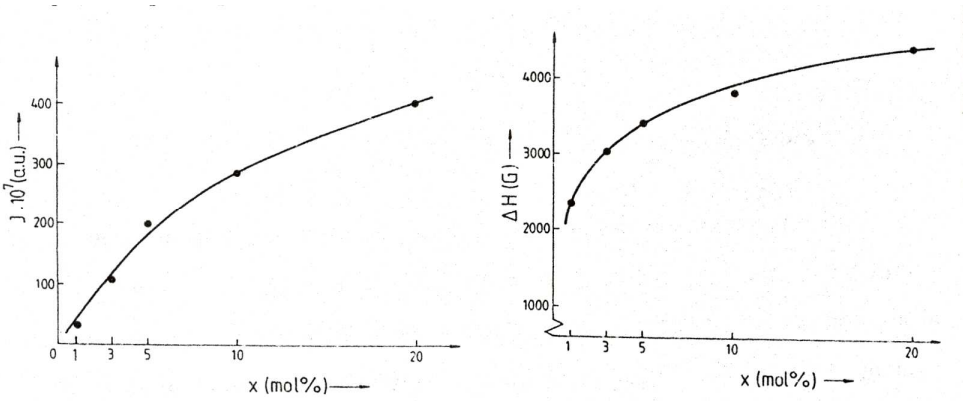

Fig.3. Line-intensity (a) and line-width (b) dependence on the Fe_2O_3 content of the sample, corresponding to absorption at $g \cong 4.3$.

In contrast to the $g \cong 4.3$ resonance's whose intensity increases on an extremely short concentration range ($0.3 \leq x \leq 1$ mol %), abruptly decreasing, and disappearing for $x > 5$ mol % Fe_2O_3, the $g \cong 2.0$ absorption are detectable only for $x \geq 1$ mol % Fe_2O_3 and their intensity increases along the investigated

concentration range (1≤x≤20 mol %). The increasing of the g ≅ 2.0 absorption is in prejudice of those centred at g ≅ 4.3 values.

The g ≅ 4.3 resonance's removal during the impurifying process is mainly due to destroying of the neighbours configuration in the iron ions vicinity. Although randomly distorted these vicinities are similar to each other having at the origin the same crystalline structure of oxides involved in preparing the vitreous matrix, and the same ability of Fe^{3+} in ordering the surrounding. These structural units are the microagregates which assure the independence of the paramagnetic ions and their specificity of "isolated" ones. The gradual increasing of the paramagnetic ions density destroys the microstructural ordering in their neighbourhood and this structural units as characteristic entities become less represented.

This restricted capacity of the matrix in accepting Fe^{3+} ions in structural units of well defined configuration and symmetry is typical for tellurite glasses due to the particularities of their structure [14, 15]. During the impurifying process the Fe^{3+} ions substitute for Te^{2+}. The microvicinity of the ion is a distorted tetrahedron in the form of a roughly planar complex, the symmetry being low enough for justifying the g ≅ 4.3 absorption.

The composition dependence of the g ≅ 2.0 absorption intensity shows an increasing which do not follows linearly the Fe_2O_3 content (Fig.3). There is a step during the impurifying process, at about 5 mol % Fe_2O_3 for the studied glasses, over which, besides Fe^{3+} iron enters the matrix as Fe^{2+} species too. Fe^{2+} ions are not involved in the EPR absorption but their interactions with Fe^{3+} influence the characteristics of the absorption lines.

According to Fig. 2 the line-width of the g ≅ 4.3 resonance's increases along the investigated concentration range, but the initial slope corresponding to the dipolar broadening at low paramagnetic ions content (0.3≤x≤1 mol %) is

changed at higher concentrations. The narrowing of the line becomes more important after x ≅ 1 mol % Fe_2O_3, where, according to the line-intensity dependence, this begins to decrease. The line-width decreasing may reflect the diminishing in number of partners involved in dipole-dipole interactions. A linear dependence at low concentrations show a random distribution of Fe^{3+} ions in the vitreous matrix [16]. When the site population deviates from randomness at higher iron concentrations, the ions may interact through superexchange-type mechanisms. Their strength is weak enough for favouring macroscopic magnetic ordering, so the sample remains essentially paramagnetic. The superexchange interactions of the nearest neighbours, even closer to each other when the Fe_2O_3 content increases, act as narrowing mechanism of the absorption line. This narrowing process is balanced by another broadening processes which now may intervene, due to the structural units disordering. Some of the low symmetry centres no more contribute to the isotropic resonance's at g ≅ 4.3 and their EPR signal is smeared out due to both its anisotropy and the distribution of parameters.

The line-width evolution of the g ≅ 2.0 resonance's in Fig. 3 may be explained having in view the clustered structure of iron giving rise to these absorption. There are superexchange mechanisms narrowing the absorption line balanced after a certain doping degree by broadening mechanisms due to interactions between Fe^{3+} ions and the Fe^{2+} ones.

CONCLUSIONS

EPR absorption due to Fe^{3+} ions were detected in $xFe_2O_3 \cdot (1)[70TeO_2 \cdot 25B_2O_3 \cdot 5PbO]$ glasses over the $0.3 \leq x \leq 20$ mol % concentration range. The structure of the spectra and the values of the EPR parameters depend on glass composition.

At small Fe^{3+} ions content resonance's centred at $g \cong 4.3$ prevail in the spectrum. They are due to isolated Fe^{3+} ions in sites of tetragonally distorted octahedral symmetry. Their number increases in the $0.3 \leq x \leq 1$ mol % range, then abruptly decreases.

Over 1 mol % Fe_2O_3 the ions interact strong enough to be incorporated gradually in a cluster structure. The corresponding EPR absorption are centred at $g \cong 2.0$. The investigated matrix is characterised by a very pronounced tendency of clustering the impurities.

REFERENCES

1. E. B u r z o and I. A r d e l e a n, *Phys. Stat. Sol*. (b) 87, K137 (1978).
2. I. A r d e l e a n , O. C o z a r , G h. I l o n c a, V. S i m o n and S. F i l i p, *Rom. Rep. Phy*s. 46, 235 (1994).
3. A. S. R a o, R. R. R e d d y, T. V. R. R a o, J. L. R a o, *Solid State Commun*. 96, 701 (1995).
4. T. C a s t n e r, G. S. N e w e l l, W. C. H o l t o n, C. P. S l i c h t e r, *J. Chem. Phys*. 32, 668 (1960).
5. D. L o v e r i d g e, S. P a r k e, *Phys. Chem. Glasses* 9, 73 (1968).
6. V. C h e p e l e v a, *Dokl. Akad. Nauk SSSR* 202, 1042 (1972).
7. M. P e t e a n u, A l. N i c u l a, *Studii ¿i Cercet. de Fizic¾* 33 (1), 29 (1981); *ibid*. 34 (1), 15 (1982).
8. A l. N i c u l a, M. P e t e a n u, Studia Univ. Babe¿-Bolyai, *Physica 1*, 42 (1976).
9. V. C e r n y, B. P e t r o v a, M. F r u m a r, *J. Non-Cryst. Solids* 125, 17 (1990).
10. D. L. G r i s c o m, *J. Non-Cryst. Solids* 40, 211 (1980).
11. V. S. K o z h o u k h a r o v, M. P. M a r i n o v, G. G r i g o r o v a, *J. Non-Cryst. Solids* 28, 429 (1978).

12. V. S. K o z h o u k h a r o v, M. P. M a r i n o v, *Compt. rend. Acad. bulg*. Sci 26 (3), 343 (1973).
13. M. P e t e a n u, I. A r d e l e a n, Studia Univ. Babe¿-Bolyai, *Physica 2*, 79 (1990).
14. G. S p e r l i c h, P. U r b a n, *Phys. Stat. Sol*. (b) 61, 475 (1974).
15. E. J. F r i e b e l e, N. C. K o o n, L. K. W i l s o n, D. L. K i n s e r, *J. Amer. Ceram. Soc*. 57, 237 (1974).
16. C. K i t t e l, E. A b r a h a m s, *Phys. Rev*. 90, 238 (1963).

EPR AND MAGNETIC SUSCEPTIBILITY STUDIES OF Cu2+ IONS IN Bi2O3· PbO GLASSES

S. FILIP[1], O. COZAR[2], V. SIMON[2], I. ARDELEAN[2]

ABSTRACT. Results of EPR and magnetic measurements performed on xCuO·(1-x)[Bi2O3·PbO] glasses with $0<x\leq 50$ mol % are reported. EPR data suggest a hexacoordinated geometry of the tetragonal-distorted octahedral symmetry for Cu2+ ions. The modification of EPR spectra with the increasing CuO content are explained by the contribution of two kinds of copper ions: isolated and clustered ions.

The magnetic susceptibility studies show that the investigated x CuO·(1-x)[Bi2O3·PbO] glasses follow a Curie type behavior, the Cu2+ ions, which represent approximately half of the Cu ions ($N_{Cu^{2+}}/N_{Cu^{2+}+Cu^{+}}\cong 0.5\div 0.6$) are magnetically isolated, do not form crystalline precipitates and seem to be randomly distributed in the Bi2O3·PbO matrix up to 50 mol% CuO.

INTRODUCTION

Electron paramagnetic resonance (EPR) studies of Cu2+ ions in oxide glasses have received a considerable attention, the EPR parameters being sensitive to the local symmetry, the character of the chemical bounds as well as to other structural factors [1-4]. In these papers the concentration effects of some network-former (B2O3, SiO2, P2O5) and network-modifier (Na2O, Cs2O, ZnO, PbO) oxides on the spin-Hamiltonian parameters and ligant field absorption energies have been studied.

Unlike the papers mentioned above, we have investigated the valence states and distribution mode of copper ions, using EPR and magnetic studies.

[1] Department of Physics, University of Oradea, 3700, Romania.
[2] ·Faculty of Physics, Babeş-Bolyai University, 3400 Cluj-Napoca, Romania.

Thus, in 19TeO2·PbO [5] and 2B2O3·K2O [6] glass matrices, the copper ions are in bivalent states, while in 2B2O3·PbO [7], 2B2O3·Li2O [8] and 70TeO2·25B2O3·5PbO [9] glass matrices, both Cu+ and Cu2+ valence states were evidenced. In past few years the glass systems based on heavy metal oxides (bismuth and/or lead) are investigated [10]. They are characterized by high density, high refractive index, high thermal expansion, low transformation temperature and excellent infrared transmission. Since network bound strengths of heavy metal oxide glasses are relatively weak compared to those of silicate and borate glasses, the glass-forming regions are comparatively limited [10-11].

Although Bi2O3 and PbO are not traditional glass formers, they can behave as main glass former in the systems based on the Bi2O3·PbO matrix, because Pb2+ and Bi3+ ions are highly polarizable and the asymmetry of their polyhedra inhibits the crystallization processes in the melts in which they participate. Nakamura et al. [12] have investigated the amorphous ferrites in the Bi2O3-CaO-Fe2O3 system and also the magnetic properties of the rapidly quenched Bi2O3-Li2O-Fe2O3 and Bi2O3-CuO-Fe2O3 [13] systems. Dimitriev and Mihailova [14] have investigated the glass formation in the binary systems Bi2O3-CuO, Bi2O3-MnO and Bi2O3-TiO2. Ardelean et al. [8,15,16] have investigated the glass formation and magnetic properties of xMO·(1-x)[Bi2O3·PbO] glasses with M=Fe, Mn or Cr.

In this paper we report EPR and magnetic susceptibility studies of xCuO·(1-x)[Bi2O3·PbO] glasses with $0<x\leq 50$ mol %, in order to obtain further information on the distribution and the valence states of copper ions in oxide glasses.

EXPERIMENTAL

The starting materials used in the present study were reagent grade purity CuO, Bi2O3 and PbO. The samples were prepared by mixing of these chemicals in suitable proportion and melting these admixtures in sintered corundum

crucibles at 1250°C for 10 minutes. The melts were poured on stainless steel plates. The X-ray patterns were characteristic for vitreous system. No crystalline phases were evidenced up to 50 mol % CuO. The magnetic data were obtained using a Faraday-type balance in the temperature range 80-300 K.

The EPR measurements were realized at room temperature, in X-band (9,4 GHz) and 100 KHz field modulation, with a JEOL-type equipment.

RESULTS AND DISCUSSION

a) EPR studies

EPR spectra of Cu2+ ions in glasses with x≤1 mol % consist of a single broad asymmetrical line, without hyperfine structure (Fig. 1a). The characteristic g values are $g_{\|}$ = 2.22 and $g_{\perp}$ =2.05.

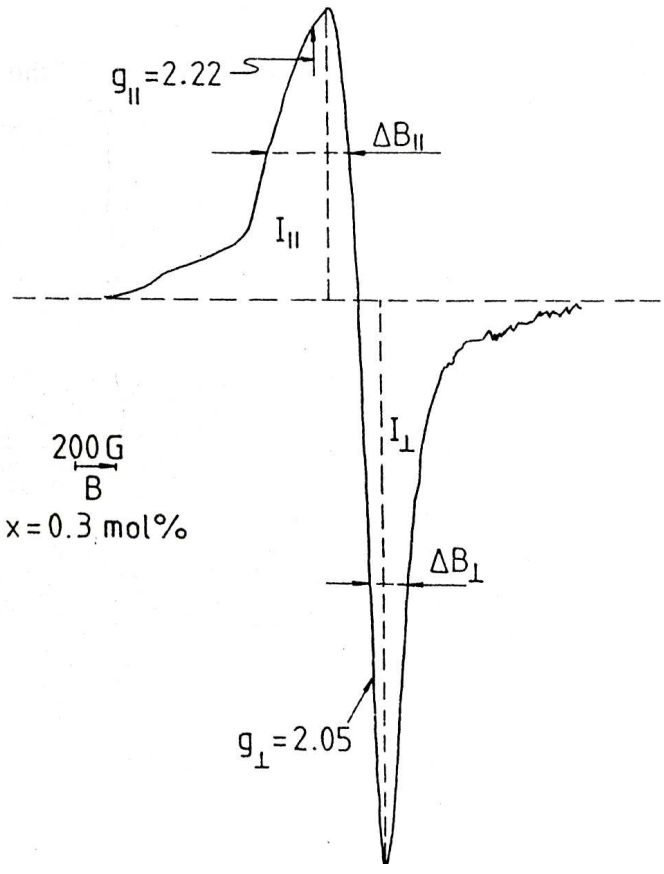

Fig.1a. EPR spectrum of Cu^{2+} ions for xCuO(1-x)[Bi_2O_3 PbO] glass with x=0.003.

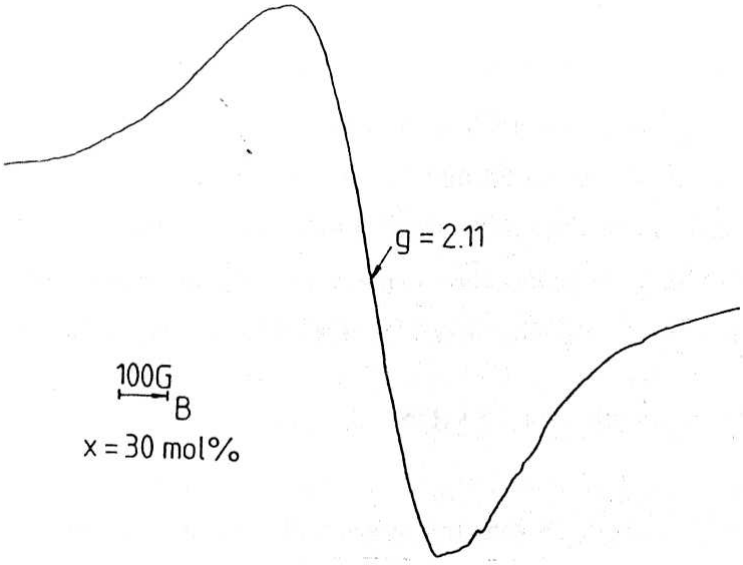

Fig.1b. EPR spectrum of Cu^{2+} ions for xCuO(1-x)[Bi_2O_3 PbO] glasses with x=0.3.

EPR spectra become symmetrical with the increasing of the CuO content, due to the contribution of clustered ions characterized by a broad symmetrical line at g ≅ 2.1 (Fig 1b).

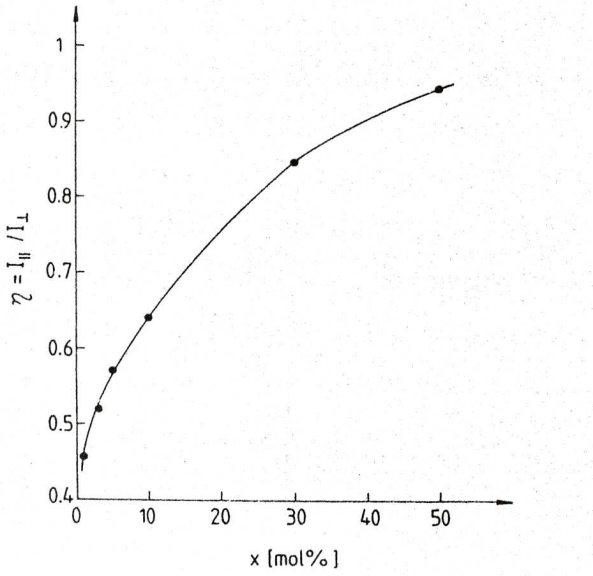

Fig. 2. The composition dependence of the EPR lineshape asymmetry (η).

The coupling between these ions is realized by dipole-dipole interaction. By defining the asymmetry parameter (η) as the heights of the $g_{\|}$ and $g_{\perp}$ absorption (Fig. 1b), an increase of the η values with the increasing of the CuO content is observed (Fig. 2). This fact may be explained by the increasing of the number of clustered Cu2+ ions with CuO content. These spectra suggest a hexacoordinated geometry of the octahedral (Oh) symmetry with a small tetragonal (↓axial) distortion for Cu2+ ions. This type of symmetry occurs by an elongation of the Cu-O bonds along the Oz axis.

The increasing of the ratio between the number of the clustered and isolated ions with an increase in x values is also suggested by the modifications of the linewidths of the parallel ($\Delta B_{\|}$) and perpendicular ($\Delta B_{\perp}$) absorptions (Fig.3). It is observed that the $\Delta B_{\perp}$ values increase with CuO content due to the contribution of clustered ions. The $\Delta B_{\|}$ values increase for x≥30 mol % due to the contribution of the broad line associated to the clustered ions.

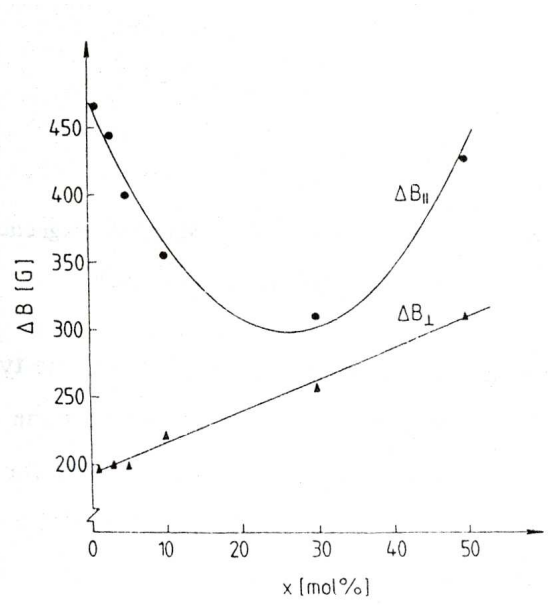

Fig. 3. Perpendicular (ΔB⊥) and parallel ($\Delta B_{\|}$) absorption linewidth vs. CuO content.

b.) Magnetic susceptibility studies

The interactions between the Cu2+ ions and their influence on the magnetic properties of xCuO·(1-x)[Bi2O3·PbO] glasses as a function of the copper concentration were studied using magnetic susceptibility measurements. The temperature dependence of the reciprocal magnetic susceptibility of various CuO-Bi2O3-PbO glasses is presented in Fig. 4.

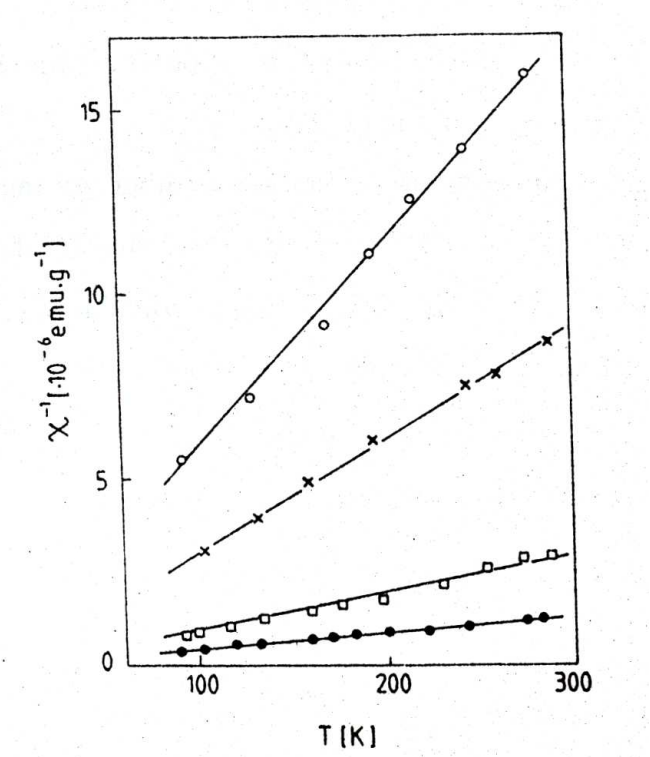

Fig. 4. The temperature dependence of the reciprocal magnetic susceptibility of CuO·Bi_2O_3·PbO glasses: (o) 5, (x) 10, (□) 30 and (•) 50 mol% CuO.

The reciprocal magnetic susceptibility follows a Curie-type behavior for these glasses up to 50 mol % CuO. These results suggest the copper ions are magnetically isolated. In this way the copper ions present the same magnetic behavior as vanadium [17], cobalt [18] and nickel [19] ions in lead-borate glasses, but it differs from that of copper ions in 19TeO2·PbO [5], 2B2O3·K2O [6], 2B2O3·PbO [7], 2B2O3·Li2O [8] and 70TeO2·25B2O3·5PbO [9] glasses.

To determine accurately the values of the Curie constants, corrections due to the diamagnetism of the glass matrix and CuO were taken into account. The molar values of the Curie constant (CM) are presented in Table 1. The experimental values of the Curie constants and consequently atomic magnetic moments of copper ions for the studied glasses were lower than those corresponding to CuO, considering that all copper ions are in the Cu2+ valence state. We therefore suppose that in these glasses both Cu2+ and Cu+ ions are present, the latter being diamagnetic. The resence of Cu2+ ions and the increase of their number with cooper oxide content was evidenced by EPR measurement.

Table 1. Curie constants, molar fractions of the copper ions in Cu^{2+} valence state and y/x ratios.

CuO content x (mol%)	CM (e.m.u.·mol-1)	Cu2+O content y (mol%)	y/x
5	**0.01165**	**3.1**	**0.62**
10	**0.02026**	**5.4**	**0.54**
30	**0.05616**	**15**	**0.50**
50	**0.09609**	**26**	**0.52**

Thus, in the melts of these glasses the Cu2+ ions can be induced according to:

$$Cu^{2+}+e^{-}\rightarrow Cu^{+}. \qquad (1)$$

In this case, bearing in mind that the atomic magnetic moment of free Cu2+ ions is $\mu_{Cu^{2+}} = 1.73\mu_B$ ($1\mu_B \cong 9.274\times10^{-24} J\bullet T^{-1}$) that was usually observed in paramagnetic salts [20], we estimated the molar fraction (denoted by y in Table 1) of the copper ions which are in the Cu2+ valence state, using relation:

$$\mu_{Cu^{2+}} = 2.83(C_M/y)^{1/2} \quad , \quad y = 2.83^2 C_M / \mu^2_{Cu^{2+}} \ . \qquad (2)$$

From these data we also estimated the $N_{Cu^{2+}}/N_{Cu^{2+}+Cu^{+}} = y/x$ ratios for the investigated glasses.

This ratio takes values of approximately 0.5-0.6 (Table 1) and indicates that more than half of the copper ions pass in the Cu2+ valence state.

The Curie constant, which is proportional to the magnetic ion concentration and the square of the atomic magnetic moment, must vary linearly with the Cu2+ ion concentration. In Figure 5 we present the Cu2+ ion concentration dependence of the molar Curie constant. This dependence suggests that the molar fractions of Cu2+ ions has been correctly estimated.

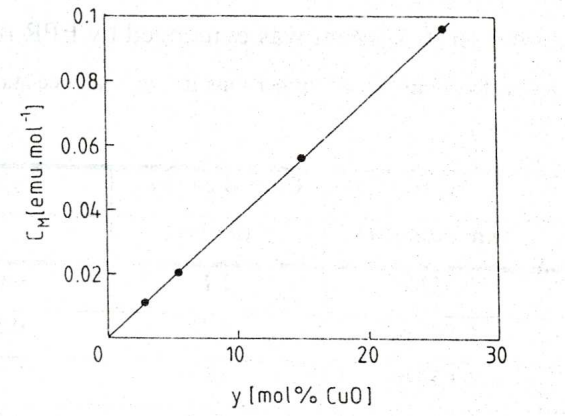

Fig.5. The composition dependence of the molar Curie constant on the $Cu^{2+}O$ concentration in $CuO{\cdot}Bi_2O_3{\cdot}PbO$ glasses.

CONCLUSIONS

In the xCuO·(1-x)[Bi2O3·PbO] system homogenous glæsses are formed up to 50 mol%. The EPR data suggest for Cu2+ ions a hexacoordinated geometry of the tetragonal-distorted octahedral symmetry.

EPR and magnetic susceptibility data indicate that the Cu2+ ions are present as magnetically isolated species. They manifest the dipole-dipole interactions with increase of the CuO content.

The Curie constant values allow to established that in these glasses both Cu+ and Cu2+ ions are present, Cu2+ representing about 50-60 % of the cooper ions in all investigated samples.

REFERENCES

1. H. Imagawa, *Phys. Status Solidi*, 30, 469 (1968).
2. L. D. Bogomolova, T. F. Dolgolenko, V. A. Jachkin, V. N. Lazukin, *J. Mag. Res.*, 15, 283 (1973).
3. H. Hosono, H. Kawazoe, T. Kavazawa, *J. Non-Cryst. Solids*, 34, 339 (1979).
4. O. Cozar, I. Ardelean, *J. Non-Cryst. Solids*, 92, 278 (1987).
5. I. Ardelean, Gh. Ilonca, M. Peteanu, *J. Non-Cryst. Solids*, 92, 278 (1987).
6. I. Ardelean, M. Coldea, O. Cozar, *Nucl. Instrum. and Methods*, 199, 189 (1982).
7. I. Ardelean, Gh. Ilonca, O. Cozar, I. Chicinas, Gh. Ciologria, *Solid State Commun*., 43, 707 (1982).
8. I. Ardelean, S. Simon, V. Simon, O. Cozar, *J. Mat. Sci. Lett*., 12, 1031 (1993).
9. I. Ardelean,, M. Peteanu, E. Burzo, S. Filip, F. Ciorcas, *Solid State Commun.*, 98, 351 (1996).
10. W. H. Dumbaugh, J. C. Lapp, *J. Am. Ceram. Soc*., 75, 2315 (1992).
11. K. Nassau, D. L. Chadwick, *J. Am. Ceram. Soc*., 65, 486 (1982).
12. S. Nakamura, Y. Hirotsu, N. Ichinose, *Jap. J. Appl. Phys*. 30A, 984 (1991).
13. S. Soeya, S. Nakamura, N. Ichino se, *J. Appl. Phys*., 68, 2875 (1992).
14. Y. B. Dimitriev, V. T. Mihailova, *J. Mat. Sci. Lett*., 9, 125 (1990).
15. I. Ardelean, Gh. Ilonca, O. Cozar, V.Simon, S. Filip, *Mat. Lett*., 21, 321 (1994).
16. I. Ardelean, O. Cozar, V.Simon, S. Filip, *J. Magn. Magn. Mat*. (in press).
17. O. Cozar, I. Ardelean, Gh. Ilonca, *Mater. Chem*., 7, 1345 (1982).
18. I. Ardelean, Gh. Ilonca, D. Barbos, *Solid State Commun*., 39, 1345 (1981).
19. I. Ardelean, Gh. Ilonca, D. Barbos, H. Adams, *Solid State Commun*., 40, 769 (1981).
20. E. Burzo, in "*Fizica fenomenelor magnetice"*, vol. 1, Edit. Academiei, Bucharest, 1979, p.241.

OPTICAL ABSORPTION STUDY ON PHOSPHATE GLASSES CONTAINING URANIUM

V. SIMON[1], I. ARDELEAN[1], D. MANIU[1], V. MIH[1], DANIELA ENIU[2], S. SIMON[1]

ABSTRACT. Two phosphate glass systems containing uranium ions $xUO_3(100-x)[2P_2O_5 \cdot PbO]$ and $xUO_3(100-x)[2P_2O_5 \cdot Na_2O]$, with $0<x\leq20$ mol % were investigated by optical absorption spectroscopy in the wave number range from 13000 to 30000 cm^{-1}. Absorption bands centered at 18400, 20400 and 23100 cm^{-1} are observed in both systems. Absorption bands at 16000 and 22000 cm^{-1} occur only for uranium ions introduced in the lead-phosphate matrix, while the absorption band centered at 15750 cm^{-1} is recorded only from samples of sodium-phosphate matrix. The absorption line intensities denote that the most uranium ions are in U^{4+} valence state, in the entire investigated composition range. The fraction of U^{4+} ions number relative to the other evidenced valence states (U^{3+} and U^{6+}) is higher in the lead-phosphate matrix than in the sodium-phosphate one.

INTRODUCTION

Oxide glasses and vitroceramics are investigated with increasing interest as possible nuclear waste hosts [1-3]. The glass matrices used for storage of radionuclides must be able to incorporate a high content of radioactive nuclides. Particular interest is accorded to uranium wastes [4]. The solubility and stability of the uranium ions in oxide glass matrices also depend on the uranium valence states. The most soluble ions are not the easiest ones to be stabilized in an oxide matrix [5, 6].

[1] "Babeş-Bolyai" University, Faculty of Physics, 3400, Cluj-Napoca, Romania.
[2] University of Medicine and Pharmacy, Faculty of Pharmacy, 3400, Cluj-Napoca, Romania.

In order to establish the valence states of the uranium ions in two phosphate glass matrices we carried out an optical absorption investigation that allow to evidence the U^{4+} ions, considered to be the best stabilized ones among the different states of uranium ions.

EXPERIMENTAL

The investigated samples belong to $xUO_3(100-x)[2P_2O_5 \cdot Na_2O]$ and $xUO_3(100-x)[2P_2O_5 \cdot PbO]$ glass systems, where $0 \leq x \leq 20$ mol %. The samples were prepared by melting UO_3, $(NH_4)_2HPO_4$ and $Na_2CO_3 \cdot 10H_2O$ or PbO powder mixtures at 1250°C for 15 minutes, followed by fast cooling at room temperature on stainless steel plates.

Optical absorption spectra were recorded at room temperature on a Specord UV-VIS spectrometer in the wave number range 13000-30000 cm^{-1} from plate samples of < 1 mm thickness and 5 mm diameter.

RESULTS AND DISCUSSION

All samples containing uranium ions are light green colored. This result indicates the presence in the glasses of U^{4+} ions which confer them the green colour while red colour is typical for U^{3+} ions and yellow colour for U^{6+} ions [5].

The absorption spectra consist of lines disposed around 14950, 15750, 18400, 20400, 23100 cm^{-1} for $xUO_3(100-x)[2P_2O_5 \cdot Na_2O]$ glasses and around 14700, 16000, 18400, 20400, 22000 and 23100 cm^{-1} for $xUO_3(100-x)[2P_2O_5 \cdot PbO]$ glasses. The intensity of these lines are given in tables 1 and 2. No absorption bands were registered for glass matrices (x = 0 % mol).

The absorption lines from 15750 and 22000 cm^{-1} were attributed to U^{3+} ions, those from 14700, 14950, 16000, 18400 and 23100 cm^{-1} to U^{4+} ions and

that from 20400 cm^{-1} both to U^{4+} and U^{6+} ions [5, 7].

Table 1. The intensity (in a.u.) of the lines from the optical absorption spectra of $xUO_3(100-x)[2P_2O_5 \cdot Na_2O]$ glasses.

Wave nr. [cm^{-1}] / x[mol %]	14950	15750	18400	20400	23100
0.1	2.0	1.0	0.5	1.1	1.2
0.5	1.2	0/7	0.3	0.4	0.5
1	2.0	1.8	0.4	0.9	1.2
3	5.7	4.3	1.6	2.7	3.9
5	6.8	5.6	2.1	3.8	6.0
10	10.4	9.7	4.5	6.7	8.4
20	9.0	8.5	4.2	7.4	9.6

Table 2 The intensity (in a.u.) of the lines from the optical absorption spectra of $xUO_3(100-x)[2P_2O_5 \cdot PbO]$ glasses.

Wave number [cm^{-1}] / x [mol %]	14700	16000	18400	20400	22000	23100
0.1	1.0	0.6	0.3	0.6	0.3	—
0.3	2.2	1.3	0.7	1.4	1.0	—
0.5	3.2	2.1	0.9	1.5	0.8	1.1
1	2.5	1.6	0.7	1.1	0.5	0.7
3	11.1	7.0	3.1	4.6	2.0	2.6
5	13.8	13.0	9.3	11.5	7.3	8.8
10	12.0	11.7	9.3	10.8	7.3	8.6
20	12.0	11.7	9.1	10.7	7.3	8.5

The uranium ions generally may appear as U^{2+}, U^{3+}, U^{4+}, U^{5+} and U^{6+}. In oxide glasses [8] their possible valence states are III, IV, V and VI. The valence state IV of the uranium ions is considered to be the best stabilized one [6] in oxide glasses.

The optical absorption lines indicate that a great part of the uranium ions introduced in the investigated phosphate glass matrices were reduced during the preparation process from U^{6+} in UO_3 to lower valence states III and IV. The presence of U^{5+} ions in these glasses is not excluded, but this valence state of

uraniu ions processes no absorbtion bands in the investigated frequency range, and they confer no colour to the oxide glass matrices into which they are introduced [5].

The ions number in different valence states was considered proportional to the intensity of the lines corresponding to that valence state. There fore the total uranium ions number was estimated by I_t obtained from the addition of all line intensities:

$$I_t = \sum_i I_i = I_{III} + I_{IV} + I_{VI}$$

According to this assumption the following ratios were calculated:

$$f_{III} = \frac{I_{III}}{I_t}, \quad f_{IV} = \frac{I_{IV}}{I_t} \quad \text{and} \quad f_{VI} = \frac{I_{VI}}{I_t}$$

as well as

$$m_1 = \frac{I_{IV}}{I_{III}} \quad \text{and} \quad m_2 = \frac{I_{IV}}{I_{VI}}$$

in order to compare the U^{4+} ions share of the other valence states evidenced by UV-VIS optical absorptionís spectroscopy.

All estimations were carried out by relative intensity measurements on the same absorption spectrum, that allowed to avoid the possible errors occurring due to the differences in thickness, face planarity and faces parallelism of the samples. From this reason we did not compare the intensity of corresponding lines arising from different samples.

The composition dependence of the relative intensities obtained as above described is plotted in figure 1 for the sodium-phosphate glass matrix and in figure 2 for the lead-phosphate glass matrix. One remarks a relative constancy of the different valence state fractions for all samples from the two phosphate systems containing more than 5 mol % UO_3. In this case the highest fraction is represented in both matrices by f_{IV}, corresponding to U^{4+} ions, followed by the fraction of U^{3+} ions, f_{III}, and that of U^{6+} ions, f_{VI}.

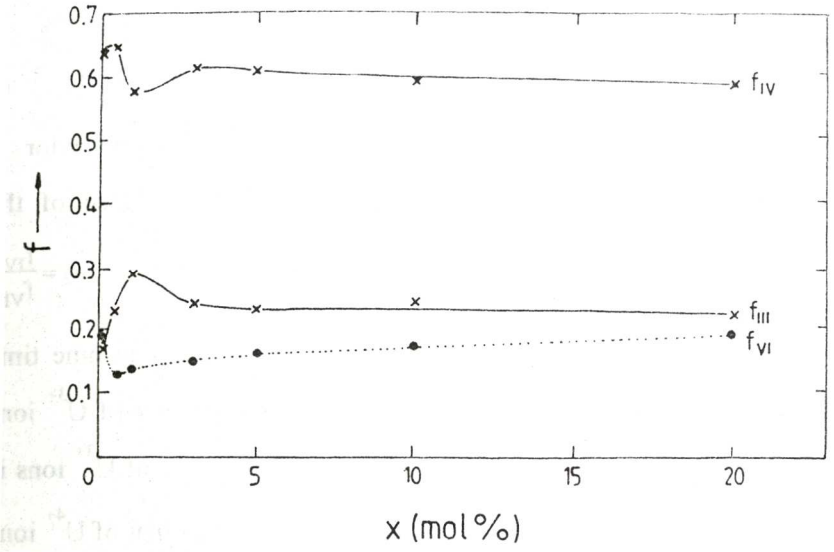

Fig. 1. The composition dependence of different valence states of uranium ions fractions in $xUO_3(100-x)[2P_2O_5 \cdot Na_2O]$ glass system.

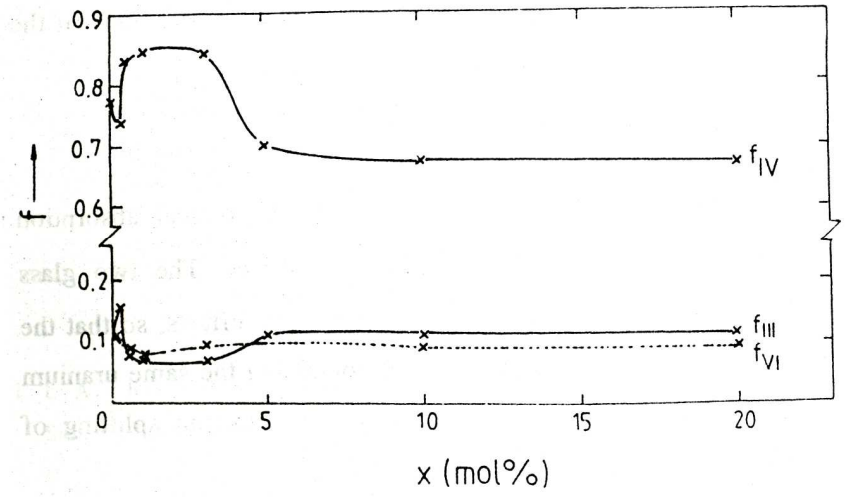

Fig. 2. The composition dependence of different valence states of uranium ions fractions in $xUO_3(100-x)[2P_2O_5 \cdot PbO]$ glass system.

An interesting composition dependence is observed for low UO_3 contents, $0<x\leq5$ % mol. In this composition range the number of U^{4+} ions exhibit a

maximum relative to the other valence states representing 65% in $xUO_3(100-x)[2P_2O_5 \cdot Na_2O]$ for $x \leq 0.5\%$ UO_3 and 85% in $xUO_3(100-x)[2P_2O_5 \cdot PbO]$ for $0.5 < x \leq 3\%$ mol UO_3. The same behavior is observed in figure 3, which illustrates the composition dependence of the multiplicity, m, of U^{4+} ions number relative to U^{3+} $\left(m_1 = \frac{f_{IV}}{f_{III}}\right)$ and U^{6+} $\left(m_2 = \frac{f_{IV}}{f_{VI}}\right)$ ions number. For lead-phosphate glasses the amount of U^{4+} ions is nine time higher than that of U^{6+} ions and seven time higher then the amount of U^{3+} ions for $5 \leq x \leq 20$ mol % UO_3. In sodium-phosphate glasses the number of U^{3+} ions is three times smaller and that of U^{6+} ions is four times smaller than that of U^{4+} ions for $3 \leq x \leq 20$ mol %. The particular behavior regarding the valence states of uranium ions in the low UO_3 content composition range of the phosphate glasses may be assigned to the structural changes induced in the structural units of the phosphate matrix [9, 10].

CONCLUSIONS

The valence states of uranium are reflected in the optical absorption spectra both of P_2O_5-Na_2O and P_2O_5-PbO glass matrices. The two glass matrices differently influence the uranium ions by structural effects, so that the absorption bands are not identical for the samples containing the same uranium content. The origin of these electronic bands is due to electron splitting of uranium ions in particular physical environment.

The position and intensity of the optical absorption lines in the 13000-30000 cm^{-1} wave number range indicate the preponderance of U^{4+} ions relative to U^{3+} and U^{6+} ones, for both investigated glass systems. The fraction of U^{4+} ions number relative to the other evidenced valence states is higher in the lead-phosphate matrix than in the sodium-phosphate one.

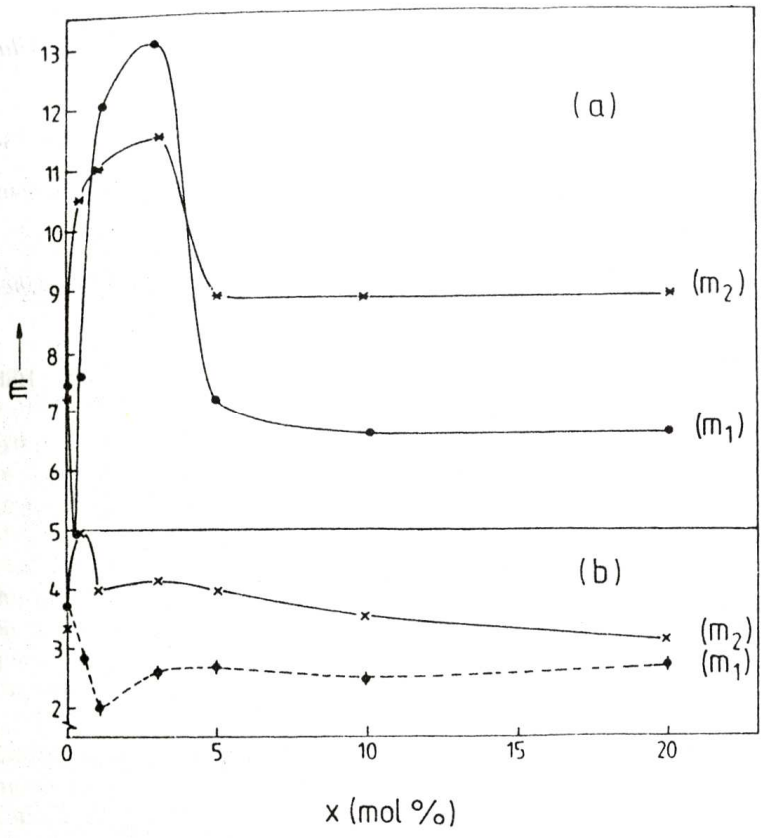

Fig. 3. The composition dependence of U^{4+} ions number multiplicity relative to U^{3+} (m_1) and U^{6+} (m_2) ions number for the lead phosphate (a) and sodium phosphate (b) glass matrix.

REFERENCES

1. L.A.Chik, R.O.Lokken, D.M.Strachan, W.M.Bowen, *J. Am. Ceram.* Soc. 69, 114 (1986).
2. P.J.Hayward, F.E.Doern, E.V.Cecchetto, S.L.Mitchell, *Canadian Mineralogist* 21, 611 (1983).
3. H.D.Schreiber, S.J.Kozak, D.G.Wetmore, C.W.Schreiber, J.S.Downey, *Ceramic Trans.* 3, 581 (1988).
4. P.J.Hayward, *Radioactive Waste Forms for the Future*, eds. W Lutze and R.C.Ewing Elserver Science, 1988, p. 427.
5. H.D.Schreiber and G.B.Balazs, *Phys. Chem. Glasses* 23, 139 (1982).

6. H.D.Schreiber, G.B.Balazs and T.N.Solberg, *Phys. Chem. Glasses* 26, 35 (1985).
7. V.Simon, I.Ardelean, O.Cozar, S.Simon, *J. Mat. Sci. Lett.* 15, 734 (1996).
8. H.D.Schreiber, *Advances in Materials Characterization*, eds. D.R. Rossington, R.A. Condrate, L.R. Snyder, Plenum, New York, 1983, p.647.
9. Y.Kowoda, H.Adacki, M.Tatsumisagi, T.Minami, *Phys. Chem. Glasses* 34, 10 (1993).
10. T.Iliescu, V.Ardelean, V.Simon, D.Lazar, Studia Univ. Babe¿-Bolyai, *Physica*, 39, 41 (1994).

STRUCTURAL STUDIES OF SOME CU(II) COMPLEXES WITH THIAZOLYLHYDRAZONE

L. DAVID[1], O. COZAR[1], L. ŞUMĂLAN[2], R. TETEAN[1], C. CRĂCIUN[1], N. POP[1]

ABSTRACT. The Cu(II) complexes with 2-N-acetyl-salicyliden-hydrazino-4-chlor-methyl thiazole (L_I) and 2-N-acetyl salicyliden-hydrazino-4-thiazolyl acetic ester (L_{II}) were prepared and investigated by electronic spectroscopy, IR, ESR and magnetic susceptibility measurements. Elementary chemical analysis show the achievement of CuLCl type compounds. IR spectra suggest that Cu(II) ion is coordinated by two nitrogen atoms (from C=N bundles, one out of thiazolic cycle and another from without) and one oxygen atom from phenolic group. The powder ESR spectrum of CuL_ICl is quasiisotropic (g=2.113) at room temperature, while for $CuL_{II}Cl$ is characteristic of monomeric species with axial symmetry (g_{II}=2.234, $g_\perp$=2.073). The isotropic ESR spectra of the CuLCl compounds in DMSO solution suggest the presence of pseudo-tetrahedral monomeric species. The anisotropic spectra were obtained for DMSO CuLCl solutions adsorbed on NaY zeolite. The parallel hyperfine structure shows the coexistence of two magnetic nonequivalent monomeric species.

INTRODUCTION

The copper(II) complexes with organic ligands are of large interest for the possible implications in pharmacology [1,2]. This paper reports the data referring to some new Cu(II)

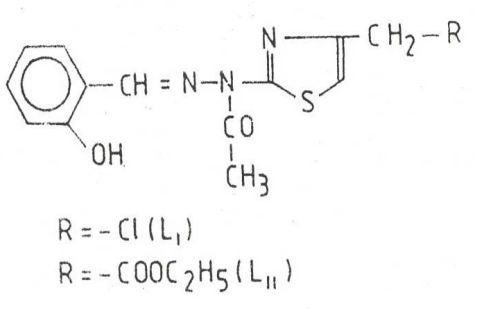

Fig.1. The ligand's structural formulae

[1] University "Babeş-Bolyai", Faculty of Physics, 3400 Cluj-Napoca, Romania.
[2] University of Medicine and Pharmacy, Faculty of Pharmacy, 3400 Cluj-Napoca, Romania.

compounds with 2-N-acetyl-salicyliden-hydrazino-4-chlor-methyl thiazole ($C_{13}H_{12}O_2N_3SCl$) (L_I) and 2-N-acetyl salicyliden-hydrazino-4-thiazolyl acetic ester $C_{16}H_{17}O_4N_3S$) (L_{II}) (Fig. 1). The choice of these ligand is motivated by their different capacity of chelation due the existence of O, N and S donor atoms in theirs molecules and by antiinflammatory and mitodepresion activity which can be increased or decreased by coordination.

In order to obtain further information concerning to the local structure of the metal ion, we have investigated the CuL_ICl and $CuL_{II}Cl$ compounds by electronic spectroscopy, IR, ESR and magnetic susceptibility measurement.

EXPERIMENTAL

The synthesis of Cu(II) compounds was performed by treating under continuous stirring the aqueous solutions of $CuCl_2 \cdot 2H_2O$ (0.1M), with the acetonic solutions (0.1M) of the ligand L_I, respectively L_{II} (0.1M), calculated for a molar rations of 1:1. The obtained dark greenish-brown micro-crystalline precipitates were filtrated, washed with acetone and dried at room temperature. The elementary chemical analysis show that the type of the compounds are CuLCl.

Anal. Calc. for CuL_ICl: Cu, 15.58; C, 38.29; N, 10.31; S, 7.86; H, 2.72; Cl, 17.42. Found: Cu, 14.83; C, 38.86; N, 10.23; S, 7.90; H, 2.51; Cl, 16.9. Calc. for $CuL_{II}Cl$: Cu, 14.27; C, 43.15; N, 9.43; S, 7.20; H, 3.62; Cl, 8.01. Found: Cu, 13.30; C, 43.33; N, 9.45; S, 7.35; H, 3.25; Cl, 7.62.

The electronic spectra in the UV-VIS region were performed with a Perkin-Elmer lambda 15 spectrophotometer. IR measurements were performed with Perkin-Elmer 848 spectrophotometer in the 400-4000 cm^{-1} region by the KBr pellets technique. ESR spectra were obtained at room temperature in the X band (9.4 GHz) using a standard JEOL-JES-3B equipment. The magnetic susceptibility measurements were performed with a Faraday balance.

RESULTS AND DISCUSSION

The most important IR bands for the ligands and their copper complexes are listed in Table 1. The bands assigned to ν(OH) phenolic are lowered by 20 cm^{-1} in the spectra of the metal complexes indicating the involving of the oxygen atom in the metal ion coordination [3]. The ν(C=N) exocyclic vibrations are lowered by 40 cm^{-1} and 10 cm^{-1} in their metal complexes suggesting the coordination of the nitrogen of imine group with the metal ion. The bands assigned to ν(C=N) endocyclic are shifted by 30 cm^{-1} and 10 cm^{-1} respectively in the spectra of the metal complexes. The ν(C=O) ester vibration band appear at 1730 cm^{-1} in the spectra of L_{II} and of their Cu(II) complexes.

The heterocyclic ring vibration appears at $1560^{-1}570$ cm^{-1}. The bands assigned to the ν(Cu-O) vibrations appears at 580 cm^{-1}. At 550 cm^{-1} and 540 cm^{-1} are observed the band characteristic of the ν(Cu-N) vibrations.

Table 1

IR absorption bands (cm^{-1})

COMPOUND	ν(OH)	ν(C=O) amidic	ν(C=N) exocyclic	ν(C=N) endocyclic
L_I	3450	1695	1650	1610
CuL_ICl	3430	1695	1610	1580
L_{II}	3440	1695	1620	1600
$CuL_{II}Cl$	3420	1695	1610	1590

The electronic spectra of the studied Cu(II) complexes show three absorption bands at 13793 cm^{-1}, 18382 cm^{-1}, 23640 cm^{-1} for CuL_ICl and 13458 cm^{-1}, 19047 cm^{-1}, 24752 cm^{-1} for $CuL_{II}Cl$ which could be assigned to $^2B_2 \rightarrow E$, $^2B_2 \rightarrow {}^2B_1$ and a charge transfer transitions, respectively [4].

The values of the magnetic moments 1.64 μ_B (CuL_ICl) and 1.75 μ_B ($CuL_{II}Cl$) obtained from the magnetic susceptibility data and the values of the electronic transitions are in agreement with a tetrahedral distorted geometry around Cu^{2+} ions [5].

The powder ESR spectrum at room temperature of CuL_ICl is quasiisotropic (g=2.113). The shape of the spectrum is not changed when the temperature is lowered at 120 K, this fact suggesting that the complex contains grossly misaligned tetragonal axis [6]. An anisotropic spectrum characteristic for monomeric species with axial symmetry (g_{II}=2.234, $g_{\perp}$=2.073) have been obtained for powder $CuL_{II}Cl$ compound.

Room temperature ESR spectra of both CuLCl compounds in DMSO solution (10 mg/cm^3) suggest the presence of pseudo-tetrahedral monomeric species. No hyperfine splitting due to the interaction of the paramagnetic electron with nitrogen nuclei was observed.

The anisotropic ESR spectra were obtained for adsorbed DMSO CuLCl solutions on NaY zeolite (Table 2). A careful analysis of the hyperfine structure from the parallel band (Fig.2) indicates the coexistence of two magnetic nonequivalent monomeric species [7]. ESR data concerning Cu(II) ions in the tetrahedral configuration are particularly due to the decreasing of hyperfine structure constants and the increasing of g-values respect to those usually observed in square-planar or octahedral-distorted environments [8]. The g_{II}/A_{II} ratio has been considered as a convenient empirical index of tetrahedral distortion for copper(II) complexes.

It has been pointed out that for square planar structures this ratio have the values in the range from 105 to 135 cm [9]. The g_{II}/A_{II} ratio have the values 118 cm for CuN_2O_2 chromophore and $168^{-1}72$ cm for CuO_4 chromophore in the case of the both monomeric species emphasized by us. There is strong tetrahedral distortion for CuO_4 relative to CuN_2O_2 chromophore.

Table 2

EPR parameters of mononuclear species obtained in DMSO CuLCl solution adsorbed on NaY zeolite

Compound	g_{II}	$g_{\perp}$	A_{II}[G]	Chromophore
CuL_ICl	2.383	2.063	128	CuO_4
	2.334	2.063	183	CuN_2O_2
$CuL_{II}Cl$	2.378	2.081	125	CuO_4
	2.336	2.081	183	CuN_2O_2

These results are in agreement with a square-planar structure for CuN_2O_2 monomeric species and a strong tetrahedral distortion for CuO_4 species when the ligand molecules are completely substituted by DMSO molecules [10].

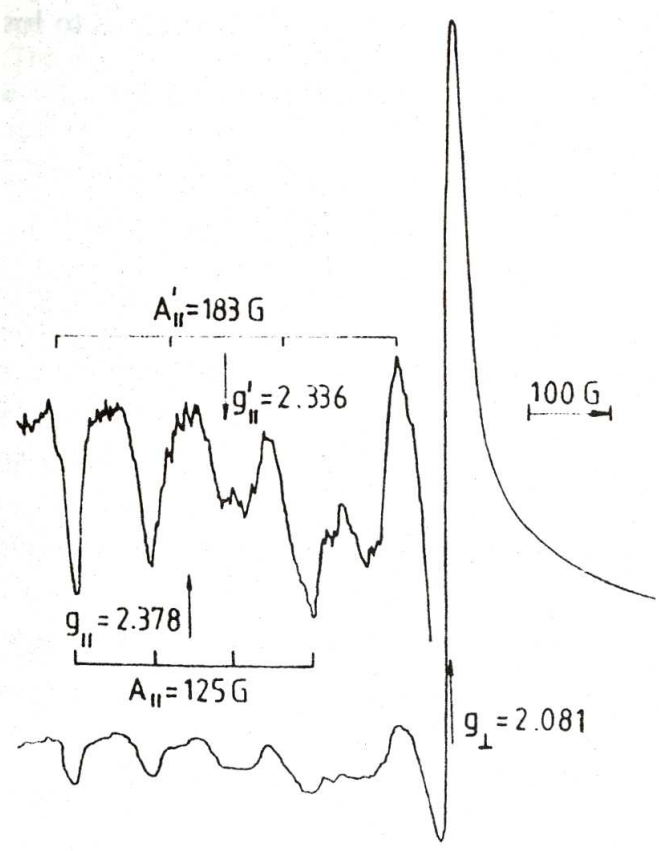

Fig.2. ESR spectrum of DMSO CulCe solution adsorbed on NaY zeolite.

CONCLUSIONS

IR spectra of thiazolyhydrazone complexes and their Cu(II) compounds show that metal ion is four coordinated by two nitrogen atoms, one oxygen and one chlorine atom. Electronic transitions and the values of the atomic magnetic moments are in good agreement with theoretical estimations to the $3d^9$ systems in tetrahedral distorted geometry. Powder ESR spectra of Cu(II) complexes are quasiisotropic for CuL_ICl and anisotropic with axial symmetry for $CuL_{II}Cl$. The anisotropic ESR spectra obtained for DMSO CuLCl solutions adsorbed on NaY zeolite suggest the presence of two magnetic nonequivalent chromophores (CuO_4 and CuN_2O_2). The values of g_{II}/A_{II} ratio show more tetrahedral distortion for CuO_4 environment than for CuN_2O_2. Also, exchanging a less electron rich O atom ligand for a more electron rich nitrogen atom tends to lower g_{II} and increase A_{II}.

REFERENCES

1. R. J. Sorenson, in H. Sigeled., *Metal Ions in Biological Systems,* Vol. 14, Marcel Dekker, New York, 1982.
2. K. Crouch, T. W. Kensler, L. A. Oberley and J. R. J. Sorenson, in K.D. Karlin and J. Zubieta eds., *Biological and Inorganic Copper Chemistry, Adenine,* New York, 1986.
3. Nakamoto, *Infrared and Raman Spectra of Inorganic Coordination Compounds,* 3th Ed. Wiley, New York, 1978.
4. B. P. Lever, *Inorganic Electronic Spectroscopy,* 2nd Ed. Elsevier, New York, 1984.
5. Drago, S. Russell, *Physical Methods in Chemistry*, W.B. Saunders Company, 1977.
6. J. Hathaway, *Struct. Bonding 57* (1984) 56.
7. David, O. Cozar, V. Chiş, A. Negoescu, I. Vlaşin, *Applied Magnetic Resonance* 6 (1994) 521.
8. Cozar, I. Ardelean, *J. Non-Crystalline Solids* 92 (1987) 278.
9. R. J. Thomas, P. Tharmaraj, V. Chandrasekhar, C. D. Bryan, A. W. Cordes, *Inorg. Chem.* 33 (1994) 5382.
10. Szabo-B., G. Peintler, A. Rockenbauer, M. Gyr, M. Varga-Fabian, Institorisz, L. Balazspiri, *J. Chem. Soc. Dalton Trans*. 8 (1989) 1925.

SOLVENT EFFECTS TOWARD ON THE MOBILITY OF THE NITROXIDE RADICALS ADSORBED ON X AND Y ZEOLITES

G. DAMIAN[1], V. ZNAMIROVSCHI, O .COZAR, M .TODICĂ, V. CHIŞ, L. DAVID, R. SALOMIR

ABSTRACT. ESR spectroscopy was used to investigate the localization and the rotational motion of 3-Carbamoyl-2,2,5,5-tetramethyl-3pyrrolin-1-yloxy (Tempyo), 4-oxo-2,2,6,6-tetramethyl-1-piperin- yloxy (Tempone) and 4-acetamide-2,2,6,6-tetramethyl-1-piperidin-yloxy (4-Acetamide-Tempo) nitroxide radicals in chloroform and deuteriated chloroform solutions adsorbed on X and Y zeolites.The changes in spectral lineshape and linewidth for adsorbed nitroxide radicals in normal and deuteriated chloroform environments are interpreted in terms of dynamic properties, interactions and localization sites in cavities.

INTRODUCTION

The ESR study of the adsorbed organic compounds with transition-metal ions on various porous surfaces give valuable information about the modification of the local structure and interactions of the molecular complexes inside pores [1,2]. The local environment has a notable influence on the magnetic characteristics of the adsorbed probes, thus the ESR signal relays information on the structure and dynamics of the probe and solvent [3].

ESR spectra of a nitroxide radicals dissolved in normal and deuteriated solvent and adsorbed on various porous materials give useful information about isotopic effects and dynamical properties. The localization of the probe molecules can be also studied by this method [4].

[1] "Babeş-Bolyai" University, Faculty of Physics, 3400 Cluj-Napoca, Romania

In this paper we report a comparative ESR study for three nitroxide radicals, Tempyo, Tempone and Acetamide-Tempo, dissolved in chloroform and deuteriated chloroform and adsorbed on NaX and NaY zeolites.

EXPERIMENTAL

A 4×10^{-4} mole/liter concentration solutions for the Tempyo, Acetamide Tempo and Tempone nitroxide radicals (Fig. 1) in chloroform ($CHCl_3$) and 99.8% deuteriated chloroform ($CDCl_3$) were preparated.

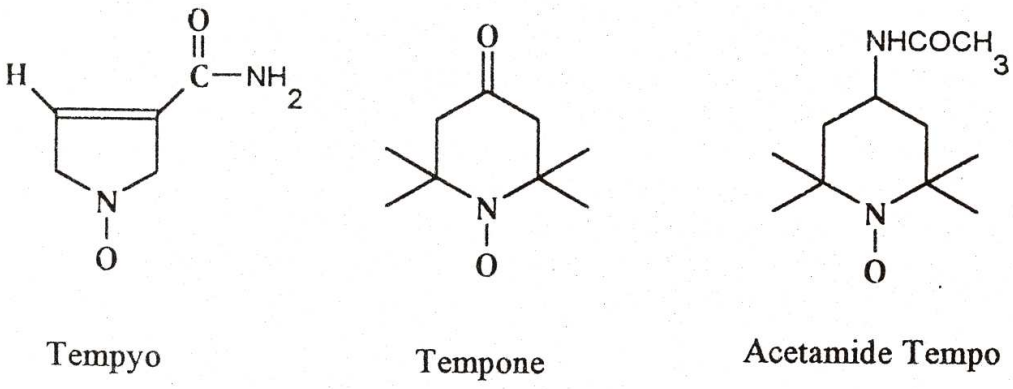

Fig.1. The structure of the nitroxide radicals

The general formula for the used Bayer zeolites are $Na_j[(AlO_2)_j(SiO_2)_{192-j}]\cdot zH_2O$ where z is about 260 and j=86 for NaX zeolite and j=56 for NaY zeolite. The zeolites were dried four hours in air at 150^{o}C before impregnation in order to remove free water. The samples were prepared by stirring two days the zeolites with nitroxide solutions. After filtering the samples were washed with fresh solvent and dried until a dry powder was obtained. ESR spectra were recorded in X-band (≈9.5GHz) at room temperature with a JEOL-JES-3B spectrometer with a field modulation of 100KHz.

RESULTS AND DISCUSSION

The shape of the ESR spectra of the adsorbed nitroxide radicals solutions are related on the molecular reorientation motion. If this motion is fast on the ESR time scale the spectra will be isotropic with the averages of the principal components of the *g*-values and hyperfine splitting factor, a^N [5]. The rate of the isotropic motion determines the relative widths of resonances: a narrow resonance for rapid motion and a broader resonance for slower motion.

The analysis of the ESR line shape and line widths has been performed in terms of rotational correlation times of the spin probes. For isotropic motion in the rapid tumbling limit, the width, ΔH_m, of an individual (hyperfine) line, in the first approximation can be written as a function of the z component of the nitrogen nuclear spin number (m=-1, 0, 1) *[5, 6, 8]:*

$$\Delta H_m = A + Bm + Cm^2 \tag{1}$$

where the A coefficient includes other contributions than motion. The terms B and C are functions related to the rotational correlational time τ for the motion and can be defined as a function of peak to peak line width of the central line, ΔH_0, and the amplitudes of the m-th line I_m [6]:

$$B = \frac{1}{2}\Delta H_0\left(\sqrt{\frac{I_0}{I_1}} - \sqrt{\frac{I_0}{I_{-1}}}\right) = 0.103\omega_e\left[\Delta g \Delta a^N + 3(\delta g)(\delta a^N)\right]\tau_B\left[1 + \frac{3}{4}\left(1 + \omega_e^2\tau_B^2\right)^{-1}\right] \tag{2}$$

$$C = \frac{1}{2}\Delta H_0\left(\sqrt{\frac{I_0}{I_1}} - \sqrt{\frac{I_0}{I_{-1}}} - 2\right) = 1.181\cdot 10^6\left[(\Delta a^N)^2 + 3(\delta a^N)\right]\tau_c \left[1 - \frac{3}{8}\left(1 + \omega_c^2\tau_c^2\right)^{-1} - \frac{1}{8}\left(1 + \omega_e^2\tau_c^2\right)^{-1}\right] \tag{3}$$

in which

$$\Delta g = g_{zz} - \frac{1}{2}\left(g_{xx} - g_{yy}\right); \qquad \delta g = \frac{1}{2}\left(g_{xx} - g_{yy}\right) \tag{4}$$

$$\Delta a^N = a_{zz}^N - \frac{1}{2}\left(a_{xx}^N + a_{yy}^N\right), \; \delta a^N = \frac{1}{2}\left(a_{xx}^N - a_{yy}^N\right) \tag{5}$$

and $\omega_N=8.8\times10^{-6}<a^N>$, a^N is the isotropic hyperfine splitting and ω_e the ESR spectrometer frequency in angular units.

In range from $5\cdot10^{-11}$ to 10^{-9} s (motion in the rapid tumbling limit) and magnetic field above 3300 G, Δg and Δa^N vanish, and the correlation times τ_B and τ_C are directly related to the *B* and *C* coefficients by the following simple relations [6]:

$$\tau_B = \tau_Z = K_1 \cdot B \tag{6}$$

$$\tau_C = \tau_{X,Y} = K_2 \cdot C \tag{7}$$

where $K_1 = 1.27\cdot10^{-9}$ *and* $K_2 = 1.19\cdot10^{-9}$. The average correlation times is:

$$\tau = 1/3(\tau_B + 2\tau_C) \tag{8}$$

In the case of slow motion, the correlation time was evaluated from the ratio of the observed splitting between the derivate extrema A_{ZZ} and principal value A_{ZZ}, determinated from rigid matrix spectrum [6,8]:

$$\tau = \alpha\left(1-\frac{A'_{zz}}{A_{zz}}\right)^{\beta} \tag{9}$$

The α and β parameters depend on the kind of the diffusion process. For small spin probe, the intermediate jump diffusion is preferable [9]. In our evaluation, we taken $\alpha=5.9\cdot10^{-10}$ and $\beta=-1.24$ [6].

With the procedures described above the correlation times for isotropics and anisotropics spectra were calculated.

The rotational correlation times, can be used to calculate the apparent microviscosity η of the partially dehydrated medium using the Debye-Stokes-Einstein relation:

$$\tau = \frac{\eta V}{kT} \tag{10}$$

where τ is the average correlation time, *V* the volume of the probe molecule, η the viscosity near the probe molecule, *k* the Boltzmann's constant and *T*, the temperature. The volume of the nitroxide molecule was calculated assuming the

prolate ellipsoid of revolution with the same short semiaxes and different long semiaxes. The optimum dimensions of the molecules was calculated using ALCHEMY program.

In general, even in isotropic media, the motion of the nitroxide molecule undergo anisotropic [6, 7]. Thus the ESR spectra must be treated in terms of two correlation times corresponding to the motion about principal molecular axis and to the translation of the molecule [6].

The motion of the nitroxide molecules inside zeolite is determinated by the existence and the strength of the acidic sites. The strength and the concentration of the sites are depending on the Si/Al ratio [8]. The zeolites with low Si/Al atomic ratio (1-1.5), (zeolites X), have higher concentration of sites with moderate acidic strength and the zeolite with Si/Al atomic ratios more than 2 have a low concentration of the sites with high acid strength (zeolites Y).

In Fig.2 and Fig.3 are presented the ESR spectra of the nitroxide radicals solutions adsorbed on NaX zeolites.

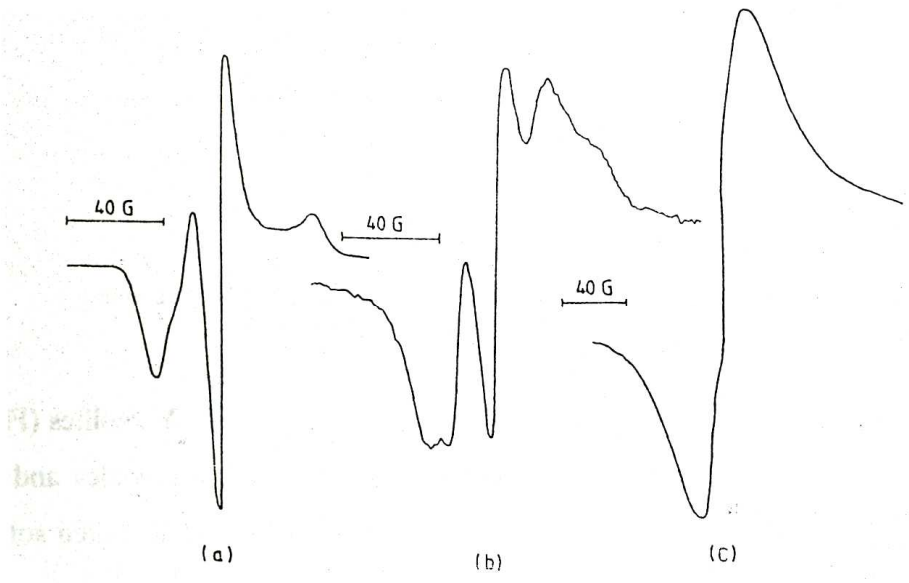

Fig.2. ESR spectra of nitroxide radicals in $CHCLCl_3$ solution adsorbed on NaX zeolite: (a) Tempyo (b) Acetamide-Tempo (c) Tempone.

The adsorbed undeuterated and deuteriated solutions of the nitroxide radicals on NaX zeolites show the existence of a isotropic spectrum (rapid reorientation) superimposed on an anisotropic spectrum (slow reorientation) corresponding to a bulk sites and to a acidic site on wall, respectively. In the case of adsorbed undeuteriated solutions the existence of the broadened signal suggests an increase of the proton interaction between nitroxide radical and OH groups on the surface and between nitroxide radical and proton from solvent molecules [9].

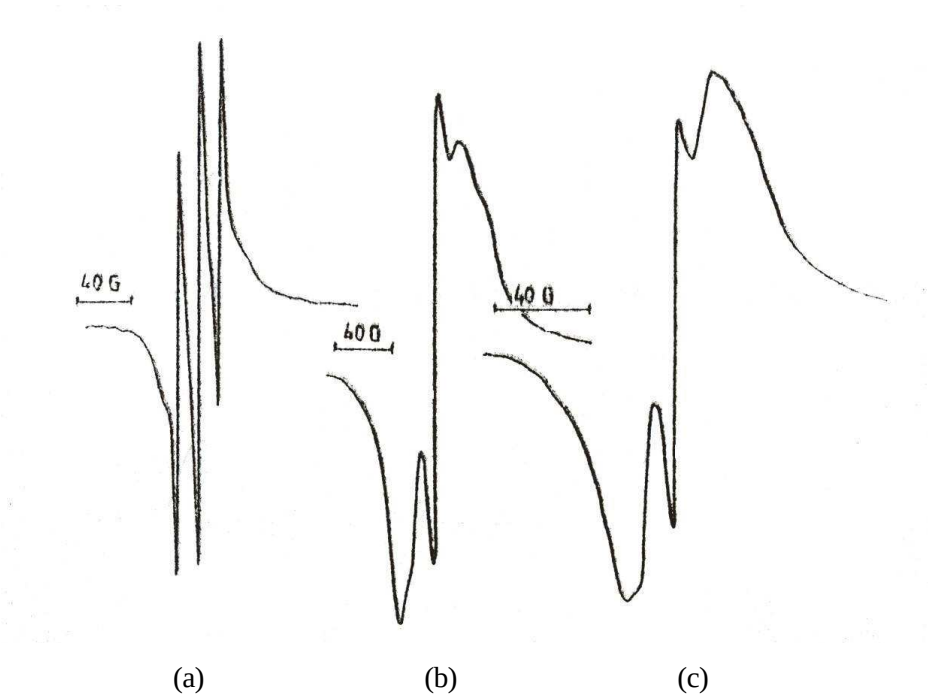

(a) (b) (c)

Fig.3. Esr spectra of nitroxide in $CDCl_3$ solution adsorbed on NaX zeolite:
(a) Tempyo (b) Acetamide-Tempo (c) Tempone.

The isotropic spectra of the adsorbed nitroxide radical on NaY zeolites (Fig. 4 and Fig. 5) show that the proton interaction between nitroxide molecules and OH groups is negligible. However, a weak interaction occurs with undeuteriated solvent giving rise to a broadening lineshape.

The ESR spectra in the last case, show a predominant slow motion of the molecules in cavities. The differences between spectra are due to the symmetry and polarities of the adsorbed molecules and to the higher viscosity of the deuteriated solvent.

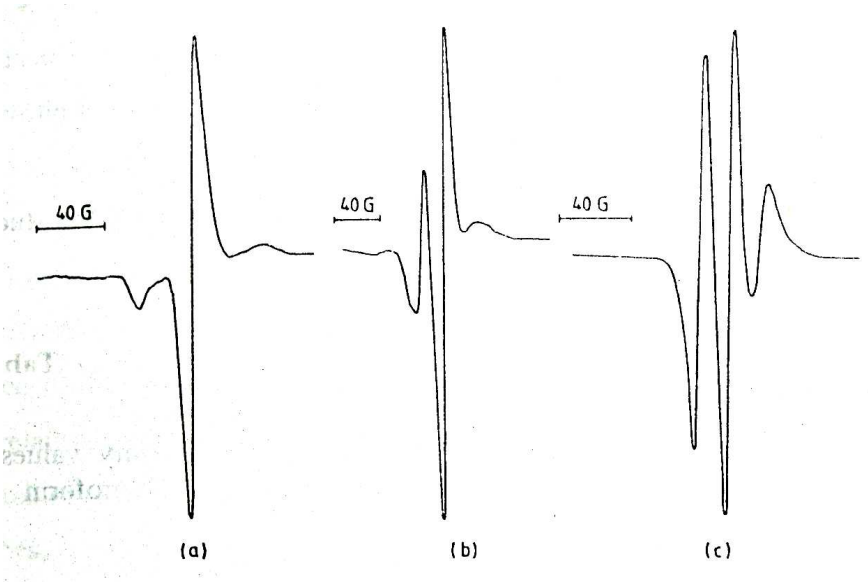

Fig.4. ESR spectra of nitroxide radicals in $CHCl_3$ solution adsorbed on NaY zeolite: (a) Tempyo (b) Acetamide-tempo (c) Tempone.

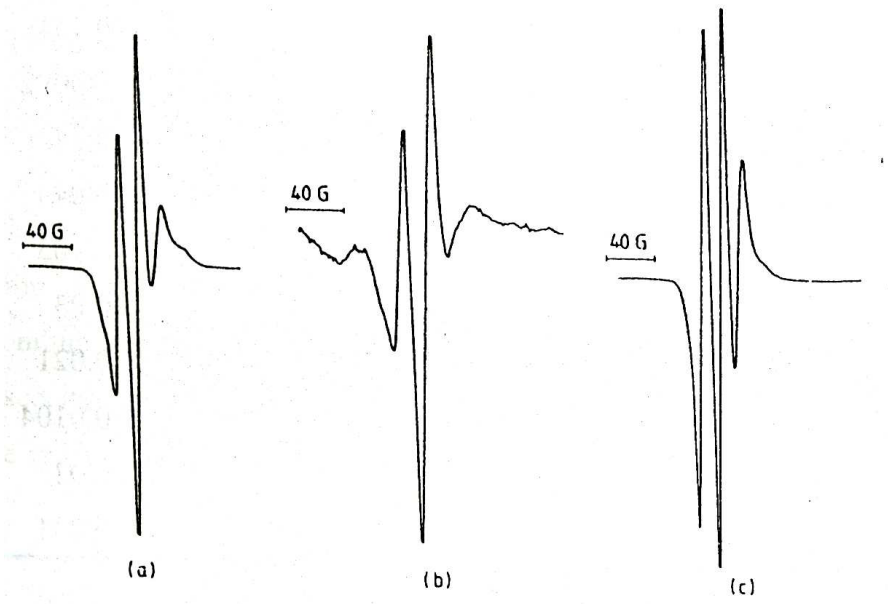

Fig.5. ESR spectra of nitroxide radicals in $CDCl_3$ solution adsorbed on NaY zeolite: (a) Tempyo (b) Acetamide-tempo (c) Tempone.

The radical mobilities were expressed in terms of the correlation times for the motion with a procedure described in reference [4].

The estimated η values are in the range from 0.0075 P to 0.14 P, depending on the nature of solvent, strength of acidic sites and on the dimension of nitroxide radical molecules.

The correlation times and apparent microviscosity obtained for the studied probes are given in Table 1.

Table 1

The correlation time, hyperfine A'_{zz} constants and viscosity values of nitroxide radicals dissolved in chloroform and deuteriated chloroform and adsorbed on NaX and NaY zeolites.

Sample	A'_{zz}(G)	τ (ns)	η (P)
Tempyo-$CDCl_3$/NaX	34.8	27.0	0.092
Tempyo-$CHCl_3$/NaX	23.7	2.2	0.0075
Tempo-$CDCl_3$/NaX	35.3	41.0	0.151
Tempo-$CHCl_3$/NaX	25.0	2.5	0.0092
Tempone-$CDCl_3$/NaX	31.0	6.8	0.14
Tempone-$CHCl_3$/NaX	23.0	2.1	0.043
Tempyo-$CDCl_3$/NaY	35.0	31.0	0.105
Tempyo-$CHCl_3$/NaY	32.4	8.8	0.03
Tempo-$CDCl_3$/NaY	30.7	5.8	0.021
Tempo-$CHCl_3$/NaY	26.3	2.8	0.0104
Tempone-$CDCl_3$/NaY	21.0	1.7	0.035
Tempone-$CHCl_3$/NaY	19.3	1.5	0.031

It can see that the correlation time depend appreciably on the solvent deuteriation even if such dependence could not be rigorously quantified. Deuteriated liquids have a mean viscosity higher than corresponding undeuteriated liquids.

The correlation time values show a dependence of mobility on the solvent nature, on the acidic character of the zeolite surfaces and the symmetry of adsorbed molecules. Thus, in the deuteriated solvent, the correlation times have the low values than in the case of undeuterated solvent. This are due to the more structurated deuteriat solvent with the consequences on the mobility and to the absence of solvent hyperfine proton interaction. For the same spin probes, the correlation times increase from τ_{NaX} to τ_{NaY} corresponding to the increase of the stretch of cationic sites on the surface support. The mobility among paramagnetic probes, expressed by correlation times, increase in the order $\tau_{Tempone} < \tau_{Tempo} < \tau_{Tempyo}$. This differences in the correlation times are due to differences of the polarizability and dielectric constants values of nitroxide radicals.

CONCLUSIONS

The studied nitroxide radicals adsorbed on X and Y zeolites show a dependence of the molecular mobility on the strength and acidic sites concentrations inside pores and on the nature of solvent. It is relevant that the correlation times in adsorbed systems were invariantly higher than in the corresponding unadsorbed systems. This could be attributed to an increase of the local viscosity sensed by the probe. The difference between radicals mobility in the same medium are due to the symmetry and polarity of guest molecules.

REFERENCES

1. C o z a r, O., D a v i d, L., C h i ş, V., C o s m a, C., Z n a m i r o v s c h i, V.,
2. D a m i a n, G., B r a t u, I., B o r a , G h., *Appl. Magn. Reson.*, 8, 235(1995).
3. C o z a r, O., Z n a m ir o v s c h i, V., D a v i d, L., D a m i a n, G., "*11th Specialized Coloque Ampere on Magnetic Resonance in Homogeneous and Heterogeneous Catalysis*", Menton, France, Sept. 1993.

4. M a r t i n i , G., O t t a v i a n i, M. F., R o m a n e l l i, M., *J.Colloid.Interface Sci.*, 94, 1, 105(1983).
5. M a z z o l e n i, F., O t t a v i a n i, M. F., R o m a n e l l i, M., M a r t i n i, G., *J.Phys.Chem.*, 97, 7, 1953(1988).
6. S c h r e i e r, S., P o l n a s z e k, C. F., S m i t h, I. C., *Biochim. Biophys. Acta*, 515, 395(1979).
7. G o l d m a n, S. A., B r u n o, G. V., P o l n a s z e k, C. F., F r e e d, J. H., *J.Chem.Phys.*, 56,716(1972).
8. H w a n g, J. S., M a s o n, R. P., H w a n g, L. P., F r e e d, J. H., *J.Phys.Chem.*, 79, 489(1975).
9. G a t e s, C. B., *Catalytic Chemistry*, Ed. John Wiley & Sons, Inc., 1992.
10. C h a c h a t y, C., *J.Chem.Phys.*, 91, 1848(1994).

SURFACE ENHANCED RAMAN SCATTERING ON THE COVERED REDOX GLASS ELECTRODES

I. MARIAN[1], S. CINTA[2], E. VERESS[3], M. VENTER[1]

ABSTRACT. Surface enhanced Raman scattering (SERS) was used for the characterisation of redox glass electrode surfaces. Depositing the thin silver film on the electrodic surfaces, the sensitivity of spectral determinations was remarkably improved. The enhancement of Raman signal at the redox glass-SCN^- ion interface was obtained. The comparative study of the spectral response from modified and unmodified redox glass surface alow the elucidation of some adsorbtion phenomena.

INTRODUCTION

The enhancement of the Raman signal from molecules placed in the vicinity of the metal has been largely reported.[1-7] Few studies were made considering semiconductor substrates for molecule adsorption.[8-11] As far as we know Raman investigations at molecule-redox glass interface have not been reported.

The aim of this paper is to prove the adsorbtion quality of the microcrystallite states contained on the redox glass surface, using SERS spectroscopy.

Electrochemical deposition (ED) of Ag thin layer on the semiconductive electrod surface modifies the spectral response of the interface. In this respect we used SERS of KSCN on Ag colloid to establish the orientation and the binding way of the molecule by adsorbtion on the Ag surface.

[1] "Babeş-Bolyai" University, Department of Chemistry, 3400 Cluj-Napoca, Romania.
[2] "Babeş-Bolyai" University, Department of Physics, 3400 Cluj-Napoca, Romania.
[3] Institute of Chemistry, 3400 Cluj-Napoca, Romania.

Also, the adsorbtion study of KSCN on the free redox glass and then, on the redox glass covered by silver, proved the adsorbtion role of microcrystallites of the glass.

The use of SCN^- ion in the study of adsorbtion at electrodic interfaces was chosen for some specific advantages:

- SCN^- ions maintain their chemical identity in both alkaline and acid media.[5]
- In case of Ag deposition on the redox glass surface, AgSCN is the only solid phase present in diluted thiocyanate system.[5]

The semiconductor glass used, has the composition (mol %): SiO_2 (30); Na_2O (5); Fe_2O_3 (8); FeO (8); B_2O_3 (35); Al_2O_3 (4).[12] A glass pearl shaped sample was fixed tightly at the end of a high rezistivity silicate glass tube (support of the electrode), by melting and rapid cheeling. By this procedure the active superficial layer (3 mm diameter) was enriched in Fe_2O_3.

Electrochemical deposited Ag island films on redox glass were obtained using an galvanic cell with redox glass as working electrod and Ag ring counter electrod. The galvanostatic conditions were: 1 mA cm^{-2} current density controled by an Tacussel potentiostat, 10 minutes deposition time, 0.1 M $AgNO_3$ aqueous solution as electrolite. Both electrodes were used after the necesary cleaning procedure.

SERS of KSCN 10^{-1} Mol L^{-1} solution dropped on 1 cm^3 Ag sol prepared according to Creighton's procedure[13, 14] was measured in 2 mL glass cell. The final concentration of KSCN in SERS-active system containing $BaCl_2$ was $2.3x10^{-4}$ Mol L^{-1} The sol solution changed in colour from yellow to purple. Adsorption studies on films were carried out in 10^{-1} Mol L^{-1} KSCN solution. Raman spectra have been recorded on a GDM 1000 double monochromator equipped with an ILA 120-1 argon-ion laser; the emission line at 488 nm was used with an incident power of 120 mW. The scattered light was collected at a 90^o geometry; the spectral slit width was 4 cm^{-1}.

Triply distilled water was used for the preparation of the solutions. All reagents used were of analitical purity. The measurements were carried out at room temperature.

RESULTS AND DISCUSSION

The IR spectrum of KSCN was recorded in the range 4000-400 cm^{-1}*. According to the structure of the SCN^- group, the most important peaks are 742 (medium), 2067 (strong) and 475, 470 (weak) assigned to the S-C, C≡N and SCN double degenerated bending vibrations, respectively. In Raman spectrum of the molecule the C≡N vibration is the most intense and it will be used in further discutions. Raman spectrum of 0.1 ML^{-1} KSCN aqueous solution is showed in Fig.1.

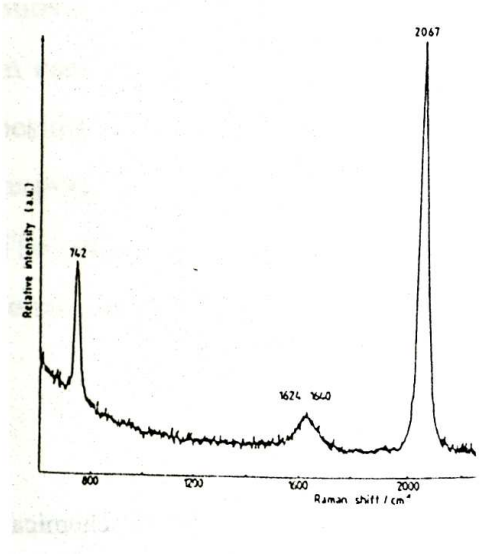

Fig. 1. Raman Spectrum of 0.1 M KSCN aqueous solution.

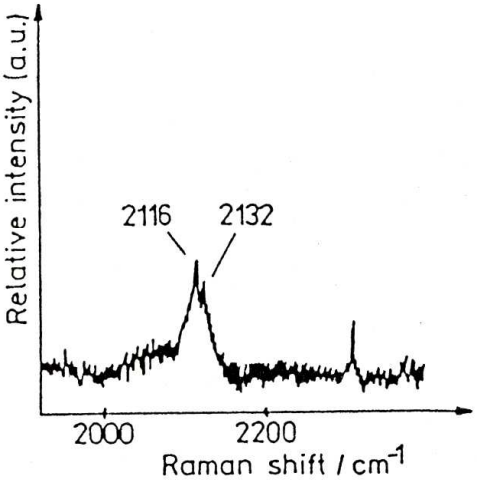

Fig. 2. SERS Spectrum of KSCN on silver sol.

* All frequencies in cm^{-1}

In case of Ag sol SERS procedure[1] on freshly prepared homogeneous phase, the SCN^- spectrum (Fig. 2) presents a large band, splitted at 2116 and 2132, respectively. The.SCN^- ion may be adsorbed on the silver surface *via* the S or N atoms. Adsorption through S atom is specific at higher than 2100 $^{cm-1}$ and through N atom at less then this value.[5] The optained values suggest the S-adsorption.The 2116 peak may be related to a monomer Ag-SCN connection with a strong Ag-S covalent ratio. The presence of 2132 peak suggests the possibility of bridging adsorption as -Ag-SCN-Ag- chain.

In Fig. 3, Raman spectra of SCN^- ion on the surface of the free redox glass (a) and on electrochemical deposited overlayer film on the redox glass (b), are presented.

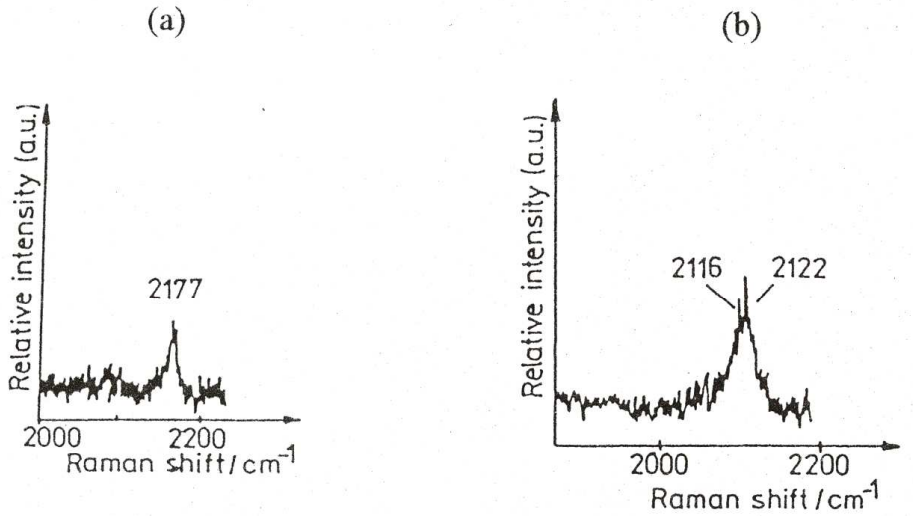

Fig. 3. SERS Spectra of KSCN on the free redox glass (a) and Ag electrochemically deposited on the redox glass (b).

The 2177 peak (Fig 3a) is close to the C≡N stretching vibration of -SCN group in organic compounds.[15] The 2067 peak from Raman spectrum shifted to 2177 indicates the chemosorption of SCN^- on the redox glass surface through the S atom.

In case of electrochemical deposited Ag film, Raman spectrum (Fig. 3b) gives a splitted band at 2116-2122, comparable to that one presented in Fig. 2. The 2116 peak can be assigned in the same manner with the corresponding peak from SERS spectrum. The 2122 peak, stronger (in relative intensity) than that of 2132 (Fig. 2) suggests the same polymer structure, but with a shorter chain. We attributed this enhancement to a short range interaction in the presence of submicroscopic roughness of the Ag film. In time, after about 20 minutes of exposure, the Raman signal is diminished because of destroying of the Ag film due to corrosion and photocorrosion. These processes are responsible for the rising of absorption coefficient in support solution.

CONCLUSIONS

The redox glass electrod surface, investigated by SERS spectroscopy, acts as follows:

- In case of strongly chemisorbed species on the metallic deposited overlayer, besides the electromagnetic enhancement, an additional efect to spectral respons can appear in time.
- The modification of adsorbtion coefficient near the electrodic surface is due to corrosion and photocorrosion.

REFERENCES

1. R. K. C h a n g, T. E. F u r t a k, *Surface Enhanced Raman Scattering*, Plenum Press, New York, 1982.
2. M. O s a w a, K. A t a k a, *Surf. Sci.*, 1992, **L118**, 262.
3. M. O s a w a, M. I k e d e a, *J. Phys. Chem.*, 1991, **95**, 9914.
4. T. Je i e s c u, I. M a r i a n, R. M i s c a, V. S m a r a n d a c h e, *Analyst*, 1994, **119**, 567.

5. R. P. Cooney, E. S. Reid, M. Fleischmann, P. J. Hendra, *J. Chem. Soc., Faraday Trans.*, 1977, **11**, 1691.
6. U. Udagava, C. C. Chou, J. C. Hemminger, S. Ushioda, *Phys. Rev. B. Condens. Matter*, 1981, **23**, 6843.
7. J. A. Creighton, *Surface Enhanced Raman Scattering*, edited by R.K.Chang and T.E. Furtak, Plenum Press, New York, 1982, 315.
8. M. L. Sanjuan, P. B. Oliete, V. M. Orera, *J. Phys. Condens. Matter*, 1994, 6, 9647.
9. E. J. Liang, D. Gottges, W. Kiefer, *Appl. Spectroscopy*, 1994, **48(9),** 1088.
10. J. L. Wynn, J. H. Kim, N. Tao, R. Dai, P. S. Song, T. M. Cotton, *J. Phys. Chem.*, 1995, **99**, 2208.
11. M. Mrozek, A. Otto, *J. Electr. Spectr. and Related Phen.*, 1990, **54/55**, 895
12. E. Veress, unpublished work.
13. M. G. Albrecht, J. A. Creighton, *J. Am. Chem. Soc.*, **99**, 5215.
14. J. A. Creighton, C. G. Blatchford, M. G. Albrecht, *J. Chem. Soc., Faraday Trans.* 2, 1979, **75**, 790.
15. N. B. Colthup, L. H. Daly, S. E. Wiberley, *Introduction to Infrared and Raman Spectroscopy*, Academic Press, New York, 1964, p. 20.

SOLVENT INFLUENCE OF THE RESIDUAL DIPOLAR INTERACTION IN THE POLYBUTADIENE TOLUENE SOLUTIONS

M. TODICĂ[1], A. V. POP[1], D. CIURCHEA[1], D. STĂNILĂ[1], G. DAMIAN[1]

ABSTRACT. The relaxation of the transversal magnetization of the protons attached to the polymeric chains was observed in order to characterize the interaction between the protons of the skeletal bonds. This interaction depends on the temperature and the polymeric concentration.

INTRODUCTION

The relaxation of the transversal magnetization of the protons attached to the polymeric chain is a reach source of information about the local and long range dynamics of the skeletal bonds of the polymeric chain, [1,2]. The main mechanism which governs this relaxation is the dipolar interaction between the protons of the polymeric chain. This interaction is affected by the dynamics of the skeletal bonds, which depends on the temperature and solvent concentration.

If the orientational motion of the skeletal bonds is an isotropic process during the NMR observation time, then the dipolar interaction is averaged to zero and the shape of the relaxation function is like in the case of the isotropic liquids. When the orientational motion of the molecular bonds is an anisotropic process during the observation time, then the dipolar interaction is not averaged to zero and the relaxation function has pseudo-solid behavior.

[1] "Babeş-Bolyai" University, Faculty of Physics, 3400 Cluj-Napoca, Romania.

EXPERIMENTAL

We studied some polybutadiene - toluene-d_8 solutions, with the polymeric concentrations 100%, 88%, 78% and 53%. The microstructure of the polymer was 40% in vinyl conformation, 36% in trans conformation, the molecular mass M_n=190000 g/mole and the glass transition temperature T_g=202K. The polymeric sample was kindly supplied by the Manufacture Michelin and the deuterated toluene was purchased from Spectrometrie Spin et Techniques, France. The solutions were enclosed in NMR tubes (diameter 8mm) and sealed under a primary vacuum. The concentration of the solutions were controlledwith an accuracy better than 1%. The glass transition temperatures of the solutions weremeasured by DSC technique with an accuracy better than 4%.

All the measurements were performed using a CXP Bruker spectrometer wor king at 45 MHz, in the temperature range of 225 K to, 334 K. The relaxation of the transversal magnetization was observed using the Carr-Purcell sequence, [3], and the echoes pseudo-solids were observed using the following sequence of impulsion: $[\pi/2]_y$-$[t$-$(\pi)_y$-$t]_n$-$[\pi/2]_x$-$[t$-$(\pi)_y$-$t]_k$-echo, [4]. The sample temperature was controlledwithin 1K.

RESULTS AND DISCUSSION

Generally, the relaxation function of the transversal magnetization is very complex and its mathematical expression is difficult to disclose from experimental data. However, important conclusions about the relaxation mechanism can be obtai ned by observing some properties of the experimental curves, like the superposition property. This property is observed for temperatures higher than a characteristic temperature for each sample, which was called *“reference temperature"*, T_{ref}.

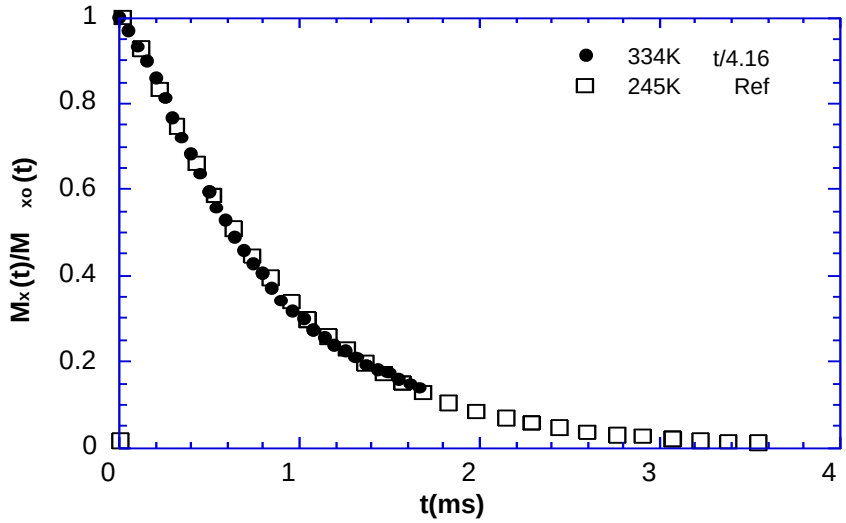

Fig. 1. The superposition of the experimental curves observed for the solution with the polymeric concentration Φ = 78%. The relaxation curves corresponds to the reference temperature, (□) Tref = 245K and (•) T = 334K.

In many cases, the experimental curves corresponding to different temperatures, $M_{x1}(T_1,t')$ and $M_{x2}(T_2,t'')$, can be superposed by dividing the time scale with a constant factor, called superposition parameter, S(T, Φ), [5, 6]. When two experimental curves are completely superposed, we can suppose that the two relaxation functions $M_{x1}(T_1,t')$ and $M_{x2}(T_2,t'')$ can be expressed by a single mathematical expression $M_x(T_{ref},t)$, where the new time variable *t* is related to the variables t' and t'' by the relations:

$$t = t'/ S(T_1, \Phi) \text{ and } t = t''/ S(T_2, \Phi).$$

We observed the superposition property for the molten polymer and concentrated solutions above T_{ref}, (Fig.1). For temperatures lowers than T_{ref}, this property is not observed. This temperatures depends on the solvent concentration and it is related to the glass transition temperature $T_g(\Phi)$ by the relation: $T_{ref}(\Phi) - T_g(\Phi) = 80\pm12$ K, (Fig.2).

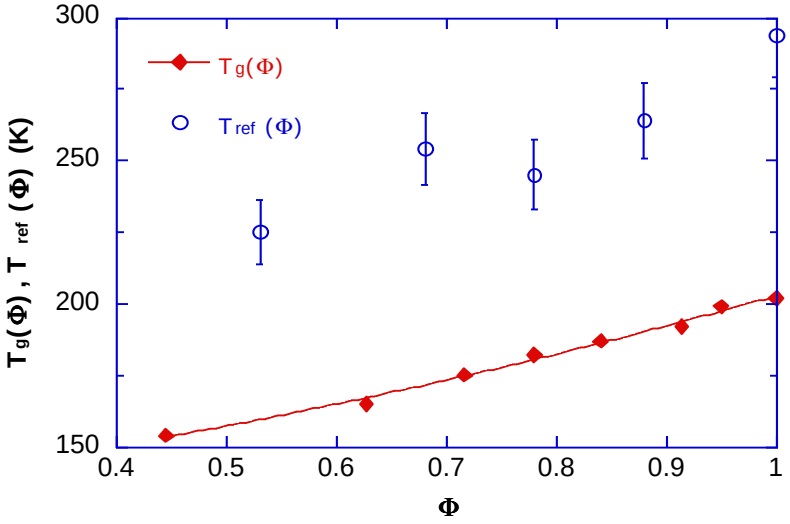

Fig.2. Concentration dependence of the reference temperature $T_{ref}(\Phi)$, (○) and the glass transition temperature $T_g(\Phi)$, (◆).

The superposition parameter S(T, Φ) has a linear temperature dependence for the molten polymer and for the concentrated solutions. This dependence is notlinearly when the solvent concentration increase, (Fig.3).

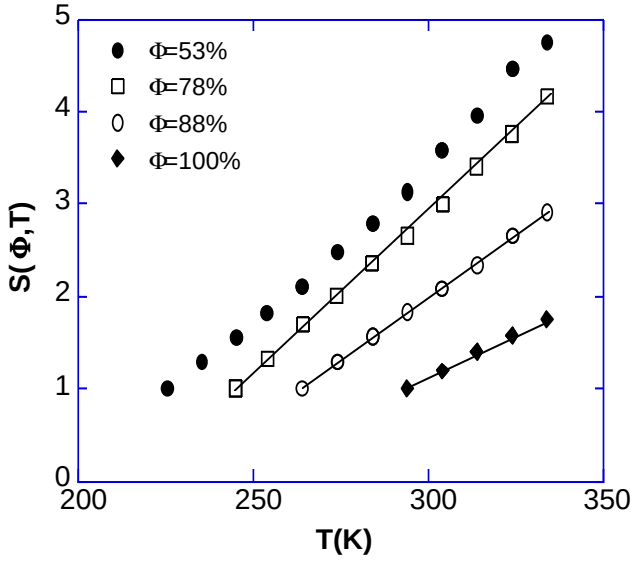

Fig.3. Temperature dependence of the superposition parameter observed for solutions with the polymeric concentration: (●) F = 53%,(□) F = 78%, (❍) F = 88%, (◆) F = 100%.

To determine the nature of the relaxation mechanism, we observed the pseudo-solid echoes in the temperature range of superposition. In previous works we shown that the relaxation is governed by the residual dipolar interaction if the superposition property is respected and the echoes pseudo-solids have specific properties, [7].

We observed this behavior for the molten polymer and concentrated solutions for temperatures higher than T_{ref}. The relaxation is governed by the residual dipolar interaction. The orientational motion of the skeletal bonds is an anisotropyc process and the dipolar interaction is not averaged to zero. We can assume that this anisotropy is due to the temporary junctions between two different chains, the entanglements. For time delay shorter than the NMR observation time, the polymeric system behave like a temporary network.

When the temperature increase, of about 60 - 80K about T_{ref}, the symmetry of the echoes is not respected. The motion of the molecular bonds is fast, so that the life time of temporary junctions is shorter than the NMR observation time. As a result the dipolar interaction between the protons is averaged to zero and the pseudo-solid character of the relaxation function vanish.

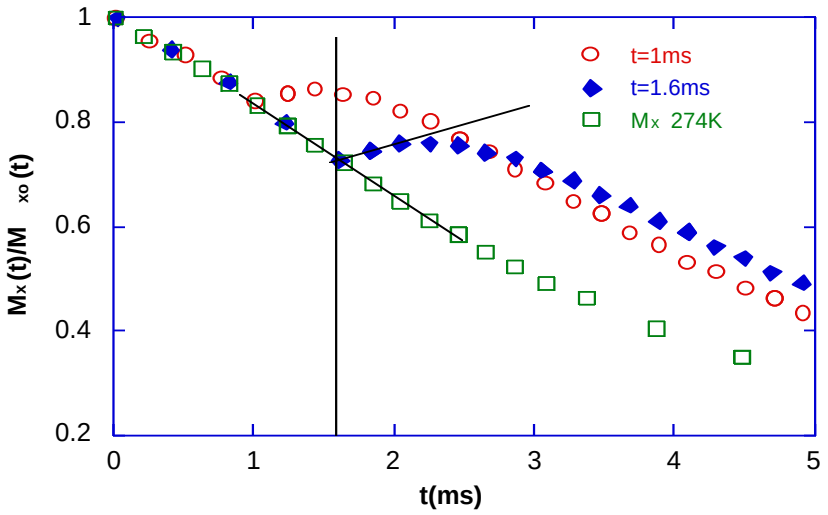

Fig.4. The echoes pseudo-solids observed for the solution with polymeric concentration Φ = 53%, at T = 274 K. The slopes of the relaxation function and the echoes function are not symmetric.

When the solvent concentration grows, the mobility of polymeric chains increase. The motion of the skeletal bonds became an isotropic process during the NMR observation time. As a result the dipolar interaction is averaged to zero, and the echoes pseudo-solids do not respect its specific properties, (Fig. 4).

CONCLUSION

The temporary junctions between the polymeric chains induces an orientational anisotropy of the skeletal bonds and thus an partial average of the dipolar interaction. This residual dipolar interaction determine the pseudo-solid behavior of the relaxation function.

The solvent molecules perturbs the junctions between the chains and induces an isotropic motion of the molecular bonds. The dipolar interaction is averaged to zero and the echoes pseudo-solids do not respect its specific properties.

REFERENCES

1. P. G. de Gennes, *Scaling Concepts in Polymeric Physics*, Cornell University Press, Ithaca, New-York, 1979.
2. J. P. Cohen - Addad, *NMR and Fractal Properties of Polymers Liquids and Gels*, Pergamon Press, London, 1992.
3. H. Y. Carr, E. R. Purcell, *Phyd. Rev*., 94, 630, 1954.
4. J. P. Cohen - Addad, C. Schmit, *Polymer*, 29, 883, 1988.
5. J. P. Cohen - Addad, A. Labouriau, J. Chem. *Phys*., 93, 4,15, 1990.
6. J. P. Cohen - Addad, *Physical Properties of Polymeric Gels*, John Wiley and Sons, Chichester, New-York, Toronto, 1996.
7. M. Todica, *Studia Physica XL 1*, "Babeş-Bolyai" University, Cluj-Napoca.

NMR OSERVATION OF THE PSEUDO-SOLID ECHOES IN MOLTEN POLYISOBUTYLENE AND POLYISOBUTYLENE-TOLUENE D_8 SOLUTIONS

M. TODICĂ[1], J. P. COHEN-ADDAD[2], A. V. POP[1], D. CIURCHEA[1]

ABSTRACT. The properties of the pseudo-solid echoes were analyzed in order to estimate the contribution of the segmental dynamics of the polymeric chain to the relaxation function of the transversal magnetization.

INTRODUCTION

The dynamics of polymeric chain is a complex process which include motions extended to a large spatial and temporary range, [1]. The elementary motions are the rapid isomeric rotations of the skeletal bonds. When the amplitude of this motions is weak and the observation time is short, this motions affect only the monomeric units. We can associate a correlation length of this motions comparable with the spatial extension of the monomeric units.

When the amplitude of this motions is strongly, this motions can affect many monomers during the observation time. The new correlation length include many monomers in this case. The new elementary link of the polymeric chain can be regarded as the segment which correspond to this new correlation length.

Generally we can consider that the polymeric segment is smaller or equal than the distance between two temporary junction between two different polymeric chains.

[1] "Babeş-Bolyai" University, Faculty of Physics, 3400 Cluj-Napoca, Romania.
[2] Lab. spectrometrie Physique, RMN-P, Univ. "Joseph Fourier", Grenoble, France.

In the molten polymers, this temporary junctions can be considered as the entanglements between the polymeric chains. The temporary junctions induces an orientational order of the conformational fluctuations and thus an anisotropy of the dipolar interaction between the protons. The dipolar interaction is not averaged to zero during the observation time. This residual dipolar interaction determine the zero solid behavior of the relaxation function, [2, 3].

In previous work we established a method to observe the existence of this temporary junctions. This method is based on the observation of the properties of the relaxation function of the transversal magnetization and the properties of the pseudo-solid echoes, [4].

Fluctuations of this junctions can be associated with the segmental dynamics of the polymeric chain. This motions diminish the anisotropy of the dipolar interaction between the protons. As a result the pseudo-solid echoes do not respect theirs specific properties. The analyze of the properties of the pseudo-solid echoes can be a way to characterize the dynamics of the polymeric segments.

EXPERIMENTAL

We studied the molten polyisobutylene and the polyisobutylene - toluene d_8 solution, with the polymeric concentrations C=79%. The glass transition temperature of the molten polymer is T_g=202 K and the glass transition temperature of the solution is T_g=165 K. The polymeric sample was kindly supplied by the Manufacture Michelin and the deuterated toluene was purchased from Spectrometric Spin et Techniques, France. The samples were enclosed in NMR tubes (diameter 8mm) and sealed under a primary vacuum. The concentration of the solution was controlled with an accuracy better than 1%. The glass transition temperatures of the solutions were measured by DSC technique with an accuracy better than 4%.

All the measurements were performed using a CXP Bruker spectrometer working at 45 MHz, in the temperature range of 264 K to, 374 K. The relaxation of the transversal magnetization was observed using the Carr-Purcell sequence, [5], and the pseudo-solid echoes were observed using the following sequence of impulsion: $[p/2]_y$ - $[q- (p)_y - q]_n$ - $[p/2]_x$ - $[q - (p)_y - q]_k$ - echo, where t = 2 n q, [6]. The sample temperature was controlled within 1 K.

RESULTS AND DISCUSSION

The analyze of the superposition property of the relaxation function of the transversal magnetization and the analyze of specific properties of the pseudo-solid echoes were utilized to observe the existence of the residual dipolar interaction. In many cases the relaxation curves obey to the superposition property and the pseudo-solid echoes has specific properties. This behavior is associated with the existence of the temporary junctions between different polymeric chains, [7, 8].

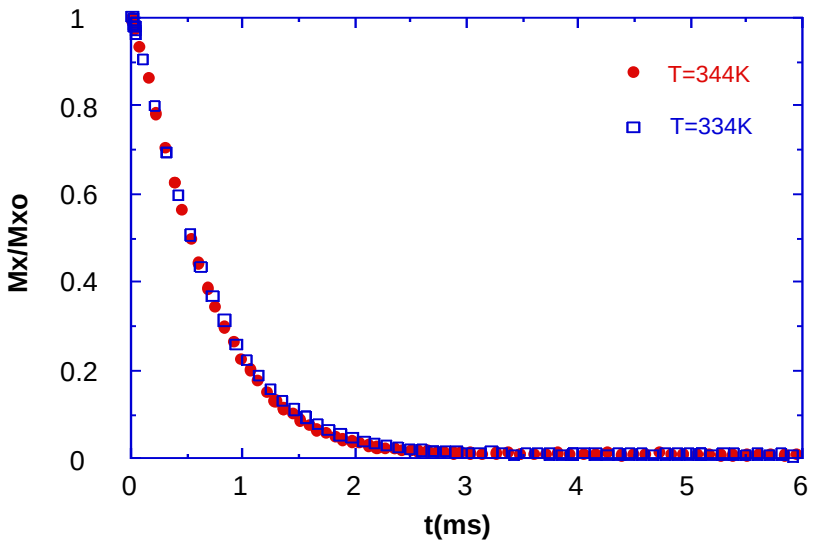

Fig. 1. The superposition of the experimental curves observed for the molten polymer. The relaxation curves corresponds to the reference temperature, ( ) Tref = 334 K and (•) T = 374 K.

We extended this analyze to the molten polyisobutylene and to the polyisobutylene-toluene d_8 solutions.

The relaxation curve is not a single exponential function. However it is possible to superpose the relaxation curves by multiplying the time scale with a constant factor, called superposition parameter, Fig. 1. This property is observed for each sample, for temperatures higher than a characteristic temperature, which was called *"reference temperature"*, T_{ref}. This temperature is T_{ref} =334 K for the molten polymer and T_{ref}=294 K for the solution with the polymeric concentration C = 79%. Below this temperature the superposition property is not observed.

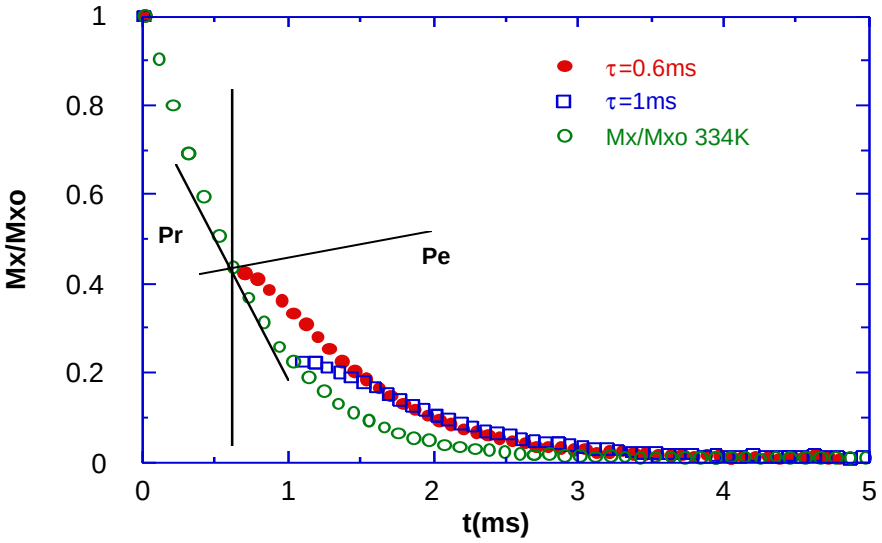

Fig. 2. The pseudo-solid echoes observed for the molten polymer at T=334 K. The slope of the relaxation function and the slope of the echo function are not symmetric.

The superposition property can be associate with the existence of the residualdipolar interaction only if the pseudo-solid echoes respect theirs specific properties. We observed that the slopes of the echoes and the relaxation curves are not symmetric, Fig.2. In this case the residual dipolar interaction is perturbed by the fluctuations of the polymeric chains.

The dominant mechanism which govern the relaxation of the transversal magnetization is the dipolar interaction between the protons attached to the polymeric chain, but this interaction is affected by two mains factors: the anisotropy induced by the temporary junctions between two different chains and the fluctuations of this junctions, [3, 9]. We can assume that the relaxation function $M_X(t)$ is expressed by the product of two others functions:

$$M_x(t) = M_x^e(t) * \Phi_e(t) \tag{1}$$

The function $M_X^e(t)$ is associated with the orientational order induced by the temporary junctions and $F_e(t)$ with the dynamics of this junctions.

The pseudo solid-echoes impulsion sequence affect the slope of the function $M_X^e(t)$, but do not perturb the function $F_e(t)$, [6]. The pseudo solidechoes is generated at the instant t. The slope $P_r(t)$ of the relaxation function represents the derivative of the total relaxation function at the instant t.

This slope can be evaluate experimentally.

$$P_r(\tau) = \frac{dM_x(t=\tau)}{dt} = \frac{dM_x^e(t=\tau)}{dt}\Phi_e(t=\tau) + M_x^e(t=\tau)\frac{d\Phi_e(t=\tau)}{dt} \tag{2}$$

When we apply the pseudo-solid echoes impulsion sequence, the evolution of the transversal magnetization after the delay t, is described by the equation:

$$\tilde{M}_x(t) = \tilde{M}_x^e(t)\Phi_e(t) \tag{3}$$

The slope $P_e(t)$ of the echoes function at the instant $t = t_+$ represents the derivative of the relaxation function $\tilde{M}_x(t)$.

$$P_e(\tau_+) = \frac{d\tilde{M}_x^e(t=\tau_+)}{dt}\Phi_e(t=\tau_+) + \tilde{M}_x^e(t=\tau_+)\frac{d\Phi_e(t=\tau_+)}{dt} \tag{4}$$

The function $F_e(t)$ is invariant to the pseudo-solid echoes impulsion sequence. Then:

$$\frac{d\Phi_e(t=\tau_+)}{dt} = \frac{d\Phi_e(t=\tau)}{dt} \tag{5}$$

On the other hand, the slope of the function $\tilde{M}_x^e(t=\tau_+)$ is the inverse of the slope of the function $M_x^e(\tau)$, [6].

$$\frac{d\tilde{M}_x^e(t=t_+)}{dt} = -\frac{dM_x^e(t=t)}{dt} \tag{6}$$

$$\text{and } M_x^e(t=t) = \tilde{M}_x^e(t=t_+) \tag{7}$$

From equations (2), (4), (6) and (7) we obtain:

$$\frac{P_r(\tau) + P_e(\tau_+)}{M_x(\tau)} = \frac{1}{2\Phi_e(\tau)} = \frac{d\Phi_e(\tau)}{dt} \tag{8}$$

Using the equation (8) we can calculate the logarithmic derivative of the function $F_e(t)$ for each instant t. To do this, we must generate many echoes for different instants t and we must measure the slopes $P_r(t)$, $P_e(t)$ and the amplitude of the relaxation function $M_X(t)$. The precision of the reconstruction of the function $F_e(t)$ depends on the total number of pseudo-solid echoes generated for each relaxation function.

We utilized this method to evaluate the function $F_e(t)$ for many temperatures, above and below T_{ref}, for the molten polymer and for the solution with the concentration C=79%. The pseudo-solid echoes were generated in the time range which correspond to the variation of the amplitude of the relaxation function from 100% to 15%. In this time domain we can suppose that the dynamics of the polymeric chains is not perturbed by the long range fluctuations, as the diffusion of the entire polymeric chains. Thus the relaxation function is sensitive to the segmental dynamics.

For temperatures higher than T_{ref}, the expression of $[P_r(t)+P_e(t)]/M_X(t)$ represent a constant, for the molten polymer and for the solution with the polymeric concentration C=79%, Fig. 3 and Fig. 4.

In this case $F_e(t)$ is an exponential function, for the time range which correspond to the pseudo-solid echoes.

$$\Phi_e(\tau) = A \exp\left(\frac{-k\tau}{2}\right) \tag{9}$$

We found for the constant k the following values:k=0.4 at T=374 K and k=1.7 at T=334 K for the molten polymer, k=0.18 at T=334 K and k = 0.72 at T=294 K for the solution.

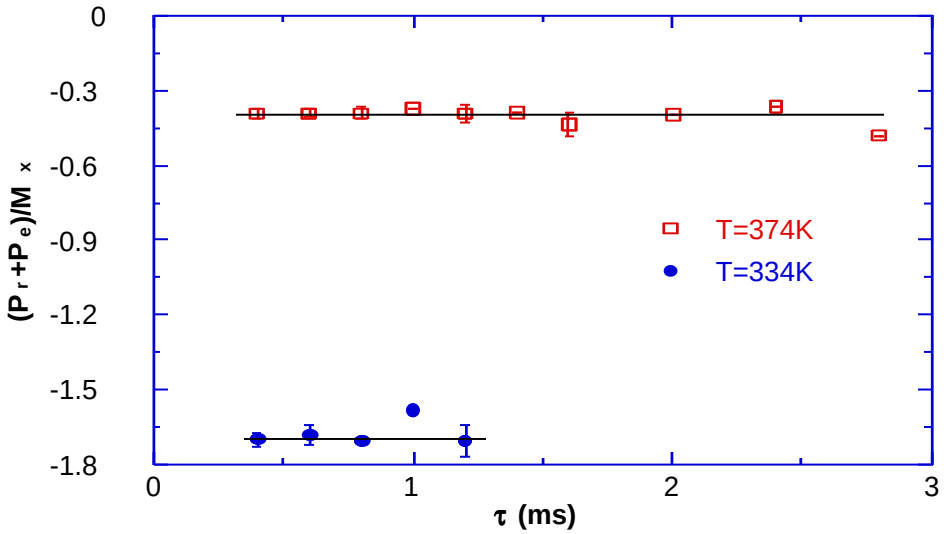

Fig. 3. Time dependence of the expression $[P_r(t)+P_e(t)]/M_x(t)$ for the molten polymer. The pseudo solid echoes were generated for the temperatures: (●) T=334 K and (□) T=374 K. T_{ref}=334.

Below T_{ref}, the expression $[P_r(t)+P_e(t)]/M_x(t)$ do not represent a constant, Fig. 4. The function $F_e(t)$ is not an exponential function. Changes of the slope of the function $F_e(t)$ above and below T_{ref} must induces changes of the shape of the total relaxation function $M_x(t)$. As a result, the total relaxation function do not respect the superposition property above and below T_{ref}. Then the temperature T_{ref} can be regarded as an important parameter which indicate changes of the dynamics of the polymeric chains.

The analyze of the pseudo-solid echoes shown that an important factor which induces changes of the dynamics of the polymeric chains is the segmental dynamics.

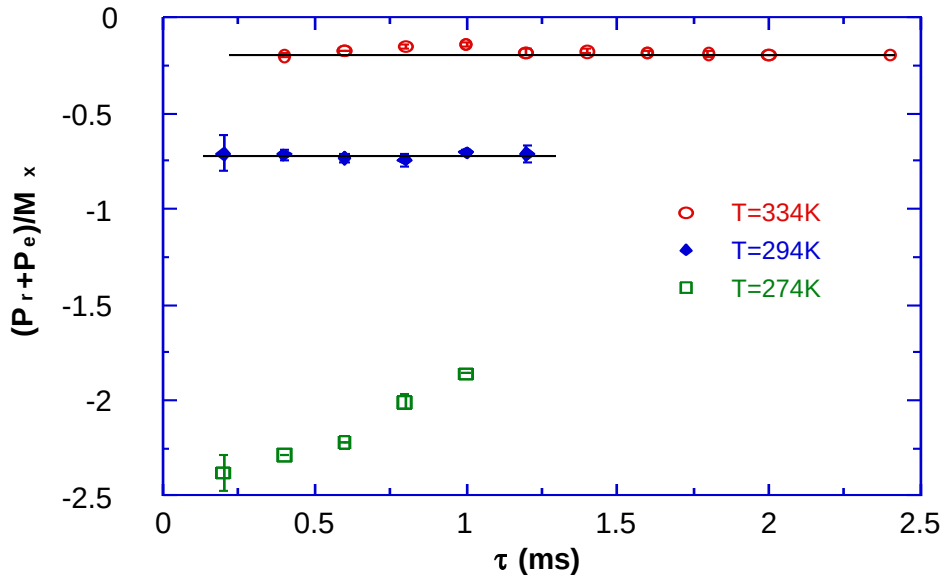

Fig. 4. Time dependence of the expression $[P_r(t)+P_e(t)]/M_x(t)$ for the solution. The pseudo solid echoes were generated for the temperatures: (❍) T=334 K, (◆) T=294 K and (□) T=274 K.

CONCLUSION

The analyze of the slopes of the pseudo-solid echoes is an important way to estimate the contribution of the segmental dynamics of the polymeric chain to the total relaxation function of the transversal magnetization. This contribution is described by the function $F_e(t)$. For the molten polyisobutylene and for the concentrated polyisobutylene - toluene-d_8 solutions, above T_{ref}, this contribution can be expressed by an exponential function. Below T_{ref}, $F_e(t)$ is not an exponential function.

Changes of the shape of the function $F_e(t)$ arise around T_{ref}. This changes indicates changes of the segmental dynamics of the polymeric chains. As a result the total relaxation function do not respect the superposition property.

REFERENCES

1. P. G. de Gennes, *Scaling Concepts in Polymeric Physics*, Cornell University Press, Ithaca, New-York, 1979.
2. J. P. Cohen-Addad, *NMR and Fractal Properties of Polymers Liquids and Gels*, Pergamon Press, London, 1992.
3. J. P. Cohen-Addad, J. *Phys*. (Paris), 43, 1509, 1982.
4. M. Todica, *Studia Physica* XL 1, "Babeş-Bolyai" University, Cluj-Napoca, 1996.
5. H. Y. Carr, E. R. Purcell, *Phys. Rev*., 94, 630, 1954.
6. J. P. Cohen-Addad, C. Schmit, *Polymer*, 29, 883, 1988.
7. J. P. Cohen-Addad, A. Labouriau, J. *Chem. Phys*., 93, 4,15, 1990.
8. J. P. Cohen-Addad, E. Soyez, A. Viallat, *Macromolecules*, 25, 1259, 1992.
9. P. Cohen-Addad, *Physical Properties of Polymeric Gels*, John Wiley and Sons, Chichester, New-York, Toronto, 1996.

NMR STUDY OF PROTON SPIN-SPIN RELAXATION ON POLYISOPRENE-TOLUENE-D_8 SYSTEM

M. TODICĂ[1], V. SIMON[1], I. ARDELEAN[1], S. SIMON[1]

ABSTRACT. The temperature dependence of the shape of the relaxation curves of the transversal magnetization and the properties of the pseudo solid echoes was observed for the polyisoprene toluene D_8 solutions and for the molten polyisoprene. The temperature to temperature and temperature to concentration superposition property of the relaxation curves observed at higher temperatures indicate similitudes of the relaxation mechanisms.

INTRODUCTION

The analyze of the relaxation process of the transversal magnetization is an important source of information concerning the local properties of the polymeric chain, like the dynamics of the macromolecules or the existence of the temporary junctions between different chains, [1, 2]. But the relaxation process is strongly dependent on the temperature , the polymer microstructure and the solvent concentration, so that the NMR recorded curves are different from sample to sample. It should be very useful for the study of the local properties of the macromolecules to observe some similitude of the relaxation process for different samples. This can simplify the analyze of the interaction between the protons of the polymeric chain.

The aim of our study is to analyze the temperature influence on the shape of the relaxation curves of the molten polymer and polyisoprene toluene solutions in order to observe some similitudes of the relaxation mechanisms.

[1] "Babeş-Bolyai" University, Faculty of Physics, 3400 Cluj-Napoca, Romania.

EXPERIMENTAL

We studied the molten polyisoprene and the polyisoprene-toluene D_8 solution, with the polymeric concentrations Φ=78%. The conformation of the molten polymer is 92% cis and the glass transition temperature is T_g=200±5K. The glass transition temperature of the solution is T_g=164±5K. The polymeric sample was supplied by the Manufacture Michelin and the deuterated toluene was purchased from Spectrometrie Spin et Techniques, France. The samples were enclosed in NMR tubes (diameter 8mm) and sealed under a primary vacuum. The concentration of the solution was controlled with an accuracy better than 1%.

All the measurements were performed using a CXP Bruker spectrometer working at 45 MHz, in the temperature range of 254 K to 344K. The relaxation of the transversal magnetization was observed using the Carr-Purcell sequence, [3] and the pseudo-solid echoes were observed using the following sequence of impulsion: $[\pi/2]_y - [\theta - (\pi)_y - \theta]_n - [\pi/2]_x - [\theta - (\pi)_y - \theta]_k -$ echo, where $t = 2 n \theta$, [4]. The sample temperature was controlled within 1 K.

RESULTS AND DISCUSSION

The main mechanism which governs the relaxation of the transversal magnetization is the dipolar interaction between the protons attached to the polymeric chain. This interaction depends on the relative position of the neighboring protons and thus on the dynamics of the polymeric links.

In the case of the rapid rotation of the protons around the molecular bonds, this interaction is averaged to zero and the shape of the relaxation function is like in the case of the isotropic liquids. If the free motion of the protons is embedded by some physical constraints, like the entanglements or the chemical links, then the dipolar interaction is not averaged to zero and the relaxation functions have specific behavior.

This behavior is illustrated by the pseudo solid echoes with characteristic properties, [5]. Changes of relaxation curves shape indicate changes of the interaction between the protons. Generally this interaction is mainly affected by the dynamics of the macromolecules. Thermal activation or the presence of the solvent molecules in the vicinity of the polymeric links are important factors which affect this dynamics.

In our work we observed the temperature dependence of the shape of the relaxation curves and the pseudo solid echoes for the molten polyisoprene and some toluene solutions of this polymer.

The relaxation curve is not a single exponential function and then it is so difficult to disclose the exact mathematically expression of this function. However we observed some particular properties of the relaxation curves, like the superposition property. For a given sample we can superpose the relaxation curves corresponding at two different temperatures, by dividing the time scale with a constant factor, (Fig.1). The relaxation curve corresponding to the temperature T=304K is chosen to reference. The time scale of the relaxation curve corresponding to the temperature T=344K was divided with the factor 1.67. This property is observed only for the temperatures higher than a characteristic temperature, which was called *"reference temperature"*, T_{ref}. We found T_{ref}=304±5K for the molten polymer and we observed that T_{ref}-T_g=100± 10K. This behavior was also observed for other polymers, [6], and indicate that the relaxation process can be described by the same mathematically function in both the cases. We suppose that the relaxation process is governed by the same mechanism.

The superposition property is not observed below T_{ref}, so that we can suppose that the relaxation mechanism change around this temperature. This specific behavior can be explained if we suppose the double dependence of the relaxation function on the asymmetry of the monomeric units rotations, at higher temperatures and the dynamics of the skeletal bonds, at lowers temperatures, [7].

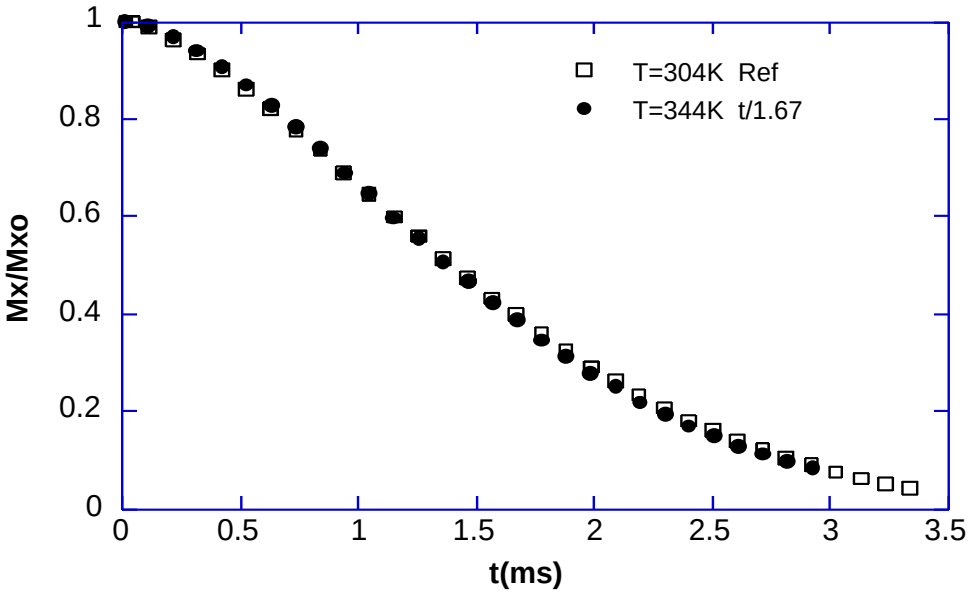

Fig.1. The superposition of the experimental curves observed for the moltenpolymer.

Thermal activation increases the mobility of the polymeric links, but the existence of the temporary or permanent junctions between different polymeric chains induces an anisotropy of the monomeric rotation. This asymmetry of the monomeric rotations induces a non zero average of the dipolar interaction, (the residual dipolar interaction). The relaxation function has a specific behavior illustrated by the existence of the pseudo solid echoes, [1]. The pseudo solid echoes with characteristic properties were observed only above T_{ref}, (Fig.2). The slope of the relaxation curve and the slope of the echo are symmetric; the echoes generated at two different instant τ_1 and τ_2 cross at the instant $\tau_1+\tau_2$.

Towards lowers temperatures the mobility of the polymeric links decrease and the polymeric backbone became more rigid. The pseudo solid echoes do not respect theirs specific properties, (Fig.3). The slope of the relaxation curve and the slope of the echo are not symmetric.

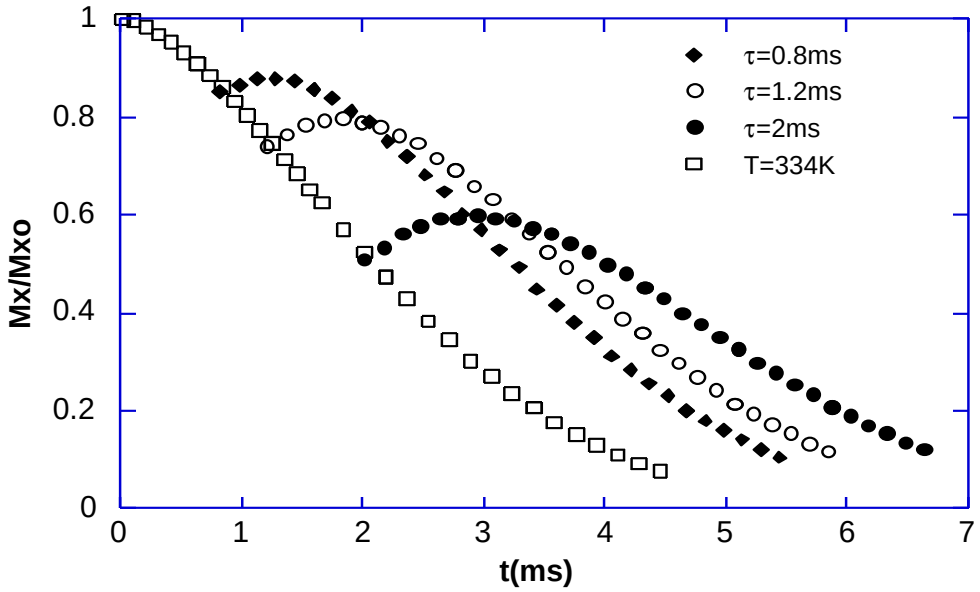

Fig.2. The pseudo solid echoes generated at different instants τ and the relaxation curve observed at T=344K for the molten polymer.

Another element which modify the mobility of the polymeric chain is the solvent. The superposition property of the relaxation functions and the pseudo solid echoes with characteristic properties were also observed for the solutions above T_{ref}. We found T_{ref}=274±5K and T_{ref} - T_g=100±10K for the solution.

The interaction between the solvent molecules and the polymeric links increase the mobility of the chain, so that the dynamics of the chain in the solution, to a given temperature, is greater that the dynamics of the chain in the molten polymer. Generally the interaction between the solvent and the polymeric chain can modify the relaxation mechanism of the transversal magnetization and then the relaxation functions which describe the relaxation process are different for the molten polymer and for the solutions. However in our case we observed an important property of the relaxation curves of the molten polymer and the concentrated solutions.

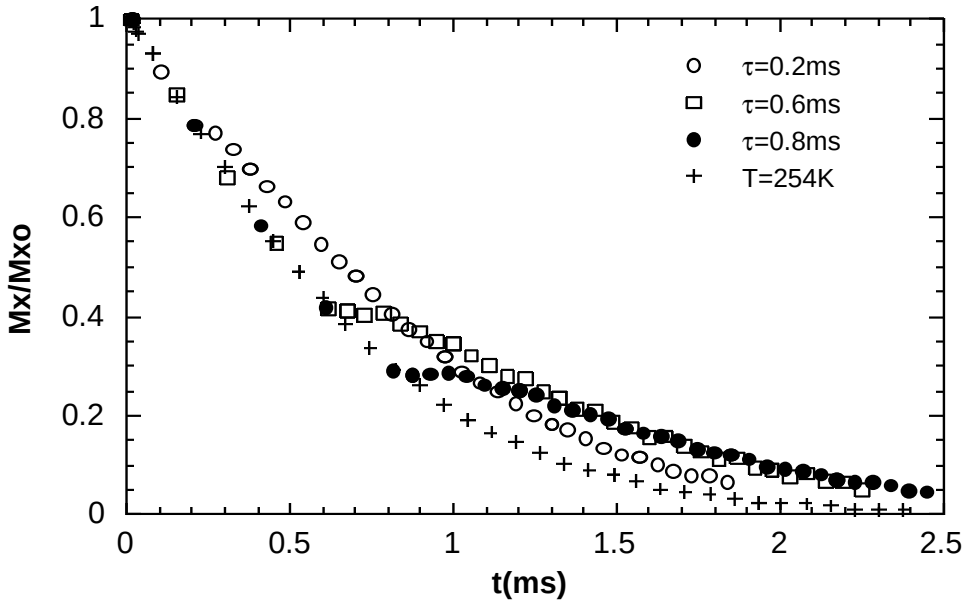

Fig.3. The pseudo solid echoes and the relaxation curve observed for the molten polymer at T=254K.

For a given temperature $T_1 > T_{ref}$ the relaxation curve of the molten polymer can be superposed on the relaxation curve of the solution corresponding to a different temperature T_2, by dividing the time scale with a constant parameter, (Fig.4). The relaxation curve of the molten polymer corresponding at T_1=294K is chosen as a reference. The relaxation curve of the solution correspond at T_2=344K, and its time scale was divided with the factor 2.83. That means that the relaxation process can be described by a single mathematically expression, depending on different variables, for both the polymer and the solution. In this case the dynamics of the polymeric chain in the solution and in the molten polymer are similar. Below T_{ref} this property is not observed. This observation simplify the analyze of the polymeric dynamics above $T_{ref.}$. When the double superposition property, concentration-temperature is observed, we can describe the relaxation process by a single mechanism.

In addition the existence of the pseudo solid echoes with characteristic properties above T_{ref} demonstrate that the relaxation is governed by the residual dipolar interaction.

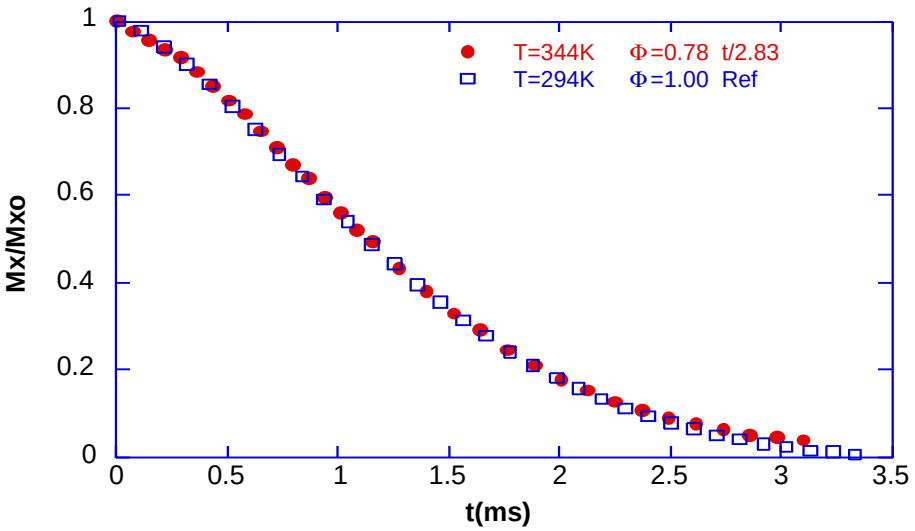

Fig.4. The concentration-temperature superposition of the relaxation curves observed for the molten polymer and for the solution.

CONCLUSION

The shape of the relaxation curves of the transversal magnetization depends on the temperature. For higher temperatures, the relaxation curves of the molten polyisoprene and concentrated polyisoprene-toluene solutions satisfy the temperature to temperature superposition property and the temperature to concentration superposition property. The pseudo solid echoes observed in the superposition domain respect theirs specific properties. In this situation the relaxation process is governed by the same mechanism, the residual dipolar interaction. For lowers temperatures the superposition property is not observed and then the relaxation process is different for the molten polymer and the solutions.

REFERENCES

1. Cohen-Addad, *NMR and Fractal Properties of Polymers Liquids and Gels*, Pergamon Press, London, 1992.
2. Labouriau, J. P. Cohen-Addad, *J. Chem. Phys.*, 94, 3249, 1991.
3. Carr, E. R. Purcell, *Phyd. Rev.*, 94, 630, 1954.
4. Cohen-Addad, C. Schmit, *Polymer*, 29, 883, 1988.
5. Cohen-Addad, *Physical Properties of Polymeric Gels*, John Wiley and Sons, Chichester, New-York, Toronto, 1996.
6. Todica, "Studia", *Physica*, XL 2, 87, 1995.
7. Cohen-Addad, E. Soyez, A. Viallat, J. P. Queslel, *Macromol.*, 4, 25, 1992.

REVIEW ON HIGH AND ULTRAHIGH FREQUENCY PLASMAS USED AS SPECTRAL SOURCES OPERATED AT ATMOSPHERIC PRESSURE

S. D. ANGHEL[1], A. POPESCU[2], A. SIMON[2], D. STĂNILĂ[1]

ABSTRACT. The modalities for generation of plasmas maintained at atmospheric pressure in radiofrequency and microwave electromagnetic fields are reviewed: inductively coupled plasma (ICP) and capacitively coupled plasma (CCP) in the radiofrequency range, and microwave induced plasma (MIP) and capacitively microwave plasma (CMP) in the ultrahigh frequency range. The possibilities to use these plasmas as spectral sources for qualitative and quantitative analysis of gaseous, liquid and solid samples are also presented.

INTRODUCTION

In the last twenty five years the spectral sources based on the gas discharge plasma sustained at atmospheric pressure in the alternative electromagnetic field have had an important role in the analytical spectrometry domain. Thus, inductively coupled plasma (ICP) and microwave-induced plasma (MIP) were successful used as spectral sources in atomic emission spectroscopy [1-4,12,14] and atomic fluorescence spectrometry [5,6] and as ionic sources for mass spectrometry [7,8]. Compared to other spectral sources, ICP has some advantages: very high temperature (8000-10000 K), low spectral interferences, large dynamic range (4-5 orders of magnitude) and very good detection limits (under 1ng.ml-1).

[1] "Babeş-Bolyai" University, Department of Physics, M.Kogălniceanu 1, 3400 Cluj-Napoca, Romania.
[2] Research Center for Analytical Instrumentation, Donáth 67, 3400 Cluj-Napoca, Romania.

Another kind of discharge maintained in alternative electromagnetic field is capacitively coupled plasma (named CCP when it is maintained in a radiofrequency field and CMP in microwave field). It was discovered in 1928 [9] and studied in the 1940s and 1950s [10]. Only in the last twenty years CCP and CMP begin to be used as spectral sources in atomic emission spectroscopy [17-20,25-33], in atomic absorbtion spectrometry [21] and as detector for gas chromatography [22,23]. Although CCP, CMP and MIP did not attained the high temperature of ICP, these techniques promise various possibilities of application because their capabilities of excitation and ionization of liquid and solid samples.

The above mentioned plasmas are gas discharges maintained in alternative electromagnetic fields having frequencies in the radio range (10-100 MHz) or in the microwave range (1-10 GHz), the absorbed power into the plasma being of 0.5-2 kW for ICP and 30-700 W for CCP, CMP and MIP. Their denominations arise from the modality in which the energy of the electromagnetic field is absorbed by the plasma: inductive for ICP (the plasma is assimilated to act as a one-turn secondary coil of a transformer of which primary is a two or three turns coil connected at a high alternative voltage), capacitive for CCP and CMP (the plasma is maintained between the plates of a condenser connected at a high alternative voltage) and inductive combined with capacitive for MIP.

These kinds of discharges can be maintained at atmospheric or subatmospheric pressures, in the first case having a larger applicability, due to its higher temperature and because of the absence of the vacuum installation.

PHYSICAL-CONSIDERATIONS

Assuming that an ionized gas, containing free electrons only, is placed in an alternative electric field, its complex electrical conductivity is expressed by the relationship:

$$\sigma = \frac{n_e e^2}{m_e(\nu_c + j\omega)} \tag{1}$$

where ne is the free electron number density, e and me are respectively the electric charge and the mass of an electron, nc is the electron-atom (molecule) collision frequency and w is the angular frequency of the electromagnetic field. The admittance of the ionized gas:

$$Y_g = A\frac{n_e e^2}{m_e}\frac{\nu_c}{\nu_c^2 + \omega^2} - jB\frac{n_e e^2}{m_e}\frac{\omega}{\nu_c^2 + \omega^2} \tag{2}$$

express its electrical properties, the first term being the active part and the second the reactive part of the admittance. In equation (2) *A* and *B* are constants depending on the discharge tube geometry. The energy absorbed from the electric field per volume unit of ionized gas per second is:

$$w = \frac{n_e E_o^2 e^2}{2m_e}\frac{\nu_c}{\nu_c^2 + \omega^2} \tag{3}$$

in which Eo is the amplitude of the alternative electric field. From equation (3) one can observe the importance of the collisions in the absorption process of energy into the plasma, because in the absence of collisions (nc = 0) the plasma does not absorb energy from the field. When the pressure is low an electron can travel a relatively long distance before it collides with an atom, and in its travel can gain enough energy from the electric field to achieve the excitation or ionization of the atom that it collides. The excited atom decays to the ground state by emitting light, and so the plasma becomes a very efficient light source.

At high pressure (particularly at atmospheric pressure) the mean free path of the electron is much smaller and there are more collisions per atom per second, enough to distribute the kinetic energy uniformly among the electrons, atoms and ions. In such plasma the particles are therefore not only excited and ionized but, as they possess considerable kinetic energy, the plasma is hot. If into a such plasma are introduced (through a certain way) the gaseous, liquid or solid

substances they are firs atomized because of the high temperature, then excited, ionized and finally deactivated.

The two mechanisms that are most often used to describe excitation in the plasma maintained in alternative electromagnetic fields are so-called radiative ionization-recombination sequence and electron impact [15]. The first step in the radiative ionization-recombination process is the Penning ionization, described by the equation:

$$M + Ar^{*} \rightarrow M^{+*} + Ar + e \tag{4}$$

followed by the radiative recombination of the generated ion with a free electron:

$$M^{+*} + e \rightarrow M^{*} + h\nu_{o} \tag{5}$$

In these equations M is an atom, e is an electron, hno is a continuum photon and the asterisk designates an excited state. If the ion generated by Penning step is excited it will decay to give its characteristic radiation:

$$M^{+*} \rightarrow M^{+} + h\nu_{y} \tag{6}$$

Similarly, the atom produced by ion-electron recombination will probably be excited and will yield its characteristic spectral line:

$$M^{*} \rightarrow M + h\nu_{x} \tag{7}$$

The excitation by electron impact can be also described by a two-step process, in which atoms or ions are excited:

$$M + e \rightarrow M^{*} + e \tag{8}$$

$$M^{+} + e \rightarrow M^{+*} + e \tag{9}$$

followed by the desexcitation reaction (7) and (6), and the emission of characteristic radiation hnx and hny respectively.

Ions excitation by electron impact, in the absence of any sort of Penning interaction, can be described by a three-steps process. This mechanism pathway would be initiated by electron impact ionization of atom to yield the ion in either the ground-state or as excited species:

$$M + e \rightarrow M^{+} + 2e \quad (10)$$

$$M + e \rightarrow M^{+*} + 2e \quad (11)$$

The decay of the excited ion on the ground state will be in accordance with equation (6).

All these mechanisms are making possible to use of atmospheric pressure plasmas maintained in electromagnetic fields as spectral sources in analytical spectrometry.

RADIOFREQUENCY-PLASMA

a. *Inductively Coupled Plasma (ICP)*

ICP can be generated when a tube containing a gas is placed into an induction coil energized by a high frequency power generator. Into the induction coil the electric field is the vectorial sum of two components: a longitudinal component Ez, because of the voltage between the two ends of the coil, and a tangential component, Eq, because of the electromagnetic induction phenomenon (Fig.1). When ICP is maintained at atmospheric pressure, the plasma gas (Ar, He) is tangentially introduced into the discharge tube with a flow rate depending on the tube dimensions and the absorbed power into the plasma. The tangential introduction of the gas assures both the cooling of the tube and the turbionary stabilization of the discharge. The gas that sustains the plasma is initially made electrically conductive by Tesla sparks. The created ions and electrons are accelerated by the longitudinal component of the electric field sustaining the

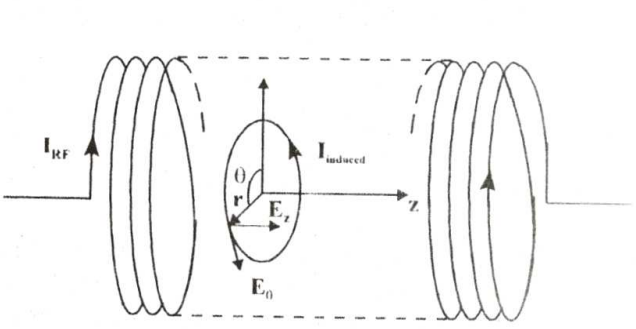

Fig. 1. - Components of the electromagnetic field in an solenoidal coil.

ionization in the flowing direction of the gas and creating a number of open-ended and distinct ion paths. This is the first step of the plasma ignition named "filamentary" phase. If the density of these filaments is sufficiently high and the helicoidal motion is strong enough for their closure, then the plasma will be able to gain additional power from the field by electromagnetic induction phenomenon. This is the second ignition step named "continuous" phase, the plasma having a homogeneous appearance. In this phase both longitudinal and tangential components of the electromagnetic field contribute on maintenance of the discharge. The ionized gas produces a conductive ring capable of absorbing enough RF power to increase further the plasma's ion density and thus to decrease its resistance.This process will continue as long as enough RF power is available and until an equilibrium state is achieved between the impedance of the plasma and the power that can be transferred to the plasma. Now, the plasma is "fully" ignited and the tangential component of the electromagnetic field has the most important role. Thus, the plasma behaves as secondary coil of a transformer whose primary is the induction coil. From electrical point of view the presence of the plasma into the coil will determine an increase of the resistance of the coil, on the one hand, and a decrease of its inductance, on the other hand.

The work coil is typically two or three turns of water-cooled tubing. The RF coil, replacing the classical electrode of an arc/spark discharge, does not come in direct contact with the plasma. In this way, the problem of elemental contamination in the source from electrodes is eliminated. The RF generator to which is coupled the coil is usually operated in the frequency range of 27-50 MHz, with a nominal power output of 1-2 kW. The oscillator and its output circuit sometimes contain only one tuned circuit [34,35]. In this case, a change in the impedance of the plasma modifies the frequency of operation but has very little effect on the power transferred to the plasma. Alternatively, there may be more than one tuned circuit, or there may be a tuned output circuit with crystal-controlled oscillator.

In these cases, a change of the plasma impedance alters the frequency to which the output circuit is tuned and the power transferred to the plasma is reduced unless the tuned circuit is re-tuned to the frequency of the oscillator. It is essential for this re-tuning to be automatically controlled. If this is done, there is not much to choose between the free-running or crystal-controlled generators.

When ICP is used as spectral source, the discharge is ignites into three concentric quartz tubes, system named "the torch" (Fig.2). The main argon flow is the plasma gas-flow (12-18 l.min-1), which has the dual function of supplying the argon that maintains the plasma and to provide a heat shield in order to protect the outer quartz tube of the torch against the high temperature of the plasma (8000-10000 K). An intermediate argon gas flow (0-1 l.min-1) may be used to adjust the vertical position of the plasma. The sample is introduced in the center of the plasma by means of the carrier gas-flow (1-2 l.min-1).

Liquid samples are converted by a nebulizer (pneumatic or ultrasonic) to an aerosol with particles of varying diameters. Spray droplets with diameters up to a few micrometers only are selected by a spray chamber to be carried to the plasma by the carrier gas-flow, while larger droplets are removed through the drain. Solid samples on the other hand can be vaporized by means of laser ablation, a spark source or a glow discharge. In both cases the aerosol and vapours are transported to the plasma by the carrier gas-flow and are introduced in its center. Due to the "skin" effect the plasma has a torroidal shape and its center is relatively cool, which facilitates the introduction of the sample (Fig.3).

After penetrating in the core of the plasma the aerosol is desolvated, dissociated, atomized (in the preheating zone) and excited (in the initial radiation zone). While the sample passes through the plasma the various excited ionic and atomic species relax to their ground states emitting characteristic radiations. For analytical purposes, the initial radiation zone and the analytical zone are considered to have a great importance.

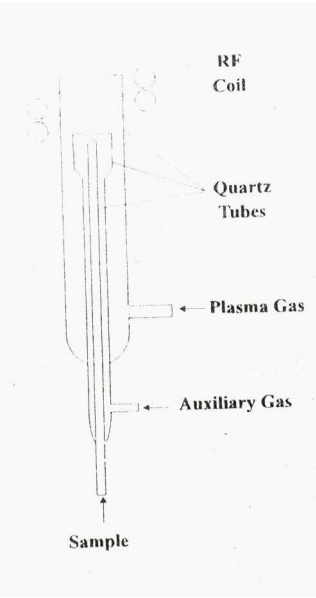

Fig.2. - Conventional torch for ICP

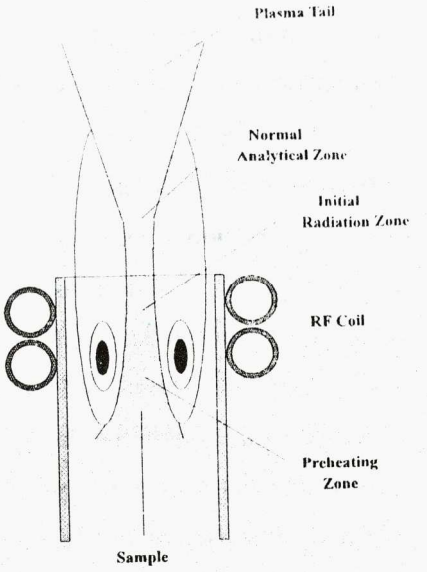

Fig.3. - Characteristic zones of ICP

b. *Capacitively coupled plasma*.

Capacitively coupled plasma or radiofrequency (RF) capacitive torch is a form of the plasma that could appear accidentally in the RF generators working at relatively high power (102-104 W), or that could be ignited deliberately with the aim of studying the ignition and maintaining mechanism, the electric characteristics or its temperature. It also can be used in analytical purposes. This kind of discharge could appear between the plates of a condenser connected at a high RF tension, or on sharp edges where the electric field is particularly intense. In the last instance it is sufficient to use a single electrode (the sustaining electrode of the plasma), the presence of the second electrode being not necessary, the RF current is closing through earth or ground clamp. If it exists, the second electrode can have different geometric forms (plate, disc, ring or sharp tip), the discharge being or not in contact with it. Many kinds of CCP are operated at different pressures, frequencies, consumed powers, the electrodes having different forms, each of these parameters being a classification criterion.

In the present work are presented some CCP at atmospheric pressure, maintained in the industrial frequency bands of 13.56, 27.12 and 50 MHz.

In the RF range one had in view the construction of generators capable of maintaining plasmas at atmospheric pressures on conditions that the total power consumption should be very low (under 100 W) and to find efficient methods for sample introduction into the plasma. The authors of the paper [21] have obtained a CCP contained in a 20 cm in length quartz tube (0.4 i.d. and 0.5 cm o.d). Power is coupled into the plasma by using two stainless steel strips, 18 cm long and 0.5cm wide, which are placed parallel to each other on either side of and in contact with the outside of this quartz tube (Fig.4).

These electrodes are connected to the RF ower supply through a coil inductively coupled with the coil of oscillating circuit. A stable plasma can be sustained at RF powers from 30 to 600 W and at a frequency of 27.12 Mhz. Plasma support gas (Ar, He, and mixtures of these gases with N_2, H_2 and air) is introduced by using an inlet on side of the main body of quartz container with flow rates ranging from 0.2 to 0.6 l.min-1. The sample is introduced into the plasma through electrothermal vaporization. Using a micropipet, before the ignition of the discharge, the sample is placed on an electrically heated tantalum strip that offers the possibility that the sample vaporization and atomization can be separated and independently optimized. A cycle of sample introduction has three steps: the drying, the ashing

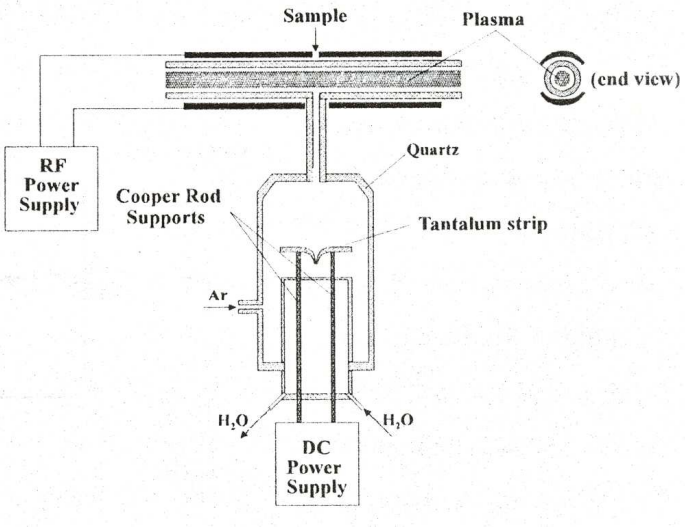

Fig.4. - CCP source for atomic absorbtion spectometry.

and the atomization. The plasma is ignited at the end of the ash step and is measured its time-response by Atomic Absorption Spectrometry (AAS) method, the discharge being longitudinal traversed by a beam from a hallow-cathode lamp. The detection sensitivities (picograms range) are comparable with that obtained through atomic absorption measurements using conventional graphite furnace.

The same authors [19,20] combine the high efficiency of atomization in electrothermal atomizers with the high efficiency of excitation in RF plasmas. They have designed an excitation source with atomization in graphite furnace for plasma emission spectroscopy (FAPES), whose schematic diagram is presented in Fig.5.

This source consists of an electrothermal atomizer (the furnace) and a RF discharge (CCP). The graphite furnace is heated using a conventional power supply and it acts as a vaporization device. To form a plasma inside the furnace, a 1 mm diameter thoriated-tungsten rod was inserted along the center axis of the graphite furnace. The RF power supply was connected through a matched impedance between the graphite furnace and the central electrode, the plasma being in contact with both electrodes.

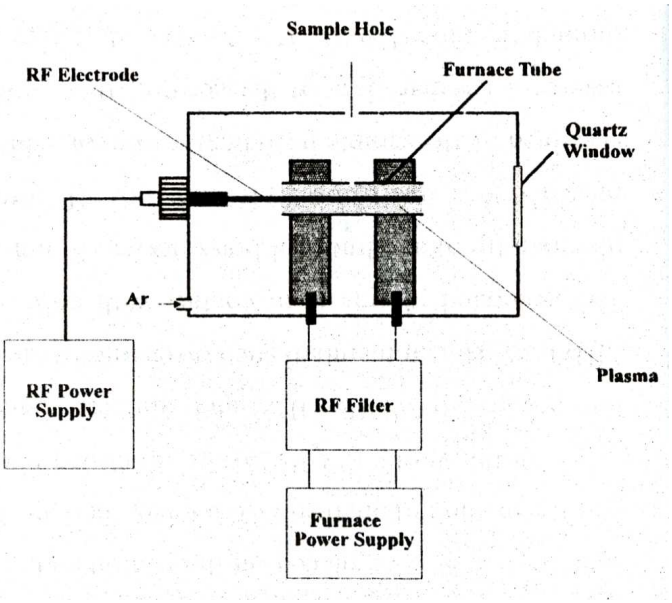

Fig. 5. - Schematic diagram of RF-Fapes source

The working frequency was 27 MHz, the power into the plasma was in the range of 10-100 W and the gas flow-rate (Ar) was 1 l min-1. While solid and liquid samples can be placed on the inner surface of the furnace tube, liquid samples can also be placed on the central rod. The detection sensitivities (AES was the method of analysis) were lower than one picogram for some elements.

In the works [29,30,36] are described two types of CCP sources, one of low power (30 W, 12 MHz) and another of mean powers (100-500 W, 27.12 MHz), which can maintain such discharges in air, Ar or a mixture of Ar and air. The generated plasma is in contact with only one electrode, which is a sharp platinum tip of a cylindrical brass device (8 mm o.d. and 60 mm in length). It is placed into a quartz tube (15 mm i.d., 18 mm o.d. and 100 mm in length) sustained by the sample introduction system, which is made of teflon (PTFE) and assures a laminar flow of the aerosol (the liquid sample pneumatic nebulized) through the tube (Fig.6). At a distance of 45 mm from the platinum tip the quartz tube is surrounded by an annular counterelectrode that assures the symmetry of the electromagnetic field lines, therefore the symmetry of the discharge. The carrier gas, which is the plasma support gas too, has a flow-rate of 1.5 l.min-1.

In contrast to previous discharges that have a homogeneous appearance, this RF discharge has four characteristic zones (Fig.6). In immediate proximity of the plasma sustaining tip one can observe a thin blue-violet layer, named superficial luminescence, with a thickness lower than 1 mm and which has all characteristics of a normal drop tension. The proper plasma consists of a thread-form core, which has the highest temperature (3500-4000 K) [37] and which in argon is brilliant-white, and a blue-light sheath, less brilliant and cooler than the core, and which surround it.

The last two zones are separated by the superficial luminescence through a dark space similar to the dark spaces of luminescent discharges in continuous current.

From analytical point of view the core and the luminescence of the plasma are important. In the core zone, the elements introduced into the plasma through pneumatic pulverization are atomized, excited and ionized.

The aerosol introduction is doing through a system that has twelve holes concentrically disposed with the sustaining tip of the plasma, and which assures the laminar flow of the carrier gas without disturbing the plasma.

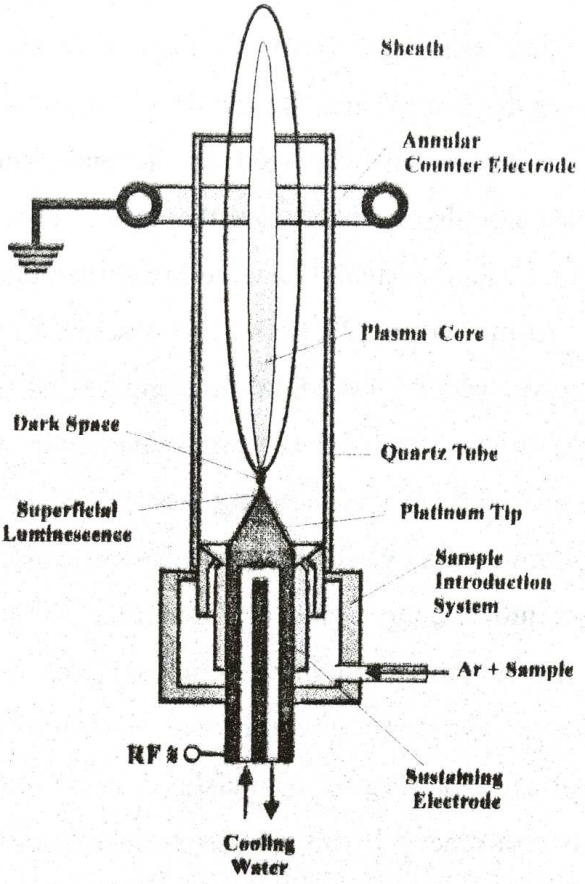

Fig. 6. - Cross section diagram of CCP torch.

Into the plasma can be introduced a low amount of auxiliary gas (with a flow-rate lower than 0.5 l.min-1) for optimize the excitation conditions for some elements. The analysis is done with the help of AES method, the detection limits being in the range of ng.ml-1 to mg.ml-1 [31]. The superficial luminescence is important because the positive ions, accelerated in its very intense field, collide the sustaining electrode and break loose atoms from this. These atoms penetrate into the superficial luminescence and into the core of the plasma, then they are excited or even ionized. Consequently, this experimental arrangement has been used for direct analysis of conductive samples [32]. The obtained detection limits are in the range of 10-3-10-2 % for eight elements.

MICROWAVE PLASMA

Microwave discharges were first observed during the early 1940's by physicists and electrical engineers as unwanted and disturbing effects in the development of RADAR equipment. Microwave plasmas are produced by interaction of electric fields at ultrahigh frequencies (usually 2450 MHz) with gases. Microwave plasmas can be classified into two groups: microwave-induced plasmas (MIP) and capacitively coupled microwave plasmas (CMP). Both types of microwave-supported discharges can be classified as working at low or medium power and at atmospheric or reduced pressures.

a. *Microwave induced plasma*

A microwave-induced plasma is usually an electrodeless discharge generated in a glass, quartz or ceramic tube, having an inner diameter on the order of few millimeters to a few centimeters. The microwave energy can be transferred to the plasma using a resonant cavity, a coaxial waveguide or another microwave structure coupled with a rectangular waveguide powered by a magnetron (microwave generator).

In the first case, the purpose of the resonant cavity is to enable the formation of astanding electromagnetic wave such that the field strength is maximized in the vicinity of the plasma torch. The resonant modes of these cavities can be classified as transverse electric (TE) or transverse magnetic (TM) modes. However, often the modes cannot be separated into purely TE or TM and are therefore called hybrid modes. The cavity which has become the most popular means of forming analytical microwave plasma is TM010 [24,38]. This is an efficient cavity which could be used to form a plasma in either argon or helium , at atmospheric pressure, and at quite low input powers (40-100 W). A schematic diagram of this cavity is shown in Fig.7. It has a shape of a pillbox and consists of a cylindrical wall with a fixed bottom and removable lid.

The discharge tube (the torch) is mounted in the center of the cavity, perpendicular to the cylindrical walls.

Microwave energy is transferred to the cavity through a coupling loop which consist of a 1mm-thick cooper wire. Cavity resonance is achieved using either a tuning stub in the bottom of the cavity or a stub through the cylindrical wall.

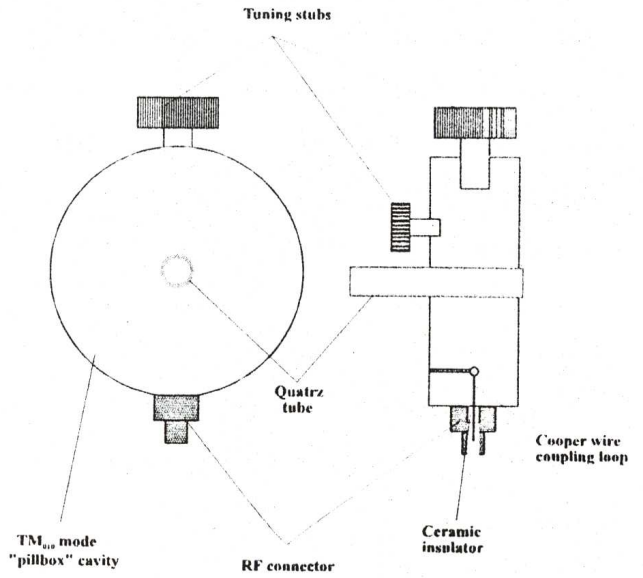

Fig. 7. - Schematic diagram of the TM010 mode cavity for MIP.

In the second case, the microwaves generated by a magnetron are transferred to a helical coil through a uniline, directional coupler, three-stub tuner, taper waveguide and a mode transformer, and are absorbed as circularly polarized waves by the plasma through a discharge tube placed inside the helical coil [4].

A schematic diagram of the mode transformer is shown in Fig.8. It consists of two parts: one is a plane rectangular waveguide with a reduced height for impedance matching between the resultant impedance of the helical coil together with the plasma and that of the microwave source; the other is a coaxial waveguide with an impedance of 50 W, coupled with the rectangular waveguide. One end of the helical coil (two turns) is connected to the inner conductor of the coaxial waveguide, and the other is terminated at the front-end plate of the outer conductor.

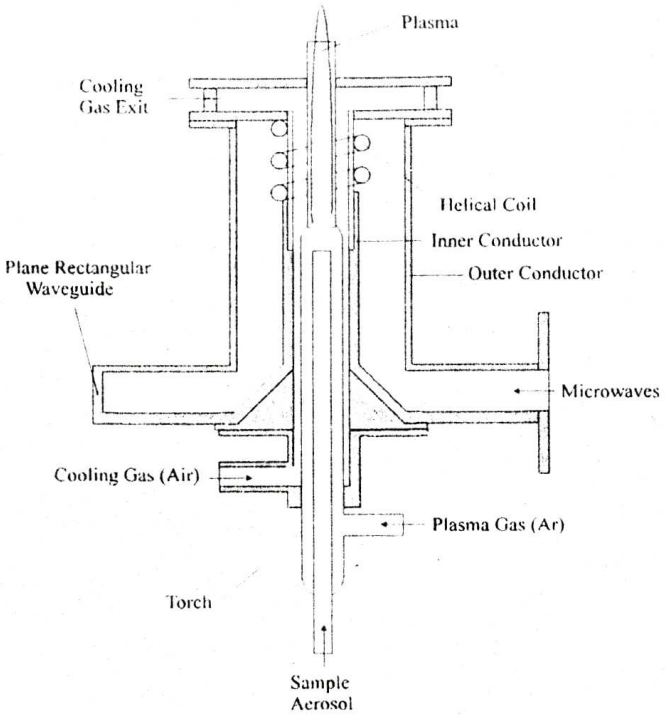

Fig. 8. - Schematic drawing of the helical coil-type microwave induced plasma.

The torch consists of two concentric quartz tubes and it is air cooled. The flow-rate of the carrier gas (Ar) for the aerosol injection is 0.35-0.5 l.min-1. The cooling air flow-rate is 60-70 l.min-1. Another structure for generating microwave induced plasmas is the surfatron, whose schematic diagram is reproduced in Fig.9. The structure can be viewed as a length of a coaxial transmission line, terminated at one end by a short-circuit and at the other end by a capacitive gap. The electric field is imposed by an electromagnetic surface wave propagating along the discharge tube. No external wave guide structure is needed, because the interface between the plasma and surrounding dielectric constitutes such a guide. The structure has a symmetry and shape capable of launching an azimuthally symmetric surface wave from the gap region along the length of the discharge tube. Tuning the surfatron is accomplished by moving the short circuits to the length of the cavity. The surface wave plasma is quite stable, since only one mode of propagation is allowed. The surfatron can be operated over a broad range of frequencies (27 MHz to 10 GHz) and a gas pressure (between 10-4 torr and a few times the atmospheric pressure). The consumption power is up to 300W.

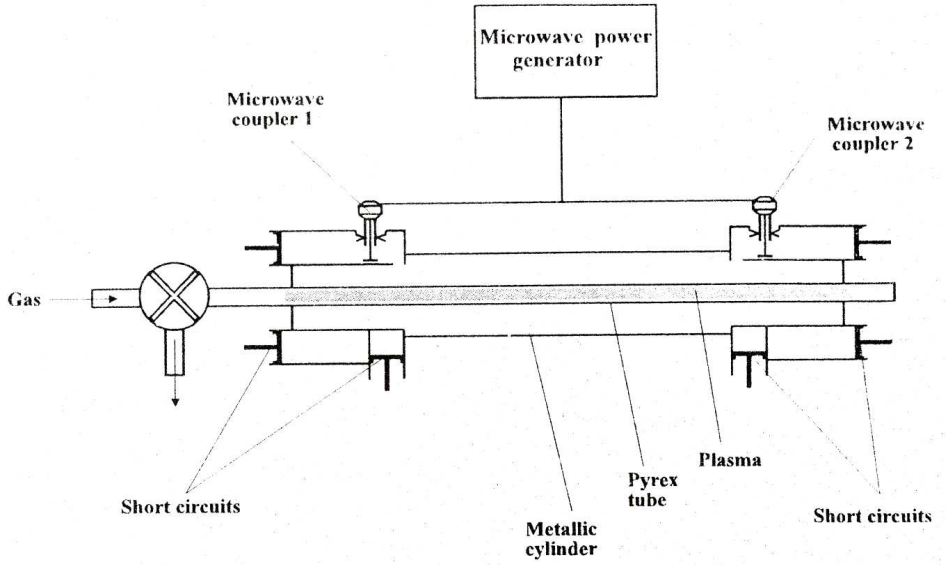

Fig. 9.- Cross section of a surfatron cavity.

For a 100 W microwave induced plasma at atmospheric pressure, the excitation temperatures are about 5000 K for Ar and 7200 K for He, and the electron densities are in the range of 1014-1016 cm-3. This plasma has been used for analysis of gaseous, liquid and solid samples, the detection limits being in the range of 10-3-103 ng.ml-1 [14].

b. *Capacitively coupled microwave plasma*

In the capacitively coupled microwave plasmas (CMP), a magnetron generates microwaves through a coaxial waveguide, via a rectangular waveguide, to the tip of a central single electrode where a flamelike plasma is formed. The central electrode can be made of Pt, W, Al, graphite or other conductive materials. It has been developed two types of the electrode configuration: in one the electrode is a rod with a sharp tip, and the sample and the carrier gas diffused into the plasma gas in the lower part of the torch bellow the solid single electrode tip [11,12], and in the other one in that is used a tubular central electrode through which the sample carried by the carrier gas is introduced directly into the plasma [16-17]. The direct introduction of sample into the plasma flame has greatly improved sample-plasma interactions, increased concentration of analytes in the

plasma viewing region, and improved signal-to-background ratio, signal-to-noise ratio and detection limits.

In the work [17] is presented a CMP from the second category, the absorbed power into the plasma being of 600 W. This power is necessary because at the powers lower than 400 W the density of energy inside the plasma isn't sufficient to assure the vaporization and atomization of the liquid and the solid samples, and the introduction of the aerosol solutions often causes an impedance mismatch of the system, thereby extinguishing the plasma. In Fig.10, a schematic diagram of the plasma system is given. The torch is likewise that used in ICP, having two tubes only. It is made of quartz, and a 5 cm long graphite tube is located on the top of the inner tube. This graphite tube is the sustaining tip of the plasma, too. The glass chimney is used to improve the plasma stability by minimizing air drafts. The chimney, 80 mm i.d. and 180 mm high, has quartz windows to enable measurement of the plasma emission. The sample was introduced by a concentric nebulizer into a spray chamber and swept by plasma torch.

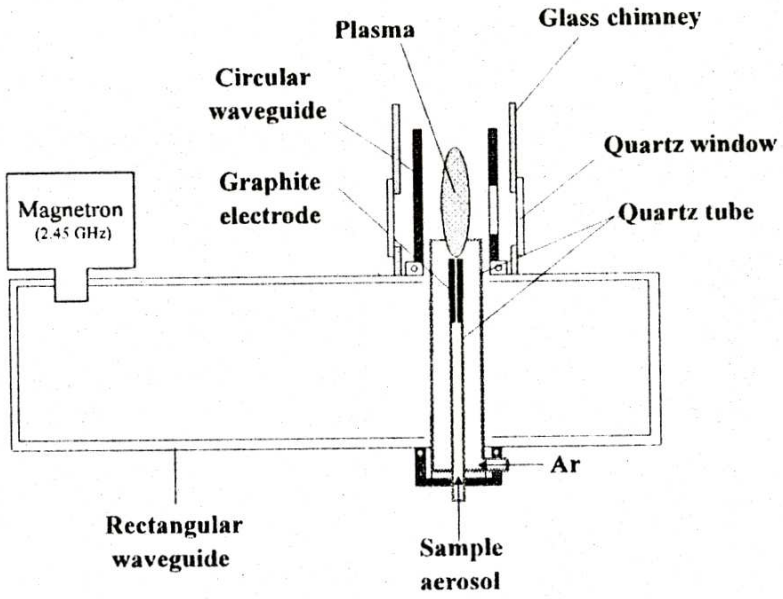

Fig. 10. - Shematic diagram of the generator for capacitively coupled microwave plasma.

The carrier gas into the plasma gas and the carrier gas (He) flow-rates were kept at 6 l.min-1 and 0.4 l.min-1 respectively. The observation height is just above the top of the electrode since the signals obtained in this area are maximal. The sample was analyzed using the AES methods, the detection limits being in the ng.ml-1 range.

At last, in the work [25] the authors present a FAPES system similar to that described in the works [19] and [20], but working in the microwave range (2450 MHz). Unlike the previously described CMP system, here the plasma is in contact with both discharge electrodes. Fig.11 presents a schematic diagram of this spectral source, in which the plasma fills uniformly the graphite tube over the length of the central electrode. With this arrangement a forward power of 50-70 W could be easily tuned for zero reflected power. The central electrode terminated in a 2.9 cm length of 1 mm diameter pyrolytic graphite coated electrographite which traversed the length of the pyrolytic coated graphite tube.

The solutions were injected on the wall of the furnace, then were dried, atomized and analyzed through AES methods, the detection limits being in the 101 pg range. Helium was used for both external sheath at a flow rate of 1.5 l.min-1 and internal purge gas, which served as the plasma support gas, at flow-rates among 50 and 360 ml.min-1. Because of long therm stability of this plasma, the authors suggest its successful use as sputtering cell for the analysis of solids.

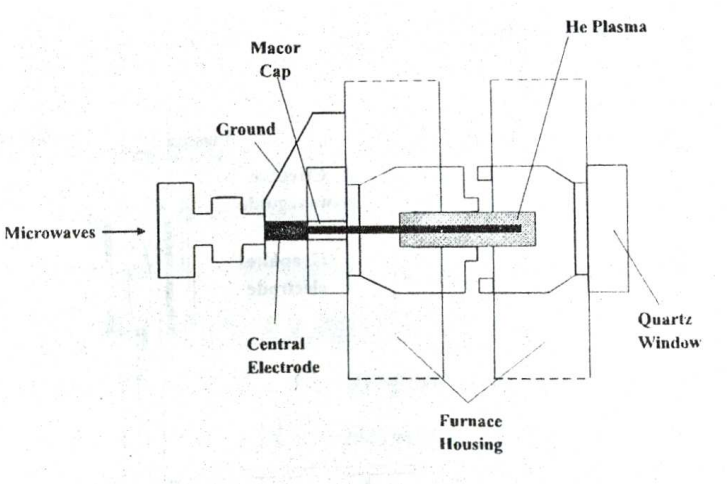

Fig. 11. - FAPES workhead for microwaves.

CONCLUSION

Plasmas maintained at atmospheric pressure in radiofrequency and microwave fields represent a spectral sources category with increase attractiveness in qualitative and quantitative analysis. Due to their superior excitation and ionization capabilities (comparatively with the traditional sources), analytical performances are very high and almost all the known elements can be analyzed. As methods for analysis of gaseous, liquid and solid samples can be used atomic emission (absorption) spectroscopy, mass spectrometry and gas chromatography.

Between the modern spectral sources, inductively coupled plasma is the most performant but also the most expensive. Due to the low price to performance ratios of microwave plasmas compared with ICP's, further investigation is required to elucidate problems associated with these modern spectral sources.

The authors hope that this short review will serve both as a useful information source and as a starting point to the future development of these kinds of plasmas.

REFERENCES

1. V. A. Fassel, *Anal. Chem.* **46**, 1155A (1974).
2. S. Greenfield and H. McD. McGeachin, *Chemistry in Britain* **16**,653 (1980).
3. R. A. Meyer, *Anal. Chem.* **59**, 1345A (1987).
4. Y. Okamoto, M. Yasuda and S. Murayama, *Jpn.J. Appl. Phys.* **29**, L670 (1990).
5. A. Montaser and V. A. Fassel, *Anal. Chem.* **48**, 1490 (1976).
6. D. R. Demers, *Spectrochim. Acta* **40B**, 105 (1985).
7. R. S. Houk, V. A. Fassel, G. D. Flesch, H. G. Svec, A. L. Gray and C. E. Taylor, *Anal. Chem.* **52**, 2283 (1980).
8. A. L. Gray, *Spactrochim. Acta* **40B**, 1525 (1985).
9. K. Baxter, *Radio News* 1204 (1928).
10. R. Grigorovici and G. D. Cristescu, *Rev. Roum. Phys.* **4**,153 (1959).
11. Yamamoto and S. Murayama, *Spectrochim. Acta* **23A**, 773 (1967).
12. Murayama, *J. Appl. Phys.* **39**, 5478 (1968).

13. W. J. M. B o u m a n s, F. J. de B o e r, F. J. D a h m e n, H. H o e l z e l and A. M a y e r, *Spectrochim. Acta* **30B**,449 (1975).
14. T. Z a n d e r qnd G. H i e f t j e, *Appl. Spectrosc.* **35**,357 (1981).
15. M. H i e f t j e, G. D. R a y s o n and J. W. O l e s i k, *Spectrochim. Acta*, **40B**, 167 (1985).
16. M. P a t e l, E. H e i t h m a n and J. D. W i n e f o r d n e r, *Anal. Chem.* **59**, 2374 (1987).
17. D. H w a n g, W. M a s a m b a, B. W. S m i t h and J. D. W i n e f o r d n e r, *Canad. Journ. Spectrosc.* **33**, 156 (1987).
18. H. A l i, K. C. N g and J. D. W i n e f o r d n e r, *J. Anal. Atom. Spectrom.* **6**, 211 (1991).
19. L. S m i t h, D. C. L i a n g, D. S t e e l and M. W. B l a d e s, *Spectrochim. Acta* **45B**, 493 (1990).
20. C. L i a n g and M. W. B l a d e s, *Spectrochim. Acta* **44B**, 1059 (1989).
21. C. L i a n g and M. W. B l a d e s, *Anal. Chem.* **60**, 27 (1988).
22. H u a n g, D. C. L i a n g and M. W. B l a d e s, *J. Anal. At. Spectrom.* **4**, 789 (1989).
23. H u a n g and M. W. B l a d e s, *J. Anal. At. Spectrom.* **6**, 215 (1991).
24. W. B l a d e s, P. B a n k s, C. G i l l, D. H u a n g, C h. l e B l a n c and D. L i a n g, *IEEE Trans. Plasma Sci.* **19**, 1090 (1991).
25. E. S t u r g e o n, S. N. W i l l i e, V. L u o n g and S. S. B e r m a n, *J. Anal. At. Spectrom.* **4**, 669 (1989).
26. E. S t u r g e o n, S. N. W i l l i e, V. L u o n g and S. S. B e r m a n, *Anal. Chem.* **62**, 2370 (1990).
27. E. S t u r g e o n, S. N. W i l l i e, V. L u o n g and J. G. D u n n, *Appl. Spectrosc.* **45**, 1413 (1991).
28. E. S t u r g e o n, S. N. W i l l i e and V. L u o n g, *Spectrochim. Acta* **46B**, 1021 (1991).
29. T ă t ă r u and S. D. A n g h e l, Vol. *Conf. Nat. Fiz.* pp. 100, Cluj-Napoca, Romania (1990).
30. C o r d o ¿, S. D. A n g h e l and A. F o d o r, *XXVII Coll. Spectrosc. Intern.* Vol. C.22, Bergen, Norway (1991).
31. A. C o r d o ¿, S. D. A n g h e l, T. F r e n ţ i u and A. P o p e s c u, *J. Anal. At. Spectro*m. **9**, 635 (1993).
32. D. A n g h e l, T. F r e n ţ i u, A. M. R u s u, L. B e s e and E. A. C o r d o ¿, *Fresenius J. Anal. Chem.* (in press).
33. H. B i n g s and J. A. C. B r o e k a e r t, *Fresenius J.Anal.Chem.* (in press).
34. D. A n g h e l, A. P o p e s c u, F. R a c z, E. T a t a r u and E. A. C o r d o š, *Rev.Chim.* **40**,344 (1989).
35. D. A n g h e l, Studia Univ. Babe¿-Bolyai, *Physica*, **XXXVIII**, 39 (1993).
36. T ă t ă r u, S. D. A n g h e l and I. I. P o p e s c u, *Rev. Roum. Phys.* **36**, 29 (1991).
37. D. A n g h e l, T. F r e n ţ i u, E. D a r v a s i, A. M. R u s u, A. S i m o n and E. A. C o r d o ¿, *Fresenius J. Anal. Chem.* (in press).
38. M a t u s i e w i c z, *Chem. Anal.* (Warsaw) 40, 667 (1995).

SOME FUNDAMENTAL CHARACTERISTICS FOR A RF CAPACITIVELY COUPLED ARGON PLASMA WITH TIP - RING ELECTRODE GEOMETRY

S. D. ANGHEL[*], E. A. CORDOŞ[**], T. FRENȚIU[**], A. M. RUSU[**], A. SIMON[***], E. DARVASI[***]

ABSTRACT. The excitation and ionisation temperatures and the electron number densities for a capacitively coupled RF plasma, sustained in Ar at atmospheric pressure, with tip-ring electrode geometry, is presented. The plasma was operated at 185 W, 27.12 MHz and 1 l/min gas flow-rate. The spectroscopically observed and investigated zone was the plasma core. Measurements were done, as function of observation height (h), for different tip-ring distances (H). The excitation temperatures for Ar were determined to be in the range of 2000-3500 K and the values of ionization temperatures in the range of 3700-4700 K. The excitation temperatures for Fe I were determined to be in the range of 3700-4700 K. The ionization temperature for Ca at an observation height of h = 18 mm was 4400 K and 4600 K for H = 10 and 40 mm respectively. Electron number densities were determined to be in the range of 2-6 $x10^{14}$ cm^{-3}.

INTRODUCTION

A gas may be regarded to be a plasma if it is ionised sufficiently for its properties to depend significantly on the ionization, the gas remaining electrically neutral macroscopically [1]. The important property of a plasma, for spectroscopic purposes, is those large quantities of electrical energy that can be transferred to it, if it is sufficiently ionised - this supply of energy will heat it to very high temperatures.

[*]University "Babeş-Bolyai", Departament of Physics, str.M.Kogălniceanu 1, 3400 Cluj-Napoca, Romania.
[**]University "Babeş-Bolyai", Departament of Chemistry, str.Arany Janos 11 and Research Institute for Analytical Instrumentation, 3400 Cluj-Napoca, Romania.
[***]Research Institute for Analytical Instrumentation, str. Donath 67, Of.P5, P.O.Box, 717, E-mail: caa@re.ro, 3400 Cluj-Napoca, Romania.

The effects of high temperatures on gases are dissociation if the gas is not monoatomic, followed by ionizations and excitations [2].

From the point of view of macroscopical investigation, the plasma is electrically neutral and containing: electrons; neutral atoms (in both ground and excited states); ions (in both ground and excited states) and photons (as a result of.relaxation processes). The distribution of these particles, as function of energy, is depending on a parameter called *absolute temperature* [3]. Plasma contains a number of different kinds of particles. Naturally it is possible and obvious to have a certain number of different distributions, and consequently, a similar number of parameters will be necessary to describe each of those distributions.

In a plasma, sustained by a monoatomic gas, there may be four kinds of *temperature*s [3]. The electron temperature (T_e) and kinetic (Doppler or gas) temperature (T_{kin}) will describe the kinetic energy distributions of electrons and gas particles (atoms and ions). The the excitation temperature (T_{exc}) will be necessary to describe the relative populations of the different energy levels of a given element and the ionization temperature (T_{ion}) to characterise the ionization equilibra. If the plasma gas is bi- or poliatomic, two more temperatures could be introduced. The rotational temperature (T_{rot}), which will governing the populations of the rotational levels, and the vibrational temperature (T_{vibr}), which will governing the populations of the vibrational levels. When all this temperatures has the same values, the system (plasma) is said to be in a state of thermodynamic equilibrium.

Thermodynamic equilibrium is an idealised state that can not be observed in reality. In spite of the well-known fact that a spectral source in local thermodynamic equilibrium (LTE) is considered to be not essential for spectrochemical analysis, this special state could be desirable on four major counts [4]: the effects of instabilities in the source is likely to be minimised , in this state the freedom from chemical interferences is almost perfect, the behaviour of a given element - introduced in the plasma - is more predictable and

in certain circumstances, some laws deduced for systems in thermodynamic equilibrium can be successfully applied to systems that are not in this state.

Electron number density (n_e) is a measure of the number of free electrons per cm^{-3} and is considered to be a fundamental parameter, largely independent from the temperature and any assumptions about the existence of LTE [4]. Consequently, if LTE exists, n_e will uniquely define the common temperature of the system. In plasmas, n_e will be the indicative of the degree of ionization. Several researchers have determined the electron number density in radiofrequency and microwave supported plasmas applying the most frequently used method: Stark broadening of the hydrogen Balmer β ($\lambda_{H\beta}$ = 486.13 nm) line [5]. Values of n_e could be determined using: the "line-to-continuum" method [6,7]; the spectral radiance of the continuum, via Kramers-Unsöld equation [8,9]; the series limit merging method [10] or the Thomson-Rayleigh scattering measurements [11].

All these considerations, presented above, are applicable for a radiofrequency capacitively coupled plasmas (RF CCP), sustained at atmospheric pressure, with tip-ring electrode geometry. The characteristic temperatures and the electron number density of this specific RF discharge are not very well known and consequently the excitation, ionization and emission processes are difficult to understand.

Therefore the aim of this paper is that to determine the excitation temperatures for Ar and Fe I, the ionization temperatures for Ar and Ca and to estimate the electron number density using only spectral line intensity measurements. At the same time, it was kept in view to determine the variations of temperature as function of observation height (h) and tip-ring distance (H), with the purpose of determining the optimum working parameters for the spectrochemical analysis.

EXPERIMENTAL

2.1. Instrumentation and operating conditions. The schematic diagram of the experimental set-up is presented in Fig.1. The plasma was obtained and operated with a 27.12 MHz RF generator, designed initially for ICP and later adapted for RF CCP [12]. The RF discharge was maintained between a water-cooled electrode, with a sharp platinum tip, connected to the ground.

Thermometric species were introduced into the plasma, using a concentric pneumatic nebulizer (Meinhard-type) in a 120 ml nebulization chamber, through a specially designed polytetrafluoroethylene (PTFE) device [13,14]. More details of the instrumentation and operating conditions are presented in Table I and Table II, respectively in reference [15]. The correction for the spectral response of the spectrometric system was made with a spectral iradiance standard lamp EPI 1604.

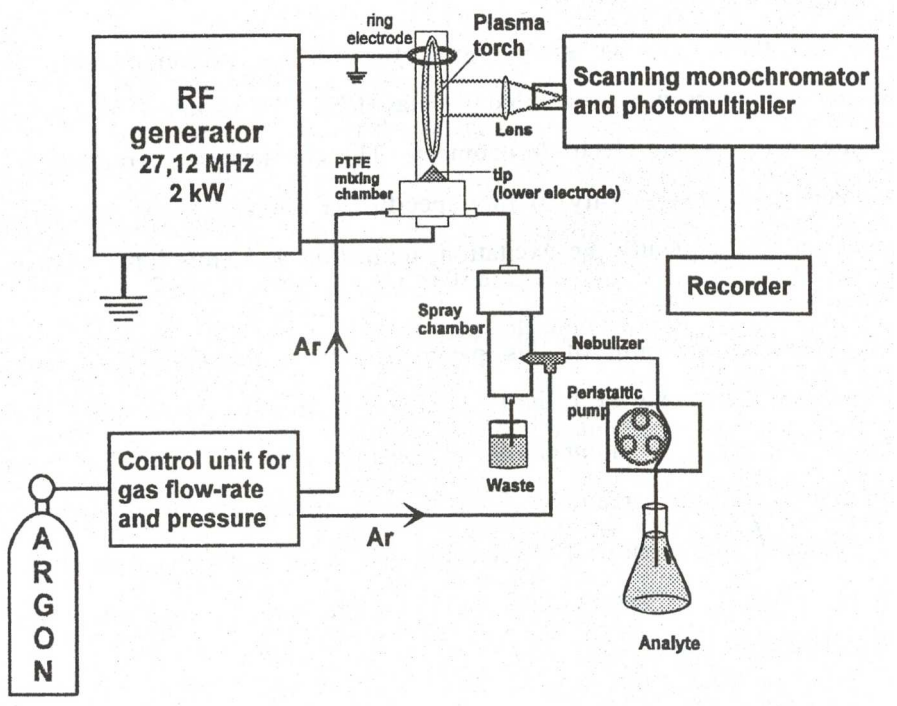

Fig.1 - Experimental setup.

Table I. Instrumentation

Apparatus	Model	Manufacturer
Plasma power supply:		
RF generator 27.12 MHz, 2 kW, free-running Colpitts type, modified for capacitive coupling and for operating at low power.(85 - 275 W)	EOP ICP	Research Institute for Analytical Instrumentation, Cluj-Napoca
Plasma torch:		
• water-cooled central electrode: 8 mm diameter, tungsten tip 90^{o} tip angle • quartz tube: 15 mm i.d., 200 mm length • brass ring counter electrode: 25 mm i.d.		Laboratory constructed
Nebulizer and analyte introduction system:		
• nebulizer: pneumatic concentric type • 120 ml glass nebulization chamber • 8 roller peristaltic pump • PTFE mixing chamber, with 12 concentric holes, 1.3 mm diameter		Research Institute for Analytical Instrumentation, Cluj-Napoca
Optics for spectra recording:		
• scanning monochromator: 35 m focal length, 1200 groves / mm grating	EU 700	Heath Co., Benton Harbor, MI, USA
• photomultiplier tube (operated at 600 V)		RCA
• photomultiplier high voltage power supply	1 P 28 EU 701	Heath Co., Benton Harbor, MI, USA
Recorder	K 201	Zeiss-Jena, Jena, Germany

Table II. Operating conditions

Frequency	27.12 MHz
Forward RF power	185 W
Capacitively coupling system	Tip-ring geometry
Plasma support gas	High purity Ar
Ar flow-rate (plasma support; sample nebulization)	1 l/min
Sample uptake rate	0.8 l/min, 10% nebulization efficiency
Focusing	quartz lens
Observation zone	plasma core (~ 2 mm width)

2.2.Procedure. The Ar excitation temperature was estimated from the slope of the Boltzmann plot, using seven neutral atom lines that are covering the wavelength-range 383.50 - 451.07 nm. For measurements the basic assumption is that excitation is thermal. Excitation temperature could be calculated from the slope of a regression line fitted according to the following equation:

$$\log\left(\frac{\mathbf{I\lambda}}{\mathbf{gA}}\right) \propto \mathbf{f}\left(\mathbf{E_{exc}}\right) \tag{1}$$

where I is the corrected line intensity; λ - the transition wavelength; g - the statistical weight of the higher level; A - the probability of spontan emission and E_{exc} - the excitation energy of the upper level of the observed transition. Table III summarises the spectroscopical data for the Ar lines used (values were compilated from several sources [16,17,18]).

Excitation temperatures for Fe I lines were calculated from the slope of the Boltzmann plot, using the following equation:

$$\log\left(\frac{\mathbf{I\lambda^3}}{\mathbf{gf}}\right) \propto \mathbf{f}\left(\mathbf{E_{exc}}\right) \tag{2}$$

where I, λ, g and E_{exc} were explained above and f is the oscillator strength.

Table III. Spectroscopic data for Ar I lines

λ [nm]	Eexc [eV]	gA 10-6 [s-1]
383.50	15.088	0.8
404.44	14.716	0.3255
425.12	14.491	0.339
427.22	14.552	0.71
430.01	14.510	1.97
434.50	14.708	0.939
451.07	16.603	1.02

For this purpose seven Fe I lines were selected. Spectral data for these lines are presented in Table IV. [4,18,19,20].

Table IV. Spectroscopic data for Fe I lines

λ[nm]	E_{exc}[eV]	$(\lambda^3/gf)x10^{-13}$
371.994	3.34	1.3855
372.256	3.42	9.8294
373.484	4.19	0.2552
373.713	3.37	1.9392
375.873	4.26	0.5308
376.379	4.29	0.8258
376.719	4.31	1.1696

With the purpose of determining the ionisation temperature, the plasma was supposed to be in local thermodynamic equilibrium and electrically

quasineutral ($n_e \approx n_i$). The LTE ionisation temperature is presented in the Saha relationship:

$$\frac{n_e \cdot n_i}{n_a} = \frac{g_e \cdot g_i}{g_a} \cdot \left(\frac{2\pi m_e k_B T}{h^2}\right)^{3/2} \cdot \exp\left(-\frac{E_i}{k_B T_{ion}}\right) \quad (3)$$

where: n is the number density of the subscripted species (e = electron; i = ion; a = atom in ground state); g is the statistical weight of the given particle ($g_e = 2$); E_i is the ionisation energy (all other symbols represents the wellknown physical constants). For Ar $g_i = 6$, $E_i = 15.755$ eV. Introducing the numerical values for the constant terms, the following equation may be obtained:

$$\frac{n_e \cdot n_i}{n_a} = 4.83 \cdot 10^{21} \cdot \frac{g_e g_i}{g_a} \cdot \exp\left(-\frac{E_i}{k_B T_{ion}}\right) \quad (4)$$

This is a more practical form of the Saha equation. Taking into account the quasineutrality ($n_e \approx n_i$), Eqn. (4) may be written as follows:

$$\frac{n_e^2}{n_a} = 28.98 \cdot 10^{21} \cdot \frac{1}{g_a} \cdot \exp\left(-\frac{E_i}{k_B T_{ion}}\right) \quad (5)$$

The relative intensity of an emitted spectral line (as compared to the ground state of the atom) is given by:

$$I = \frac{hc}{\lambda} \cdot (gA) \cdot \frac{n_a}{g_a} \cdot \exp\left(-\frac{E_{exc}}{k_B T_{exc}}\right) \quad (6)$$

By combining Eqn.(5) and Eqn.(6), and taking account the LTE condition ($T_{exc}=T_{ion}$), the following equation may be obtained:

$$\frac{hc \cdot gA}{I \cdot \lambda} = 28.98 \cdot 10^{21} \cdot \frac{1}{n_e^2} \cdot T^{3/2} \cdot \exp\left(\frac{E_{exc} - E_i}{k_B T_{ion}}\right) \quad (7)$$

Ionisation temperature could be estimated from the slope of a regression line fitted in accordance with the following equation:

$$\ln\left(\frac{hc \cdot gA}{I \cdot \lambda}\right) = f\left(-\frac{E_{exc} - E_i}{k_B T_{ion}}\right) = a + b\left(E_i - E_a\right) \quad (8)$$

where: $\mathbf{a = 51.721 - 2 \cdot \ln(n_e) + 3/2 \cdot \ln(T_{ion})}$ and $\mathbf{b = -1/(k_B T_{ion})}$

In Eqn.(5) **a** and **b** are two parameters, which depend on ionisation temperature. Presuming that T_{ion} was previously estimated from the slope of

Eqn.(5)., electron number density could be calculated from parameter **a**, which represents the intersection of the Boltzmann plot with the axis of **ln[hc·gA/(Iλ)]**. Following this mathematical order of ideas, the practical expression for n_e may be written as:

$$\mathbf{n_e = \exp\left\{51.721 - a + \frac{3}{2}\ln\left(T_{ion}\right)\right\}} \tag{9}$$

Eqn. (9) represents the electron number densities which were estimated using only spectral line intensity measurements.

Calcium ionisation temperatures were calculated using an expression given by Boumans and De Boer [21]:

$$\left(\frac{I_i}{I_a}\right)_{LTE} = 4{,}83 \cdot 10^{21} \cdot \frac{1}{n_e} \cdot \left(\frac{gA}{\lambda}\right)_i \cdot \left(\frac{\lambda}{gA}\right)_a \cdot T^{3/2} \cdot 10^{-\frac{E_i + \Delta E_i - \Delta E_a}{k_B T}} \tag{10}$$

where: I_i/I_a - ionic to atomic intensities ratio; ΔE_i and ΔE_a represents the transition energy of ionic and atomic lines. The *i* and *a* indexes refer to singly charged ions and neutral atoms respectively.

Three atomic and one ionic line was used for the calculation of T_{ion} from the slope of a regression line fitted in accordance with the following equation:

$$\log\left(\frac{I_i}{I_a}\right)_{LTE} = f\left(\frac{E_i + \Delta E_i - \Delta E_a}{k_B T}\right) \tag{11}$$

The relevant spectroscopic data for Ca are summarised in Table V [22,23].

Table V. Spectroscopic data for Ca lines

λ [nm]	Transition energy [eV]	gA [x10^{-8} s^{-1}]	Obs.
430.253	2.882	7.1	atomic line
445.673	2.784	7.5	atomic line
393.367	3.152	0.91	ionic line
422.67	2.932	1	atomic line

It was assumed that, addition of an analyte specie to the plasma has no significant effect on the electron number density, which was estimated for the "unseeded" system using Eqn.(9).

2.3 Reagents. Stock solutions (1000 μg/ml) were prepared by dissolution of the high-purity metals or their salts in HNO_3 (1+1) - for Fe and in HCl (1+1) - for Ca. Single element working standard of 50 mg/ml were obtained by diluting the stock solutions with high purity 2 % v/v HNO_3 and HCl 1:1 respectively.

RESULTS AND DISCUSSION

3.1 Plasma shape and spectra. The Ar plasma obtained with a tip-ring electrode geometry has a filamentar shape with an intense purple core and a barely visible bluish outer mantle (sheath). The discharge extends up to the upper electrode above which the heated gas forms a larger bluish plume. It is very stable and completely noiseless.

The plasma shape and especially the core length is power dependent [13]. At 85 and 125 W the core does not exceed 20 mm in height, while at 185 W it extends up to the ring electrode (≈ 65mm) and at 275 W is well above it. The width of the plasma mantle (sheath) gradually increases with power and at 275 W completely fills the quartz tube. If higher power or lower Ar flow-rates are used, the plasma heat will affect the quartz tube.

The optical emission could be observed either below or above the ring electrode. The plasma background spectra were recorded in the 200-800 nm range with distillated water as blank and Ar or Ar and air as support gas using similar conditions as for the analytical determinations. The prominent feature of the emission spectra are the OH bands, the NO bands, the N_2 bands and the Ar lines. The background from 450 to 800 nm is smooth [11].

3.2 Excitation temperatures. A typical Boltzmann plot for Fe I lines is shown in Fig.2. Measurements were done at 185 W RF power, 1 l Ar flow-rate and h = 15 mm observation height for different tip-ring distances (H = 10, 20 and

40 mm). Mean electronic excitation temperatures were found to be in the range of 3700-4700 K.

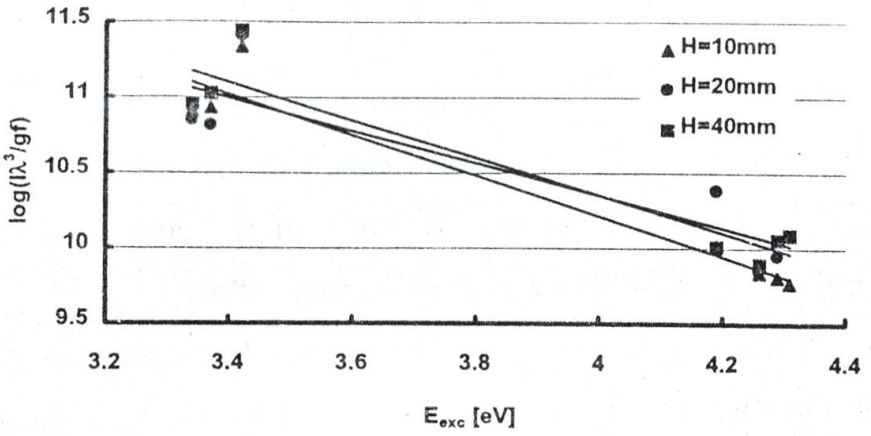

Fig. 2 - Boltzmann-plot for Fe

The electronic excitation temperatures for Ar were found to be in the range of 2000-3500 K, and were obtained at the same operation conditions like for Fe lines. In Fig.3 is shown the effect of observation height on Ar excitation temperatures, for different tip-ring distances.

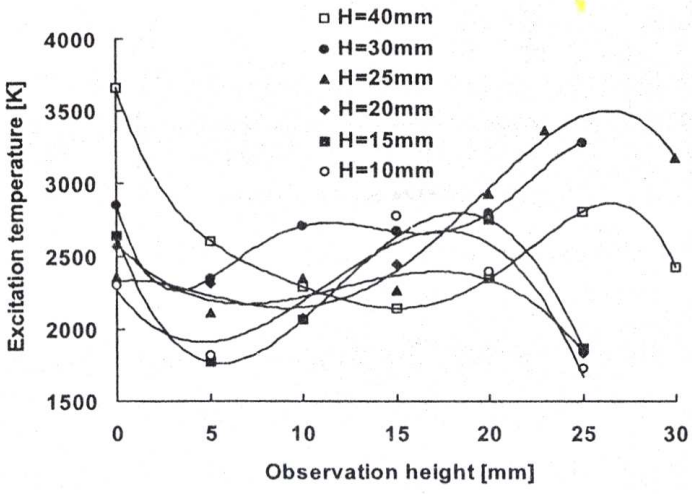

Fig. 3 - The Ar excitation temperatures as function of observation height and distance between electrodes (H)

3.3 *Ionisation temperatures.* The ionisation-recombination temperatures of Ar were determined to be in the range of 2500-4500 K. In Fig.4 is shown the effect of observation height on Ar ionisation temperatures, for different tip-ring distances.

The plots for T_{exc} and T_{ion} as function of observation height and tip-ring distance have similar shapes. The curves have two maximums situated close to the electrodes. The maximums are the result of the cumulated effect of the distribution of the RF field lines and the support gas flow.

The ionisation temperature of Ca determined according to Eqn.(10) was 4460 K, for a tip-ring distance of H = 10 mm and 4620 K for a tip-ring distance of H = 40 mm. Measurements were done at an observation height of h = 18 mm.

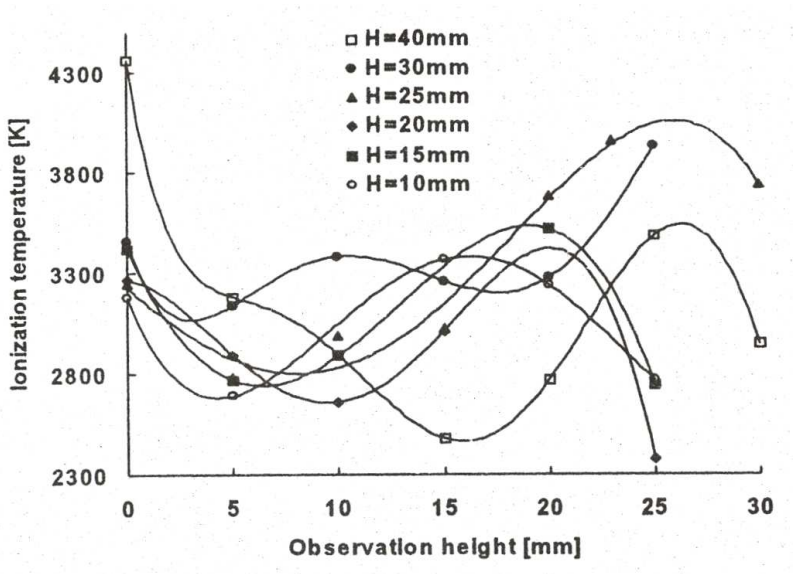

Fig. 4 - The Ar ionisation temperatures as function of observation height and distance between electrodes (H)

*3.4 Electron number density***.** The results for n_e, using Eqn.(6), were found to be in the range of 2-6x 10^{14} cm^{-3}. The effect of observation height on electron number density, for different tip-ring distances is presented (plotted) in Fig.5 and obviously it has the shape of T_{exc} and T_{ion} (with a similar explanation).

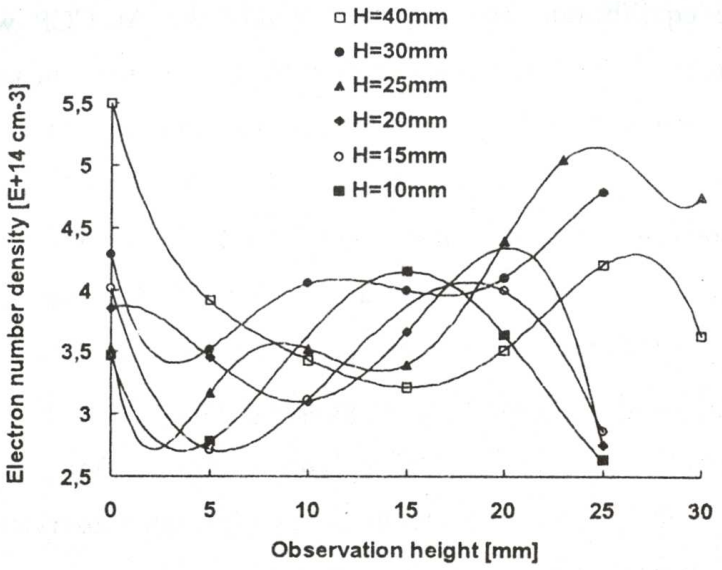

Fig. 5 - The electron number density as function of observation height and distance between electrodes (H)

CONCLUSIONS. A presentation of some fundamental characteristics for a RF Ar CCP, with tip-ring electrode geometry has been given. The plasma was investigated for electronic excitation temperature, ionisation-recombination temperature and electron number density. Table VI presents the characteristic temperatures and electron number densities derived in this study.

Table VI. Characteristic temperatures and electron number densities

Specie	T_{exc} [K]	T_{ion} [K]	n_e [10^{14} cm^{-3}]
Ar	2000 - 3500	2500 - 4500	2 - 6
Fe I	3700 - 4700		
Ca		4600 - 4700	2 - 6

These temperatures reflect the degree of excitation/ionisation of the relevant spectral lines used as thermal indicators. Due to the non-equivalence of the various state distribution temperatures, it may be concluded that

thermodynamic equilibrium does not exist within the Ar CCP with tip-ring electrode geometry. Taking into consideration the precision of measurements (± 15%) we may suppose that the plasma core is not very far from LTE and the analyte species are probably excited mostly by collisions with electrons (the excitation temperature has a close value to the ionisation temperature).

The values presented in Table VI are similar with the results obtained by other authors for capacitively coupled low power Ar plasmas [4, 24, 25, 17, 26].

The analytical performances are in good agreement with the explanations given for the shapes of T_{exc}, T_{ion} and n_e curves. For example, decreasing H, T_{exc} increases in the plasma core among 15 and 20 mm (observation heights) and this part of the plasma yields the best results for analysis of nebulised liquid samples. For liquid samples the optimum observation height corresponds always to the second maximum (Fig.3). At this height the desexcitation rate of the analyte specie is the greatest.

REFERENCES

1. S. Greenfield, H. McD. McGeachin, *Chemistry in Britain* **16**, 653 (1980).

2. S. Greenfield, H. McD. McGeachin, P. B. Smith, *Talanta* **22**, 1, (1975).

3. S. Greenfield, *The Spex Speaker* **XXII**, 1 (1977).

4. R. E. Sturgeon, S. N. Willie, V. T. Luong, *Spectrochim. Acta* **46B**, 1021 (1991).

5. Shi-Kit Chan, Akbar Montaser, *Spectrochim. Acta* **44B**, 175 (1989).

6. S. Bastiaans, R. A. Mangold, *Spectrochim. Acta* **40B**, 885 (1985).

7. P. J. Galley, G. M. Hieftje, *Spectrochim. Acta* **48B**, E 1725 (1993).

8. G. R. Kornblum, L. de Galan, *Spectrochim. Acta* **29B**, 249 (1974).

9. V. M. Goldfarb, S. V. Dresvin, *High Temperature* **3**, 303 (1965).

10. A k b a r M o n t a s e r, V. A. F a s s e l, G. L a r s e n, *Applied Spectroscopy* **35**, 385 (1981).

11. D. S. H a n s e l m a n, N. N. S e s i, M. H u a n g, G. M. H i e f t j e, *Spectrochim. Acta* **46B**, 495 (1991).

12. S. D. A n g h e l, A. P o p e s c u, F. R a c z, E. T ă t a r u, E. A. C o r d o ş, *Revista de Chimie* **40**, 344 (1989).

13. E. A. C o r d oş, S. D. A n g h e l, T. F r e n ț i u, A. P o p e s c u, *J.A.A.S.*, **9**, 635 (1994).

14. E. A. C o r d o ş, T. F r e n ț i u, A. F o d o r, M. P o n t a, A. M. R u s u, S. N e g o e s c u, *Acta Chimica Hungarica*, **132**, 313 (1995).

15. E. A. C o r d o ş, T. F r e n ț i u, A. M. R u s u, G. V â t c ă, *Analyst*, **120**, 725 (1995).

16. I. K l e i n e m a n n, J. Č a j k o, *Spectrochim. Acta* **25B**, 627 (1970).

17. R. E. S t u r g e o n, S. N. W i l l i e, V. T. L u o n g, J. G. D u n n, *Applied Spectroscopy* **45**, 1413 (1991).

18. M. W. B l a d e s, B. L. C a u g h l i n, *Spectrochim. Acta* **40B**, 579 (1985).

19. R. R e z a a i y a a n, G. M. H i e f t j e, *Anal.Chem*. **57**, 412 (1985).

20. W. R. L. M a s a m b a, A. H. A l i, J. D. W i n e f o r d n e r, *Spectrochim. Acta* **47B**, 481 (1992).

21. P. J. W. M. B o u m a n s, F. J. d e B o e r, *Spectrochim. Acta* **32B**, 365 (1977).

22. D. L i t t l e j o h n, J. M. O t t a w a y, *Analyst* **104**, 208 (1973).

23. C. H. C o r l i s s, W. R. B o z m a n n, *Nat.Bur.Stand.Monogr*., **53** (1962).

24. M. W. B l a d e s, *Spectrochim. Acta* **49B**, 47 (1994).

25. D. C. L i a n g, M. W. B l a d e s, *Anal. Chem.* **60**, 27 (1988).

26. M. W. B l a d e s, P. B a n k s, C h r i s G i l l, D. H u a n g, C h. L e B l a n c, D. L i a n g, I.E.E.E. *Trans. on Plasma Sci*., **19**, 1090 (1991).